UNIVERSITÀ DEGLI STUDI DI GENOVA

Scuola di Scienze Matematiche, Fisiche e Naturali

Corso di Dottorato in Fisica

Study of the modulation of $GABA_A$ receptors by using RuBi-GABA uncaging with linear and non-linear photoactivation in rat cerebellar granule cells *in vitro*

Supervisori

Chiarissimo Prof. Alberto Diaspro

Chiarissimo Prof. Mauro Robello

Candidata

Virginia Bazzurro

XXXIII Ciclo di Dottorato

“Mi domando – disse – se le stelle sono illuminate

perché ognuno possa un giorno trovare la sua.”

(Antoine de Saint – Exupéry)

In memory of Giancarlo, who loved the Science

Contents

Introduction

The research project that I present with this Ph.D. thesis is the result of these years of work and study at the Biophysics Laboratory of the Physics department of the University of Genoa, and it has evolved under the supervision of my Professors Alberto Diaspro and Mauro Robello.

This research concerned a receptor, $GABA_A$ receptor, which allows modulating the neuronal transmission in the Central Nervous System through its activation by the inhibitory neurotransmitter GABA.

The methodological approaches can be multiple and can be faced from different points of view, as well as a faceted mirror reflects the different aspects of the same reality.
In this case, a reality that affects the study and observation of events involving the infinitely small, such as neurons, and which cannot be seen with the naked eye.

The neuronal transmission regulates our emotions, thoughts, relationships with the external world, and our life, integrating and transforming the information from electric signals of our neuronal circuit brain.
These signals come from the passage of ions through channels in the cellular plasma membrane; an imbalance is enough to cause pathologies involving the Central Nervous System, i.e., epilepsy and other neuropsychiatric conditions.

Therefore, it is necessary to combine the use of techniques that allow identifying biological mechanisms based on neuronal conduction to understand and, in this way, to be able to modulate the function.

This is how it was thought to couple two distinct physical techniques, electrophysiology, and optical microscopy, to precisely follow the $GABA_A$ receptor activation in a limited cell portion with the uncaging method.

This method enables selecting a region of interest on the neuron for verifying differences in the $GABA_A$ receptor modulation after the activation by its neurotransmitter and pharmacological molecules.

The purpose can be achieved thanks to the use of inert or inactive molecules until they are activated by light where and when needed: these are the caged compounds. The release of photoactivable compounds is suitable to control interactions in living cells.

In the last decades, in the literature, several papers have been published works about caged compounds [*1-10*]; in this project, the uncaging of a caged molecule, RuBi-GABA, was exhaustively investigated and characterized.

The first part of the thesis deals with the biological background: GABA and GABAergic transmission, cerebellum, and Antisecretory Factor.

In the second chapter, caged compounds are considered; the attention is focused on caged neurotransmitters and, in particular, caged GABA.

Biophysical approaches are then described, in which the physical methods of electrophysiology and optical microscopy are presented as techniques for the study of biological mechanisms and their function.

In chapter 4, the instrumentation and the preparations used for carrying out the experiments are reported in materials and methods.

The thesis ends with the results and their analysis.

In the first part of the results, the uncaging method was studied as a useful technique for activating the receptor in localized areas of interest.

Hence, various physical parameters that may influence $GABA_A$ receptor activation during the uncaging event have been considered, chosen, and studied in a spatially and temporally confined way [*11*].

After studying all the physiological variations due to changes in these parameters, it was decided to move on to the use of the Antisecretory Factor, a pharmacological molecule previously studied during my Master's Thesis [*12*].

This factor was provided by Dr. Stefan Lange of the University of Gothenburg (Sweden), discoverer of this molecule, who also studied and investigated its function in various body areas [*13-16*].

The Antisecretory Factor has a facilitating action on the $GABA_A$ receptor in the presence of the neurotransmitter GABA.

The second part of the results reports how this pharmacological molecule action mechanism might change on a limited number of receptors and in different parts of the neuron, such as soma, growth cones, and neurites.

The study of the receptor responses in a confined cell area may open the door to future studies that can be used for the topical application of drugs on a specific target without activating the non-specific response of cells not of interest, thanks to the photoactivation of selective caged compounds.

Chapter 1: Biological background

1.1 GABA and GABAergic receptors

1.1.1 The neurotransmitter GABA

γ-aminobutyric acid (GABA) is the principal inhibitory neurotransmitter in the Central Nervous System of mammalians; it is at least in 30% of the synapsis [*17*]. It carries out its function binding receptors in the plasma membrane of pre and postsynaptic neurons.

Eugene Roberts and Sam Frankel identified it for the first time in the '50, but its inhibitory function was discovered later.

It is not uniformly distributed in the nervous system; *substantia nigra*, *globus pallidus*, hypothalamus, *corpora quadrigemina*, cerebral cortex, hippocampus, and cerebellum are the structures with the highest GABA concentration.

GABA is synthesized in the neuronal cytoplasm from the amino acid glutamine: glutamine is converted into glutamate by a glutaminase. After a decarboxylation reaction, glutamate is transformed in GABA by the glutamate decarboxylase enzyme (GAD) thanks to the cofactor pyridoxal-phosphate [*18-22*].

The neo-synthesized GABA is stored in the axonal terminal in synaptic vesicles through vesicular transporters (VGAT) by electrical and pH gradient generated by a proton pump. A stimulus opens calcium channels; calcium enters into the cell, and, because of the increase of its concentration, GABA is released into the synaptic space after the vesicle fusion with the plasma membrane of the neuron.

This neurotransmitter acts on receptors in the postsynaptic neuron membrane, inducing activation of inhibitory signals, but at the same time, it works on presynaptic receptors allowing a modulation in the release of the neurotransmitter.

After GABA binding to the receptors and its physiological action, the presynaptic neurons, and glial cells (astrocytes) pick it up through membrane transporters (GAT). It may be directly accumulated in the synaptic vesicles, ready to be released after a new stimulation (presynaptic neuron); or it is catabolized by the enzyme GABA transaminase (GABA-T) and by the NAD-dependent succinic semialdehyde dehydrogenase.

The transaminase deaminates GABA to succinic semialdehyde and transfers the amino group to a molecule of α-ketoglutarate to produce glutamate [*23*]. NAD-dependent succinic semialdehyde dehydrogenase oxidizes succinic semialdehyde forming succinic acid, which enters the Krebs' cycle (Figure 1.1).

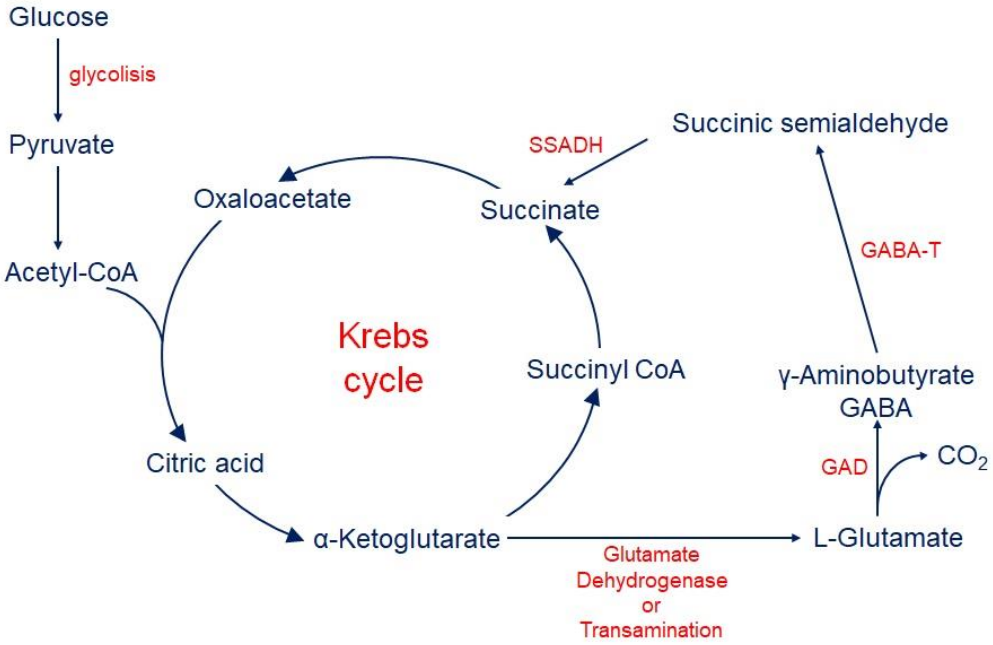

Figure 1.1: Metabolic pathway of GABA.

A glutamine synthase converts glutamate into glutamine, which is released and captured by the GABAergic termination for the production of new GABA molecules (Figure 1.2) [*24*].

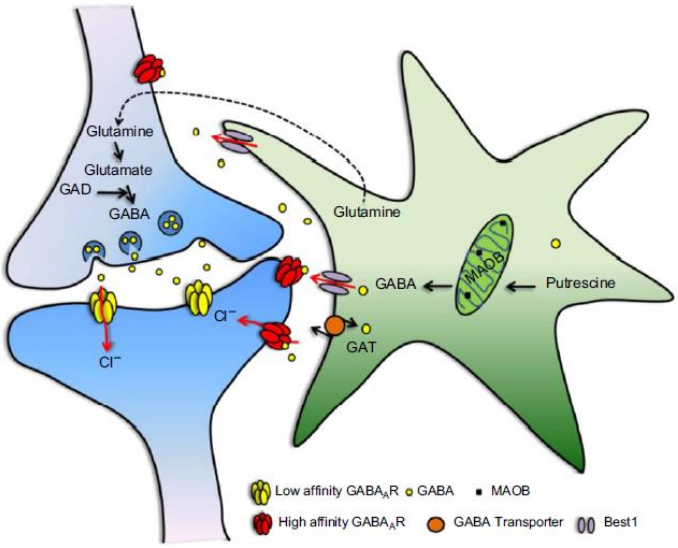

Figure 1.2: Synthesis, release, and catabolism of GABA by a GABAergic synapse. Copyright (2014) Wiley. Used with permission from Yoon B. E. et al. Glial GABA, synthesized by monoamine oxidase B, mediates tonic inhibition. J Physiol, The Physiological Society [*25*].

GABA controls the neuronal excitability in the nervous system. In essence, the modulation of its activity, particularly positive and facilitating, at the receptor level is the mechanism of action of a large number of sedative, muscle relaxant, hypnotic, and anti-epileptic drugs, benzodiazepines, and general anesthetics.
GABA can interact with three different types of receptors: $GABA_A$, $GABA_{B,}$ and $GABA_C$.

1.1.2 GABA receptors

GABA receptors are divided into three different types: $GABA_A$, $GABA_{B,}$ and $GABA_C$. The differences among them are based on the molecular structure, signal transduction mechanism, distribution, and pharmacological profile.

$GABA_A$ receptor is a ligand-gated receptor of 5 subunits assembled to form a central anion-selective transmembrane pore that allows chloride passage.
Chloride permeability involves membrane hyperpolarization (chloride enters into the cell), which decreases the probability that excitatory postsynaptic potentials can reach the threshold for generating the action potential.

In different regions of the Central Nervous System (i.e., spinal cord, the dendrites of some hippocampal and cortical neurons) [*26*], a membrane depolarization can occur because of the activation of receptors that determines a loss of negative charges (Cl^- moves out the cell). The resulting depolarization can generate an action potential for the activation of the voltage-dependent Na^+ channels [*24*]. This phenomenon is due to a pre-existing electrochemical gradient for Cl^-, which results in a driving force for the exit from the cell of this anion. In turn, this is determined by the presence on the neuronal membrane of a Na^+, Cl^- transporter (to be precise: a Na^+, K^+, $2Cl^-$ cotransporter) which accumulates chloride in the inside of the neuron utilizing the energy released by the simultaneous transport of Na^+ along its electrochemical gradient [*27*]. Instead, when the increase of Cl^- permeability results in hyperpolarization, this is due to the activity of a K^+, Cl^- cotransporter (KCC2) which sets the equilibrium potential for Cl^- at the equilibrium potential for K^+, which is hyperpolarized in respect of the resting membrane potential.

In particular, the cells have a resting membrane potential (V_m) which results from an unequal distribution of ions on both sides of the plasma membrane. The factors affecting

the membrane potential are the ion concentration and the membrane's permeability to these ions.

The equation that describes the membrane potential for a single ion is the Nernst equation; for any ion, this potential is defined as equilibrium potential and is given by:

$$E_{ion} = \frac{RT}{zF} ln \frac{[ion]_{out}}{[ion]_{int}} \quad (1.1)$$

Where R is the ideal gas constant, T the temperature, F the Faraday constant, z the charge of the ion, and [ion] is the concentration of the ion outside (out) and inside (int) the cell.

The concentration of chloride in the extracellular fluid (≈ 108 mM) is higher than the concentration in the cytoplasm (≈ 10 mM); the equilibrium potential for the chloride ion is:

$$E_{Cl^-} = \frac{61}{-1} ln \frac{108}{10} \approx -63\ mV \quad (1.2)$$

Sodium, potassium, and chloride are the ions that influence the membrane potential; the contribution of each ion to the membrane potential is proportional to its ability to cross the membrane. Goldman equation is used to calculate the potential resulting from these ions:

$$V_m = \frac{RT}{F} ln \frac{P_K[K^+]_{out} + P_{Na}[Na^+]_{out} + P_{Cl}[Cl^-]_{int}}{P_K[K^+]_{int} + P_{Na}[Na^+]_{int} + P_{Cl}[Cl^-]_{out}} \quad (1.3)$$

Where R is the ideal gas constant, T the temperature, F the Faraday constant, P_K, P_{Na}, and P_{Cl} the permeabilities of the membrane to the ions K^+, Na^+ and Cl^- respectively, and $[K^+]$, $[Na^+]$ and $[Cl^-]$ the concentrations of K^+, Na^+, and Cl^- ions [*28*].

$GABA_A$ receptor has several binding sites for different molecules; for this reason, it is an essential target of drugs such as benzodiazepines and barbiturates to treat various neuropsychiatric conditions [*29*] and drugs for the induction and maintenance of general anesthesia [*30, 31*].

The second type of GABA receptor identified is the $GABA_B$ receptor; it is a metabotropic receptor associated with a G protein. It is made up of 7 transmembrane domains, an extracellular N-terminal portion, and an intracellular C-terminal portion.

These receptors are mainly distributed presynaptically and act as autoreceptors for GABAergic neurons or heteroreceptors on non-GABAergic terminals. Even if less abundantly, they are also found on the postsynaptic membrane, dendrites, and soma.

They are activated by the endogenous ligand GABA and by the agonist baclofen; they do not respond to drugs active on $GABA_A$ receptors such as benzodiazepines and barbiturates and the competitive antagonist bicuculline [*32*]; their antagonists are saclofen [*33*] and phaclofen.

The functional $GABA_B$ receptor consists of a heterodimer. The interaction of two subtypes composes it, $GABA_BR1$ and $GABA_BR2$, which interact with their C-terminal domains (coiled-coil structure) [*34*]. $GABA_BR1$ contains the binding site for GABA, agonists, and antagonists; $GABA_BR2$ interacts with a G protein and transfers the receptor complex on the plasma membrane.

The activation of presynaptic $GABA_B$ receptors leads to a decrease in Ca^{2+} voltage-dependent channel conductance, a reduction in the flow of Ca^{2+} ions, and resulting inhibition of the release of neurotransmitters by exocytosis [*33*, *35*]. In the postsynaptic neurons, these receptors induce a K^+ channels conductance increase with a hyperpolarizing effect due to the increment in the efflux of K^+ ions [*24*, *33*, *36*].

$GABA_C$ receptor is an ionotropic receptor, as $GABA_A$ receptors. It is a pentameric channel receptor, permeable to chloride, and it is mainly localized in the vertebrate retina. It can produce homomeric or heteromeric complexes. It is composed of ρ subunits (ρ_1, ρ_2, and ρ_3) that are considered part of the $GABA_A$ receptor subunit family [*37*].

These receptors' physiological function is not yet clear, but they have a high sensitivity to GABA, produce small currents, and do not desensitize [*37*].

They are insensitive to the antagonists active on $GABA_A$ (bicuculline) and the agonist of $GABA_B$ receptor baclofen, do not respond to the administration of benzodiazepines, barbiturates, and general anesthetics. However, picrotoxin inactivates them [*38*].

1.1.3 $GABA_A$ receptors

Structure and subunits

$GABA_A$ receptor is a ligand-gated receptor permeable to Cl^- ions, highly sensitive to the selective agonist muscimol, and the competitive antagonist bicuculline.

It consists of 5 subunits assembled to form a central transmembrane pore; each subunit presents an extracellular N-terminal domain of about 200 amino acids, a small extracellular C-terminal portion, and four transmembrane hydrophobic regions called M1, M2, M3, and M4 (Figure 1.3).

These receptors belong to the Cys-loop receptor superfamily with the nicotinic acetylcholine, the glycine, and the 5 -HT_3 receptors. In the first portion of the N-terminal region of each subunit, there is a loop of 13 amino acids between two cysteines which form an SS-bond. The M2 segment forms the structure and the ionic selectivity of the channel; a long variable intracellular stretch (loop) is between M3 and M4 segments. In some subunits, this loop consists of consensus sequences for phosphorylation [*24*].

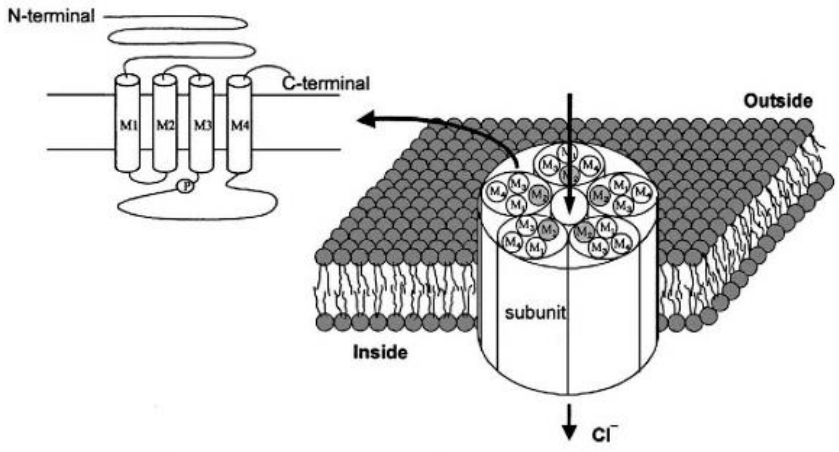

Figure 1.3: Schematic representation of the $GABA_A$ receptor. Transmembrane domains (M1-M4), amino and carboxy-terminal are represented on the left; on the right is shown the arrangement of the transmembrane regions in the various subunits of the receptor for the formation of the central pore permeable to Cl^-. Copyright (2002) Wiley. Used with permission from Watanabe M. et al. GABA and GABA receptors in the central nervous system and other organs. Int Rev Cytol, Elsevier [*37*].

Significant variability among $GABA_A$ receptors is known due to the presence of 16 different receptor subunits encoded by 19 genes: 6 subunits α (α_{1-6}), 3 β (β_{1-3}), 3 γ (γ_{1-3}), δ, ε, θ and π [*39*]. The combination of different classes of subunits leads to the formation of $GABA_A$ receptors with various pharmacological properties.

Each subunit of the same class has a homology of 60-80%, and the homology between subunits of different classes is 30% [*40*]. Functional $GABA_A$ receptors have two α subunits, two β subunits, and one of γ, δ or ε subunits. The most expressed receptors are composed of the combination α_1-β_2-γ_2 in a ratio 2: 2: 1 [*41*].

GABA neurotransmitter binds $GABA_A$ receptor in a site that involves α and β subunits; each receptor consists of two α and two β subunits. Therefore two molecules of GABA allow the activation of the receptor (Figure 1.4).

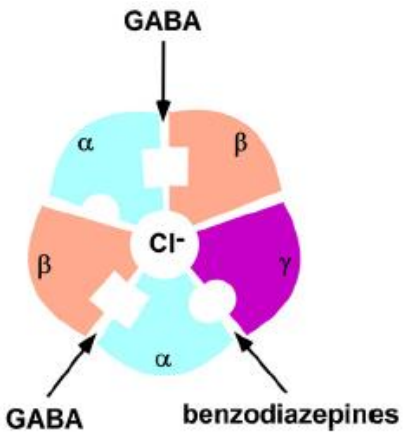

Figure 1.4: Transverse view of the $GABA_A$ receptor. The subunits and binding sites for GABA and benzodiazepines are highlighted. Copyright (2016) Wiley. Used with permission from Gravielle M. C. Activation-induced regulation of $GABA_A$ receptors: Is there a link with the molecular basis of benzodiazepine tolerance? Pharmacol Res, Elsevier [*17*].

Immunohistochemistry and *in situ* hybridization studies have allowed verifying the distribution of the different subunits in several brain regions:

- α_1, β_2, β_3, and γ_2 are widely diffused in different cell types in the brain and show the same pattern of diffusion [*42*];
- α_2, α_3, α_5, and δ are limited to some cell populations [*42*];
- α_1 is in regions where α_2 is not expressed or where it is not much expressed [*43*];
- α_3 is localized where levels of α_1 are low [*42*, *43*];
- α_4 is mainly distributed in the hippocampus and thalamus [*42*, *44*, *45*];
- α_5 is prevalent in brain regions linked to memory and learning functions such as the hippocampus [*42*];
- α_6 is expressed almost exclusively in cerebellar granule cells [*46*];
- ε is only found in some portions of the hypothalamus and hippocampus [*47*].

θ subunit is not well known; π subunit was detected in organs not belonging to the Central Nervous System such as uterus, prostate, lungs, and thymus [*48*], it can form $GABA_A$ receptor in association with α, β and/or γ subunits and it allows the bond with pregnanolone, an endogenous steroid.

Binding sites, agonists, and antagonists

Different binding sites for several compounds characterize the $GABA_A$ receptor because of the combinations of different subunits: the sites for GABA, benzodiazepines, barbiturates, picrotoxin, neurosteroids, general anesthetics, and ethanol are the most known and studied.

GABA binding site

It is between α and β subunits. It is well conserved among the different isoforms. The interaction with the endogenous molecule or with a GABA-mimetic (muscimol) allows, after a modification of the receptor complex, the opening of the Cl^- permeable channel, and generally results in membrane hyperpolarization, and the generation of an inhibitory signal. Competitive antagonist bicuculline and gabazine block this interaction.

Benzodiazepine binding site

It is in $GABA_A$ receptors composed of α, β, and γ subunits.

This site is located between α and γ interfaces; the receptor sensitivity depends on isoform type. Receptors formed by the γ_2 subunit show higher sensitivity to benzodiazepines than those with the γ_1 subunit [*49*].

Benzodiazepines or non-benzodiazepine agonist interaction, in the presence of GABA, allows an increase in the receptor activation. The Cl^- permeability improves the GABA action with a consequent rise in the ion channel opening frequency. The effects are anxiolytic, muscle relaxant, sedative, and hypnotic. In particular, if benzodiazepines interact with $GABA_A$ receptors with α_1 subunits, the results are sedatives, anesthetics, and anticonvulsants, anxiolytic with α_2 subunit, while with α_3 or α_5, the final effect is muscle relaxation.

α_1 subunit exhibits high sensitivity to benzodiazepines such as diazepam and quazepam and ligands as the imidazopyridine zolpidem. Zolpidem has an intermediate affinity for α_2 and α_3, and it binds α_5 subunit with low affinity; receptors composed of α_4 and α_6 subunits in combination with β and γ_2 subunits do not bind traditional benzodiazepines and non-benzodiazepine agonists such as zolpidem but interact with high affinity with imidazobenzodiazepines, typically flumazenil [*50*].

Therefore, the efficacy and potency of the benzodiazepines depend on the α component [*39*].

This site is also recognized by a class of negative mediators, such as the inverse agonist β-carboline, which determines an opposite (inverse) action of benzodiazepines: it generates anxiogenic and convulsive effects.

The evidence that benzodiazepines and inverse agonists bind the same site is demonstrated by the fact that the competitive antagonist flumazenil can block both the anxiolytic and anxiogenic effects. The capability to determine opposite effects depending on the interaction with inverse agonists or agonists is due to the GABA allosteric site modulation with a consequent activation or decrease of ion channel activity.

Barbituric binding site

It is between M2 and M3 transmembrane domain interfaces. When it is activated by barbiturates, the Cl^- conductance increases, the channel opening time is extended, and the neuronal activity decreases, also when GABA is not present.

Barbiturates, widely used in the past as hypnotics and sedatives, are dangerous, causing tolerance and dependence. For this reason, benzodiazepines have replaced these drugs. However, phenobarbital is still used as an anti-epileptic drug, especially in developing countries [*51*].

Active antagonists are unknown for this binding site.

Picrotoxin and TBPS binding site (t-butylbicyclophosphorothionate)

It is inside the Cl^- channel; the bond to the non-competitive antagonist picrotoxin or the TBPS blocks the channel function and induces opposite effects than those mediated by GABA.

Picrotoxin interacts with the M2 transmembrane region of α and β subunits [*37*] and blocks the channel; this site is also known as the "convulsant site" because it causes anxiety and convulsions [*50*].

Neuroactive steroid-binding site

Two binding sites for neuroactive steroids have been identified. The first is in the M1 transmembrane region of the α subunit, and it facilitates the action of GABA by determining an allosteric modulation, and the second one is between α and β subunits. It involves modulation of the channel receptor similar to the action of barbiturates.

The different isoforms of the subunits that form the receptor lead to various sensitivity towards different neuroactive steroids. For example, studies on recombinant receptors consisting of α_1, α_2 or α_6 subunits in combination with β_1 or β_2 are more sensitive to the action of the neurosteroid allopregnanolone compared to subunits α_3, α_4, and α_5. δ subunit is not directly involved in forming the binding site, but it plays an essential role in increasing these active molecules' activity on the $GABA_A$ receptor.

Receptors with the γ_1 subunit are more sensitive to the interaction with neuroactive steroids; on the other hand, those formed by ε subunit are insensitive [*24*].

Ethanol and anesthetic binding site

The binding site for ethanol and volatile anesthetics appears to be at the interface between M2 and M3 transmembrane domains. Two amino acids (S270 and A291 of α_1 subunit) in this receptor region are involved in allosteric modulation [*52*]

It is not yet clear how ethanol acts on the $GABA_A$ receptor. Different studies have led to contradictory results [*50*].

Ethanol enhances the $GABA_A$ receptor function. Its effects, which can be overlapped with those of benzodiazepines and barbiturates, are increased by GABA agonists such as muscimol and reduced by antagonistic agents such as bicuculline.

Anesthetics raise the inhibitory function of the receptor even in the absence of the endogenous neurotransmitter if they are administered intravenously and in high concentrations; this action, called GABA-mimetic, determines a direct effect on the channel for Cl^-.

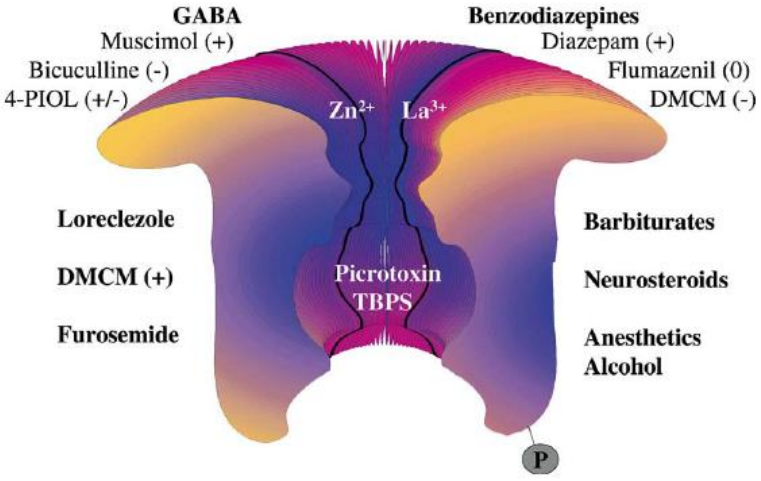

Figure 1.5: Schematic representation of the structure of the $GABA_A$ receptor. Copyright (2002) Wiley. Used with permission from Korpi E. R.et al. Drug interactions at $GABA_A$ receptors. Prog Neurobiol, Elsevier [*50*].

1.2 The Cerebellum

The cerebellum is an organ of the Central Nervous System mainly involved in the regulation of muscle tone, planning and coordination of movements, posture and balance [*53*].

It develops from the neural tube, which forms three primary vesicles in its anterior part: forebrain, midbrain, and hindbrain; the posterior part remains cylindrical and originates the spinal cord.

The hindbrain gives rise to the myelencephalon, from which the *medulla oblongata* develops, and the metencephalon, that forms the cerebellum [*54*].

The cerebellum consists of a central part, called *vermis*, and two cerebellar hemispheres; it is located dorsally to the brainstem, with which it is connected through three peduncles, and below the occipital poles, from which it is separated by the *tentorium cerebelli*, a lamina of *dura mater*.

The external surface shows a series of large transversal fissures, the deepest of which divides it into lobes; according to the phylogenetic origin, it is separated into three portions. The oldest part, the archicerebellum, and the paleocerebellum already appear in the "lower vertebrates". The neocerebellum, which includes the cerebellar hemispheres, is only in the "higher vertebrates".

The cerebellum has a cortex of grey matter surrounding a medullary center of white matter; the cerebellar nuclei are localized in the medullary center, while the cortex is subdivided into three different zones: the granular layer, the ganglion or Purkinje cell layer, and the molecular layer.

Two neuronal cell types form the **granular layer**, the cerebellar cortex innermost layer: the Granule and the Golgi cells. The Granule cells project their axons towards the molecular layer, where they divide into T and run parallel, forming Parallel fibers.

The Golgi cells modulate the activity of Granule cells.

The **intermediate layer** consists of Purkinje cells, neurons with a typical flask shape. The soma base originates an axon that reaches the medullary center after crossing the granular layer. They are the only cell type to leave the cerebellar cortex to interact with the nuclei of white matter: in fact, the axons of the other neurons are involved in the formation of intracortical circuits.

From the cell body of Purkinje cells, a dendrite originates and, after reaching the molecular layer, branches off, creating a dendritic arborization that receives Parallel fibers through synaptic contacts.

The **molecular layer** is the outermost layer; it contains inhibitory interneurons (Basket and Stellate cells) that interact with Purkinje cells, the dendritic arborization of Purkinje cells, Parallel fibers formed by Granule axons, and Climbing fibers.

The afferent fibers that reach the cerebellum are the Climbing and the Mossy fibers. The Climbing fibers, which originate from the inferior olivary nucleus, cross the first two cortical layers and in the molecular layer surround the Purkinje cell arborizations. The Mossy fibers, which derive from the *pons* and spinal cord neurons, project into the granular layer and make contacts with Granule cells' dendrites and the axons of Golgi cells.

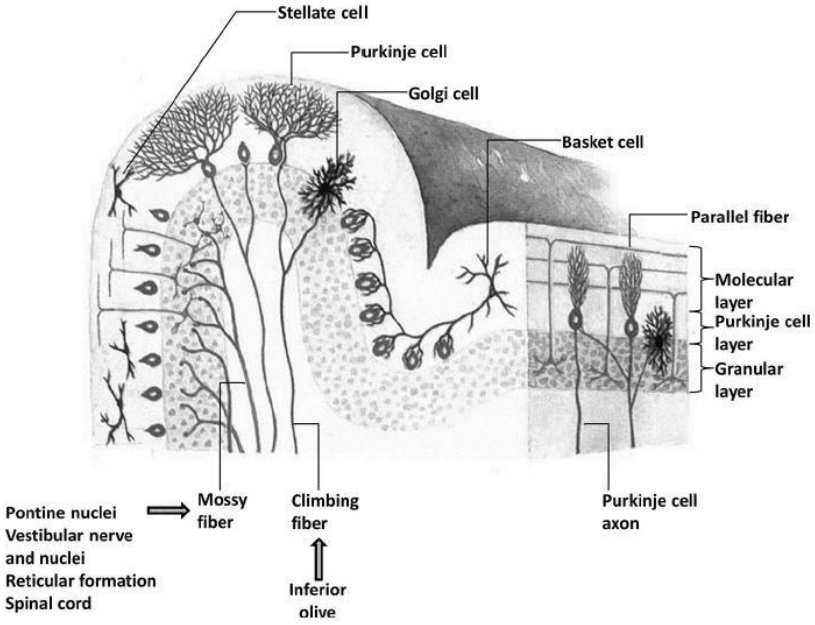

Figure 1.6: Subdivision of the cerebellar cortex and related neuronal types. Copyright © 2015 Mosconi M. W., Wang Z., Schmitt L. M., Tsai P. and Sweeney J.A. The role of cerebellar circuitry alterations in the pathophysiology of autism spectrum disorders. Front Neurosci 9: 296. Frontiers Research Foundation. doi: 10.3389/fnins.2015.00296 [*55*].

Typical synaptic structures formed by the excitatory terminations of the Mossy fibers are the "*glomeruli*", where single large ends of Mossy fibers innervate more dendrites from different cerebellar Granule cells, which also receive GABAergic inhibitory innervation by Golgi cells [*56*].

The deep cerebellar nuclei of the cerebellum in the medullary center are four pairs. They are reached by the Purkinje cells' axons and collaterals of the Climbing and mossy fibers before entering the cortex and emit neurites going out from the cerebellum.

In the middle-lateral part, the deep cerebellar nuclei are distinguished in the globose and emboliform nuclei, which form the interposed nucleus, and the dentate nucleus, more developed and related to the neocerebellum.

The axons are directed to the brain motor cortex through the cerebello-thalamo-cortical and the cerebello-rubro-thalamo-cortical pathway from the nuclei. The information is transmitted from the cerebellum to the telencephalon allowing gradual movements.

The inputs that arrive at the cerebellum allow programming movements and motor learning; through the spinocerebellar tract, the proprioceptive information concerning the body's position comes from the periphery, and through the cortico-ponto-cerebellar fibers, the cerebellum receives the motor information elaborated by the cerebral cortex.

All neurons in the cerebellar cortex synthesize the inhibitory GABA neurotransmitter except for Granule cells that release glutamate, an excitatory neurotransmitter.

Only the axons of Purkinje cells leave the cortex and contact the cerebellar nuclei; we can consider these as the principal cells that modulate the nuclei function through an inhibitory stimulus.

Also, the Climbing and Mossy fibers interact, in an excitatory way, with the cerebellar nuclei.

Therefore, the cerebellum activity result derives from the integration of inhibitory signals coming from the cortex and excitatory on the deep cerebellar nuclei through the Mossy and Climbing fibers.

Purkinje cells are excited by Climbing and Parallel fibers and inhibited by all other types that contact them [*53*].

1.3 The Antisecretory Factor

1.3.1 The discovery of a new molecule

The Antisecretory Factor is an endogenous protein of 41 kDa expressed in different mammalian tissues and plasma [*57*]. This factor was identified in the 1980s, and it has an inhibitory function against hypersecretion induced by exposure to enterotoxins (especially to CT, cholera toxin) or due to chronic inflammatory diseases.

This protein was purified for the first time from the intestinal mucosa and the pig pituitary gland [*13*] using methods such as isoelectric focusing, gel filtration, and agarose gel affinity chromatography [*16*].

The cDNA sequence was then cloned [*57*], and experiments were conducted to find the active site presents in the molecule [*58*]. Several peptides containing the sequence with antisecretory activity were synthesized to verify the possible pharmacological use in different conditions that induce intestinal hypersecretion and in situations of imbalance in the transport of liquids in other body compartments.

Although the Antisecretory Factor (AF) mechanism of action is mostly unknown, it is hypothesized that the antisecretory activity occurs through the nervous pathway. However, it can not be ignored direct action on ion channels that are involved in the hypersecretion of Cl^- ions and H_2O: in fact, it regulates ion transport in Deiters cells, inhibiting the passage of chloride ions through the cell membrane [*59*]. Furthermore, the intestinal fluid hypersecretion causes a nervous stimulation which, conducted centrally by the vagus nerve, acts on the adenohypophysis inducing the release of the AF factor in the blood to reach the peripheral organs with the activation of a further secretion/activation of the AF itself.

The distribution of the Antisecretory Factor was studied by immunohistochemistry and *in situ* hybridization of messenger RNA [*15*]; some cellular populations (i.e., different types of epithelia, leukocytes, endocrine cells, and neurons) have shown high expression, synthesis, and accumulation capacity of this protein [*16*].

Some foods, such as hydrothermally processed cereals (HPC), can increase AF blood levels by a mechanism of "false" intestinal hypersecretion due to a hypertonic signal in their passage into the small intestine. This capacity has clinical applications to improve the symptomatology of chronic inflammatory bowel diseases [*60*]. In Sweden, it has allowed preventing gastrointestinal diseases in pig and cattle breeding, avoiding the use of antibiotics [*14*]. The hydrothermal treatment of these cereals in a process similar to

malting produces many monomers/dimers of carbs and amino acids [*16*]. In particular, the carbs derive from the hydrolysis of the starch of the cereals themselves. With the substitution of single macromolecules with many smaller molecules, this process determines hypertonicity on the "wet" surface of the cereals in contact with the intestinal mucosa. This hypertonic signal causes an osmotic "suction" of liquid from the intestinal epithelium that "mimics" the abnormal release of fluid in diarrhea processes. This signal sets in motion the reaction of the endogenous homeostatic system, implying the release of AF.

1.3.2 Structure and active sites

Thanks to cloning, the AF sequence was obtained, and it was possible to study its structure.

The genes encoding for AF are located on human chromosomes 1, 19, 23, and pseudogenes are present on chromosomes 10 and 15 [*16*].

The complete length of the human AF sequence is 1309 bp, in which a coding part of 1131 bp can be distinguished [*57*]. In the mouse, 5 different variants were identified (Rpn10a – Rpn10e) with a 67 – 96% homology with the human protein. In particular, the first 250 amino acids are conserved, while the C – terminal sequence differs [*16*].

AF subjected to enzymatic digestion with trypsin has an antisecretory activity twice as high as the action of the whole protein; this increase in the inhibitory capacity led to the synthesis of peptide fragments of different lengths for the identification of the active antisecretory site [*58*].

Nine peptides from the recombinant protein and four smaller fragments were synthesized, a total of 13 peptides (see Table 1.1): five of them did not show antisecretory activity, and seven, containing amino acids 36 – 42, were particularly active.

The data showed that the antisecretory site is in the region between the amino acids 35 and 43, and it has the sequence (I)VCHSKTR.

In the N-terminal region of the AF molecule, four cysteine groups form disulfide bridges where the active site is present. These are necessary to guarantee the antisecretory activity [*58*].

Code	Oligonucleotide	Peptide	Inhibition of cholera secretion (pmol)
AF-1	1–1131	1–376	1–10
AF-2	186–1131	63–376	> 100
AF-3	361–1131	121–376	> 100
AF-4	1–315	1–105	6
AF-5	1–240	1–80	4
AF-6	106–240	36–80	6
AF-7	61–153	21–51	5
AF-8	61–108	21–36	> 100
AF-9	124–207	42–69	> 100
AF-10	(106–153)	36–51	5
AF-11	–	35–46	14
AF-12	–	35–42	15
AF-13	–	36–41	> 100

Table 1.1: Peptide fragments synthesized from the recombinant AF protein; for each peptide is shown the nucleotide and amino acid length and the dose (moles injected into the rat), which determines the inhibition of 50% of the secretion induced by the cholera toxin. Copyright (1997) Wiley. Used with permission from Johansson E. et al. Identification of an active site in the antisecretory factor protein. Biochim Biophys Acta, Elsevier [*58*].

The AF peptide formed by 16 amino acids (AF-16), including the antisecretory site, is the most stable fragment during laboratory experiments, determines a protective and regulatory effect in several damaged tissues, normalizes intracranial pressure, and decreases mortality in rats with encephalitis [*61*].

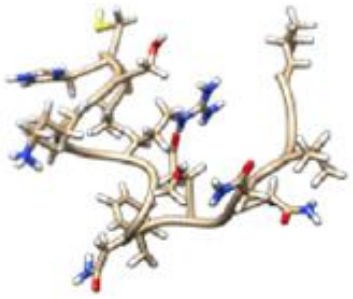

Figure 1.7: Molecular structure of the AF-16 peptide. Reprinted (adapted) with permission from Matson Dzebo M. et al. Enhanced cellular uptake of antisecretory peptide AF-16 through proteoglycan binding. Biochemistry, 53(41): 6566-6573. Copyright (2014) American Chemical Society [*62*].

Also, the site in the N-terminal region is involved in the anti-inflammatory action. Studying the immunohistochemical distribution of AF, it has been hypothesized a possible role in the immune system. In lymphoid organs (i.e., spleen, lymph nodes, and thymus), AF is expressed abundantly in macrophages and cells with dendritic morphology; in the central nervous system, it is present in perivascular cells, necessary for the regulation of anti-inflammatory reactions, and in the intestine is widely localized in Peyer's plaques [*63*].

From protein structure prediction models based on the sequence information [*64*], it appears to be a von Willebrand domain between residues 5 and 188 of the N-terminal that would mediate protein-protein interactions [*16*].

The C-terminal portion of AF presents a site involved in ubiquitination and forms part of the 19S proteasome regulatory subunit [*65*].

Fascinating is that the AF factor interacts with the flotillin-1 protein in the nervous system [*66*, *67*]. Flotillin-1 is a membrane protein and a component of the so-called lipid rafts that participate in transport processes of receptors at postsynaptic sites of the neuronal plasma membrane [*67*].

1.3.3 Function

In vivo experiments have shown that AF is a potent inhibitor of intestinal secretion induced by cholera toxin [*13*] and toxin A produced by *Clostridium difficile* [*68*]. The cholera toxin, and probably also the toxin A produced by *Clostridium difficile,* causes hypersecretion of chloride and water from the epithelial cells of the small intestine due to the prolonged opening of anionic channels due to their phosphorylation. The AF factor could reach its effect by acting on the nervous system interneurons and secretory complexes.

The influence of the antisecretory factor in GABAergic transmission was considered: GABA represents the primary inhibitory neurotransmitter of the Central Nervous System of mammals and is present with its $GABA_A$ receptors in the Enteric Nervous System [*29, 69, 70*]. However, such receptors in the Enteric Nervous System appear to have above all an excitatory function [*29, 69, 70, 71*], although the final result of their activation depends on whether they are in circuits that innervate motor or excitatory or inhibitory neurons. Ultimately, it does not appear possible in the Enteric Nervous System to apply the convenient conclusion that seems valid in the adult mammalian brain: increased activity of the $GABA_A$ receptors equal more significant inhibition and behaviourally anxiolytic, sedation, anti-epileptic action.

Thus, the influences of the AF factor on the Enteric Nervous System and the secretory phenomena through effects on $GABA_A$ receptors should be evaluated in the context of intricate enteric nerve circuits.

A more simplistic approach was to directly assess the effects of the AF factor on the large anionic channels potently activated in the intestine's epithelial cells from the cholera toxin. One model used was studying the chloride ion permeability properties of the plasma membranes of the large Deiters neurons of the mammalian brain trunk. This approach has suggested that AF can function directly as a blocker of such anionic channels, as a sort of "plug" [*59*].

Returning to the *"$GABA_A$ centric receptor"* approach, neuronal systems of the Central Nervous System were studied as models. In the CA1 region of the hippocampus, the effect of AF on pyramidal cells and their interneurons was studied; AF promotes an increase in the GABAergic inhibitory signal on the interneurons of the radiated layer, primarily by increasing the extrasynaptic tonic inhibition resulting in an AF mediated disinhibition of the pyramidal neurons [*72*].

However, it remains clear that these last approaches and the one presented here are among these, have the purpose fundamentally to understand the "modules" of the functioning of the factor that can later be used and integrated within a better understanding of the mechanisms of the Enteric Nervous System.

In recent years, the focus on AF function has also turned to clinical purposes. In the plasma of healthy people, it predominates the inactive form of AF; if exposed to agents that cause gastrointestinal disorders, AF is rapidly transformed into an active form to regularize and normalize the transport of water and ions in the gut [*66*].

Consumption of cereals hydrothermally treated with a process similar to malting by individuals suffering from inflammatory bowel disease increases plasma levels of AF and, at the same time, is accompanied by an improvement in physical well-being and quality of life with reduction of clinical symptoms [*60*].

Children with acute and chronic diarrhea may present a health improvement after consuming egg yolk rich in AF. This food with high doses of preformed antisecretory factor could be useful for prophylaxis in populations where gastrointestinal diseases are endemic [*73*, *74*].

AF's possible role is the regulation of endolymph transport in the inner ear: vertigo symptoms in patients with Ménière's syndrome could be due to an imbalance in the production and/or transport of endolymph [*75*]. The treatment with AF would determine homeostasis control in the inner ear by regulating the secretion of endolymph. Furthermore, hydrothermally processed cereals (HPC) consumption has led to a reduction in vertigo because of the increase in AF production in treated patients [*75*-*77*].

A more recent randomized double-blind study with placebo controls led to discordant results compared to previous work. In essence, 53% of patients (17 patients out of 32) treated with HPC showed a functional improvement, but this did not result statistically significant compared to 44% (14 patients out of 32) found in placebo patients [*78*]; this would require an investigative approach aimed at analyzing and deepening this aspect of the antisecretory factor for the understanding of its mechanism of action and its role.

However, the work of *Ingvardsen and Klokker* [*78*] is not immune to criticism, having been conducted on no-hospitalized patients and therefore not adequately evaluated from "compliance" in treatment (in this case, a particularly decisive aspect). Moreover, in this type of approach, it would be necessary to monitor AF blood levels in parallel to confirm its activation.

Chapter 2: Caged compounds

In cell biology, an important issue is how particular molecules or ions influence cell functions. This question can be investigated by introducing probes of interest in live cells and observing the effects. A conventional method is microinjection of the molecules into cells or using a probe that can be photo-activated and precisely controlled in space and time [*79*].

These probes, called "caged compounds", are chemically modified, and their biological activity is masked until UV-visible light activate them when and where the exposure occurs. This approach is suitable because illumination can be easily controlled in timing, location, and amplitude.

The term caged is based on the concept that biologically active species could get trapped inside a large molecule that would be open or dismembered after illumination [*1*].

These optical probes are similar to pro-peptides whose activity is suppressed by the presence of sequences covalently linked to the molecule, inhibiting their function.

Chemical thermal reactions release the functional peptides from the precursors such as photolysis breaks the covalent bond in caged compounds, enabling the active form [*8*].

The caged group must fulfill some principles to be useful for physiology:

- It should cause the biomolecule to become inert at the working concentration; adding the caging chromophore to a functionally crucial side of the biomolecule usually renders it inactive towards its target [*1, 80*].
- It should instantly release the biomolecule in high yield; it is essential how excitation translates to release of the caged molecule, a property measured as the quantum yield (QY; Φ, unitless). Furthermore, most ionotropic neurotransmitter receptors activate on a fast time scale; the photolytic release must occur faster than the signaling to be activated for mimicking endogenous receptor signaling [*1, 80*].
- It should have an efficient light absorption, measured as the extinction coefficient (ε, unit: M^{-1} cm^{-1}) [*80*].
- It should have hydrolytic stability at physiological pH during the experiments [*80*].
- It should be soluble at the experimental concentration [*80*].
- It should not interact or interfere with other molecules [*1*].
- It should not be damaging to the biological system.

Several caged compounds are available, i.e., amino acids, neurotransmitters, enzymes, and peptides; different caged probes allow studying intracellular ion levels, typically calcium and sodium, which regulate and transduce cytoplasmatic signals.
Also, caged fluorophores are attached in biomolecules for measuring the system steady-state or dynamics conditions after the photolysis reaction [*1, 79*].

Nowadays, different caged frameworks have been described and are commercially accessible; the widely used are the nitroaromatic groups as CNB, DMNB, MNI [*81*, *82*], CDNI [*8*], that are activated by light in 300-410 nm range [*1*, *8*, *83*, *84*] or DEAC450 [*6*], and RuBi [*2*, *85*] with an uncaging absorption spectrum into the blue range (440-500 nm) [*8*].

The spatially precision of the uncaging is realized by focusing the light. The localized illumination can reveal the spatial diffusion of caged compounds and provide a reduction in their use.

Conventional lighting through microscope objectives is related to a double cone, as in confocal microscopy; although the highest photon density is in the focus plane, the planes above and below the focus collect photons.
For favoring the photolysis as firmly as possible to the focus plane, it is required the absorption of more than one photon; in particular, the two-photon regime is the most diffused [*1*].
In this way, two red-infrared photons are simultaneously absorbed by a molecule and emitted as a single photon with a half wavelength [*86*]; this phenomenon necessitates tight focusing of a pulsed laser of 10^{-13} s width repeating every 10^{-8} s.
Also, infrared wavelengths provide less scattering and damage but more penetration than UV in tissues.

Besides one- and two-photon uncaging, other significant parameters are reported in the literature, as well as laser power [*6*, *87-89*], exposure time [*90*], and plane distance from the cell target [*2*, *6*, *8*, *88*, *91*].

Uncaging has many useful features and advantages compared to other methods. The intracellular compartment is accessible to the photorelease, cells are transparent to uncaging light, and the inert compound can be loaded [*83*].
It is fast (from sub-microseconds to milliseconds), so channel-gating kinetics can be calculated. It is possible to repeat and control the release of the caged compound,

calibrating the uncaging efficiency as a function of incident light intensity or via intracellular imaging techniques [*83*].

Finally, caged compounds provide a much less invasive means of producing concentration jumps than rapid flow techniques, causing physical perturbation of the sample [*83*].

Other characteristics of caged compounds are related to purity and stability. Caged compounds should be extremely pure; impurities could cause a response before the illumination of the caged compound [*83*].

Moreover, they must be hydrolytically and enzymatically stable for the duration of the experiment; chemical instability of certain caged neurotransmitters could liberate enough of the caged species to produce desensitization before illumination [*83*].

2.1 Caged neurotransmitters

The uncaging method has proved useful in some physiological studies. A process is measured while a light flash is applied to manipulate a physiologically relevant or pharmacologically active photosensitive molecule. In particular, it is the case of the investigation of receptor activations in the nervous system [*92*].

These probe compounds are prepared via covalent appendage of a light-sensitive protecting group (the "cage") to a signaling molecule that is unable to activate its target until the light brokes the bond [*93*].

Once uncaged, the neurotransmitter becomes active, and it can interact with its receptor site, inducing a physiological variation that can be measured with a suitable experimental apparatus.

Caged neurotransmitter compounds are composed of aromatic rings to produce photosensitivity. The simplest type of caging chromophores is quite water-soluble; no organic solvents should be present in the buffer, even small amounts of it can be toxic and jeopardize the experiment success [*94*].

The first caged neurotransmitters described were a series of photoactivatable acetylcholine, active on nicotinic acetylcholine receptors (AChR) and studied coupling the uncaging with the electrophysiological techniques [*1*].

The most known was Bis-Q, a reversible agonist in its *trans* form, but with not negligible side effects as desensitization and inactivation of the receptors [*95*]; for this reason,

carbamoylcholine replaced it [*96*]. This new probe was the beginning of the development of most caged neurotransmitters, such as glycine [*97*], glutamate [*98*], serotonin [*99*], dopamine [*4*], and GABA [*2, 8, 87, 100, 101*].

The functional distribution and connectivity of neurons are studied by optical stimulation of postsynaptic receptors using caged neurotransmitters in neuronal culture and *ex vivo* (i.e., brain slices) [*6*].

Some caged neurotransmitters are two-photon sensitive, which allows reaching a photolytic reaction with a remarkable spatial resolution and analyzing cellular processes with a more exceptional spatiotemporal control [*3*], as at the level of dendritic spines [*4*].

The use and relevance of caged neurotransmitters have been described in different papers [*3, 6, 8, 88, 102, 103*]. In particular, glutamate and GABA are the most critical neurotransmitters mediating excitatory and inhibitory neurotransmission in the Central Nervous System, respectively; the balance of these is essential for normal signal processing in the brain, and its malfunction has been determined to be a fundamental cause of several neurological diseases [*80*]. In this work of Thesis, one and two-photon uncaging are considered for studying the modulations of $GABA_A$ receptor responses activated by a caged GABA (RuBi-GABA) in the cerebellar granule cells in a novel approach, after the variation of physical key parameters as described in Chapter 5.

2.1.1 Caged GABA

Since GABA is the primary inhibitory neurotransmitter in the Central Nervous System (CNS), several caged GABA molecules are synthesized and commercially available; among these, the most representatives in literature are CDNI-GABA, BCMACM-GABA, CNB-GABA, DEAC450-caged GABA, and RuBi-GABA.

CDNI-GABA

CDNI caged compounds absorb light in the 300-380 nm range, extended beyond 400 nm; violet lasers can photoactivate these probes [*8*].

It was employed to study $GABA_A$ receptor localization to dendritic spine heads, even if the function is not entirely understood [*8*].

Also, 720 nm wavelengths photolyze CDNI-caged neurotransmitters during non-linear excitation. They are useful for performing two-color uncaging experiments, partnering blue light photoactivated caged compounds [*8*].

BCMACM-GABA

BCMACM caged compounds possess a coumarin chromophore linked to the biomolecule by an ester bond. Since this bond should be hydrolyzed by intracellular esterase, these caged neurotransmitters could be used extracellularly.

It shows an adequate solubility in aqueous buffer at pH 7.2, is stable for 1 h in the dark at room temperature but is gradually hydrolyzed with half-lives of longer than 200 h. However, hydrolysis is not found after 2 days, when HEPES is added to BCMACM-GABA at pH 7.2 and stored at -4 °C in the dark.

The quantum yield of photolysis is 0.20 for photolysis on irradiation with 390 nm light, and the fluorescence lifetime is 760 ps [*104*].

CNB-GABA

It is a GABA bond to an α-carboxy-o-nitrobenzyl group, released from this compound when exposed to ultraviolet light [*105*]. It has a quantum yield of 0.02 and photolysis half-times of about 1.5 ms [*106*]. It possesses almost ideal characteristics such as rapid photolysis and prolonged spontaneous breakdown [*106*, *107*].

However, *Gee et al.* reported that CNB-GABA behaves as an agonist or antagonist action on $GABA_A$ receptors at concentrations as high as 500 μM [*82*, *105*, *106*].

DEAC450-caged GABA

Linear and non-linear excitation photo-release this caged GABA; its maximum absorption is at about 450 nm towards a one-photon regime. It has a quantum yield of 0.39; it is soluble and stable in physiological buffer.

It is excited at 900 nm but is inactive at 720 nm during two-photon uncaging. Therefore, it is used for performing two-color uncaging when paired with nitroaromatic caged glutamate that is excited at those wavelengths. In this way, the two neurotransmitters can be photo-release, with one- and two-photon excitation, around a single spine head of neuronal brain slices [*6*].

RuBi-GABA

Ruthenium-bipyridine-triphenylphosphine GABA (RuBi-GABA) is a caged GABA photolyzed by visible wavelengths.

RuBi-GABA is a ruthenium-based photosensor that releases ligands with a single, clean and fast photochemical step. It is composed of a ruthenium polypyridine core linked to four 2,2′ bipyridines, triphenylphosphine, and GABA [*2*].

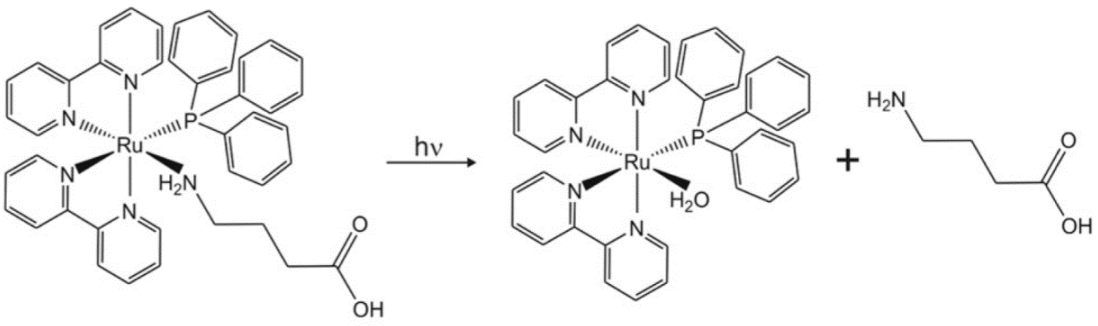

Figure 2.1: GABA release from the photolysis of RuBi-GABA. Copyright © 2008 Rial Verde E. M., Zayat L., Etchenique R. and Yuste R. Photorelease of GABA with visible light using an inorganic caging group. Front Neural Circuits 2:2. Frontiers Research Foundation. doi: 10.3389/neuro.04.002.2008 [*2*].

Ruthenium-based caged GABA compound provides multiple advantages compared to the other available UV-sensitive caged GABA compounds:

- The inorganic-based photo-release is usually much faster than organic approaches [*2*]
- The quantum yield of uncaging is higher than the previous standards for GABA uncaging [*108*]
- The uncaging with visible light results in less scattering (better spatial resolution), less phototoxicity (UV wavelengths damage cell DNA and proteins), and penetrates deeper into tissue [*109*]
- The complex is also active in the two-photon regime (2PE), allowing uncaging with IR light using a Ti: Sapphire laser [*110*]

RuBi-GABA produces chloride current activating $GABA_A$ receptors, and it enables receptor and input mapping from various interneuron types.

The chemical versatility and fast photo-release make RuBi-GABA an ideal caged compound for studying neuronal biophysics and neuronal circuits.

Chapter 3: Biophysical approaches

3.1 Patch-clamp

Patch-clamp is a technique developed by Nobel laureates Erwin Neher and Bert Sakmann in 1976. This technique allows electrophysiological studies recording ionic currents using glass micropipettes, which determine high resistance in contact with the plasma membrane.

This method enables studying the activity of individual ion channels. It comes from the voltage-clamp technique, and it can be applied to any type of excitable cell (i.e., neurons, cardiomyocytes and muscle fibers, cell cultures, and tissue slices).

Cellular processes are studied by measuring the ionic flux by blocking the difference of the potential in a small portion (patch) of the plasma membrane.
While the potential is set constant, the current is measured. Any change in the current flow reflects changes in the state of the ion channel opening [*111*].

A 1-2 μm glass micropipette, which adheres to the cell membrane, electrically isolates the small area. A seal with a resistance exceeding 10 GΩ, called Gigaohm seal, is created with negative pressure.

After the seal formation, single or whole channel measurements are performed, depending on the microelectrode and cell membrane final configuration, the composition of the electrolyte solution inside the microelectrode, and the external solution where the sample is maintained [*112*].

The patch-clamp is based on the electrical, biological activity due to the movement of charges across the plasma membrane, in particular, Na^+, K^+, Ca^{2+}; the flow of current through an ion channel is due to a driving force which can be defined by Ohm's law:

$$I = \frac{V}{R} \tag{3.1}$$

Where I is the current, V the potential, and R the resistance; the current is proportional to the potential.

Recordings of current changes allow verifying changes in ion channels' opening and closing state [*113*].

For obtaining the Gigaohm seal, certain conditions must be fulfilled. In particular, the plasma membrane must be clean; no extracellular matrix residues must be present. The solutions used in the bath and the micropipette must be filtered before the experiments to avoid impurities; the glass microelectrodes must be changed at each measurement. They must have resistance between 2 and 5 Megaohms, and the instruments used must be placed on an anti-vibration table to ensure mechanical stability and electrically isolated, employing a Faraday cage [*114*].

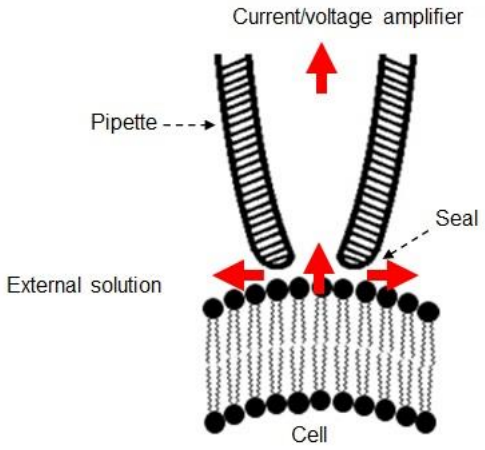

Figure 3.1: Relationship between the tip of the micropipette and the cell membrane during the seal formation.

The cell membrane can be assimilated to an equivalent electric circuit RC which includes a resistance R_m and a capacitance C_m: the resistance is that offered to the ionic flow through the channels, therefore dependent on the number and permeability of the different ion channels; the capacitance is related to the dielectric power of the lipid phase, that is to the properties of the phospholipid bilayer which allows the separation of positive and negative charges, making the plasma membrane assume a behavior similar to a capacitor.

The micropipette is filled with an electrolytic solution and contains a chlorinated silver electrode connected to an amplifier. The current flows the membrane in the tip and is recorded by the amplifier thanks to negative feedback. This mechanism provides an equal

amount of current, but of opposite sign, to the current flowing the cell. Thus, the membrane potential can be blocked and the current recorded.

The patch-clamp can be used in different configurations to follow different purposes: i.e., recordings of the activity of a single channel, of channels activated by a ligand, or of the total cell currents.

3.1.1 Patch-clamp configurations

- *Cell-attached*

  It is the most straightforward configuration to reach. The microelectrode is brought closer to the cell of interest with manipulators. The final approach is favored thanks to micromanipulators that allow movements of a few micrometers; when the tip of the microelectrode is in correspondence with the cell, slight negative pressure is applied to enable the formation of the Gigaohm seal; the cell-attached configuration leaves the cell intact and allows the measurement of individual channels [*111*].

- *Whole-cell patch*

  It is obtained by applying negative pressure after reaching the cell-attached configuration. The cell plasma membrane inside the tip of the microelectrode breaks, the solution inside the micropipette becomes continuous with the cell cytoplasm. This configuration is generally the most used and allows the study of the response of all the ion channels on the cell membrane [*111*]. Components in the cytoplasm can diffuse into the micropipette, causing significant ion channel function effects during measurement.

  In the whole-cell patch-clamp, two recording methods can be considered depending on the amplifier configuration: the voltage clamp or the current clamp. In the first case, potential pulses are applied, and the ionic membrane current is measured, while in the second one, the alterations in the membrane potential are studied after the variations in the injected current. Potential pulses of variable duration and different amplitudes are used to separate particular ion currents [*115*].

- *Inside-out patch*

  After reaching the cell-attached configuration, quickly retracting the microelectrode, the part of the membrane in contact with the tip can rupture: a small vesicle is formed, which remains attached to the tip of the micropipette. The air exposure destroys the vesicle. This lets a portion of the membrane intact on the tip, and in particular, the membrane layer inside the cell remains in contact with the solution present in the bath, while the outer part is exposed to the internal solution of the microelectrode [*111*].

  This configuration is useful for conducting studies on a single ionic channel function and verifying cytosolic factor effects on a channel [*116*].

- *Outside-out patch*

  It is possible to reach the outside-out configuration by slowly retracting the microelectrode tip from the whole-cell configuration. A part of the cell membrane is detached and closed on itself due to the phospholipid properties. The outer layer of the membrane remains in contact with the bath's external solution and the inner part in contact with the solution inside the microelectrode [*116*].

  This type of configuration is useful for studying single ion channel functions in response to the application of extracellular compounds on the plasma membrane's outer layer [*111*].

- *Perforated patch*

  In the microelectrode solution, compounds such as the nystatin and gramicidin fungicides are added, determining the formation of ion channels on the plasma membrane after reaching the cell-attached configuration. Ions can pass through the channels., but not other molecules necessary for cell metabolism [*111*].

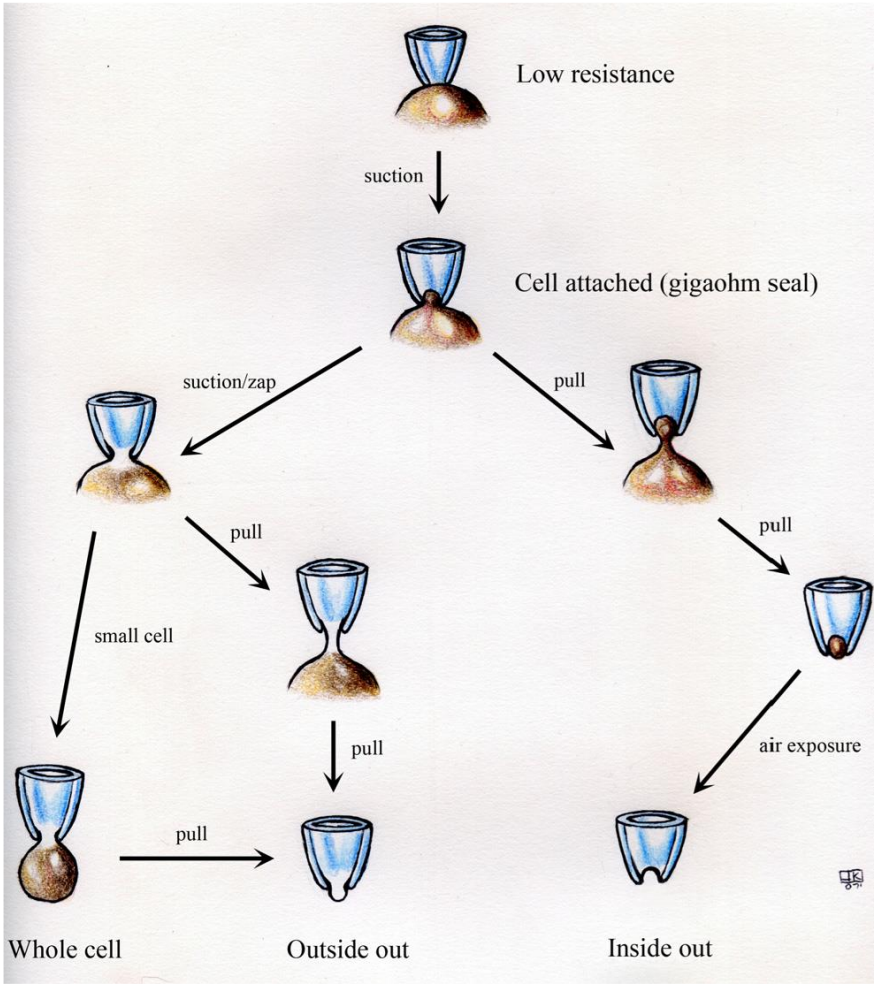

Figure 3.2: Representation of the various patch-clamp configurations. Copyright (2007) Wiley. Used with permission from Kornreich B.G. The patch clamp technique: principles and technical considerations. J Vet Cardiol, Elsevier [*111*].

3.2 Optical Microscopy

Microscopy is the use of a microscope for investigating details that cannot be observed by the naked eye.

Microscopes have been developed in the seventeenth century and are currently applied in several branches, as in scientific and clinical research and industry.

Three attributes are crucial: magnification, contrast, and resolution. Magnification is a fundamental requirement, resulting in an enlarged image from which the eye's sensory elements can collect more information than the smaller naked eye image [*117*]. Contrast is related to the capability to make the details visible to the human eye. Finally, the resolution, or resolving power, is the principal characteristic of a microscope, and it is classically referred to as the ability to distinguish two near objects as distinct objects [*118*].

In optical microscopy, the interaction between the specimen and a beam of electromagnetic waves (light) is the critical point; this interaction modifies the beam, bringing information about the sample, and is presented as an image.

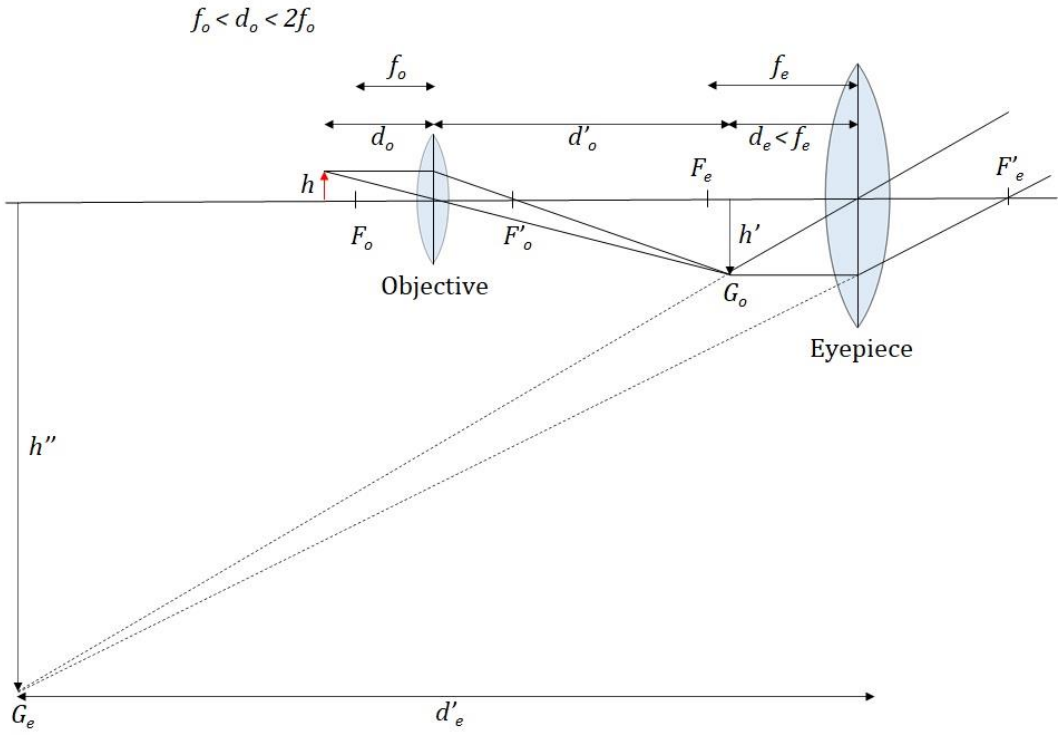

Figure 3.3: Schematic representation of a compound microscope.

Inadequate equipment or technique may affect the image quality, but the principal limitation of light microscopy is due to physics laws and the phenomenon of diffraction that occurs whenever a wave motion meets an object [*117*].

Ernst Abbe first elucidated the role of diffraction as the limiting factor in the performance of the microscope in 1873 [*119*] and found that the light, with a wavelength λ, traveling in a *medium* with refractive index *n* and converging to a spot with half-angle α, has a minimum resolvable distance of:

$$d = \frac{\lambda}{2n\,sin(\alpha)} \tag{3.2}$$

$nsin\alpha$ is also referred to as the numerical aperture of an objective lens (NA), a dimensionless number that specifies the ability to collect light and resolve fine specimen detail at a fixed object distance: a high NA objective can gather more light than one with a low numerical aperture.

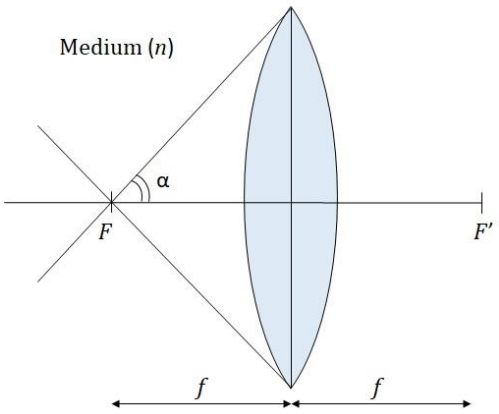

Figure 3.4: Numerical aperture of an objective lens in an optical microscope; α is the half-angle of the maximum light cone, *n* the refractive index of the *medium* between specimen and lens, *F* is the objective object focal point, F' is the objective image focal point, and *f* is the objective focal length.

Light microscopes can be classified: i.e., bright field, fluorescence, phase contrast, quantitative phase, and others [*120*].

More details about confocal and Two-Photon microscopy are given in the following paragraphs.

3.2.1 Fluorescence

Fluorescence is a methodology used widely in scientific disciplines. Its detection is highly sensitive, and fluorescence imaging can reveal the localization and measurements of intracellular molecules, sometimes at the single molecule's detection level.

It is a form of luminescence resulting from a three-stage process in particular molecules: when illuminated with a specific wavelength, some materials emit light with another wavelength; the Jablonski diagram well describes this phenomenon (Figure 3.5).

In the first stage (excitation), a molecule (fluorophore) absorbs a photon of energy $h\nu_{EX}$ supplied from an external light source, creating an excited electronic singlet state (S_2). During the excited state, the fluorophore is susceptible to conformational variations and is exposed to interactions with its molecular environment. The S_2 energy is partly dissipated, resulting in a relaxed singlet excited state S_1 (second stage). In an excited singlet state, the electron in the excited orbital is paired, by opposite spin, to the second electron in the ground-state orbital. Therefore, the electron can return rapidly to the ground state with the emission (third stage) of a photon of energy $h\nu_{EM}$.

The fluorescence emission rates are typically 10^8 s^{-1}; a typical fluorescence lifetime τ, the average time between a fluorophore excitation and return to the ground state, is near 10 ns [*121*].

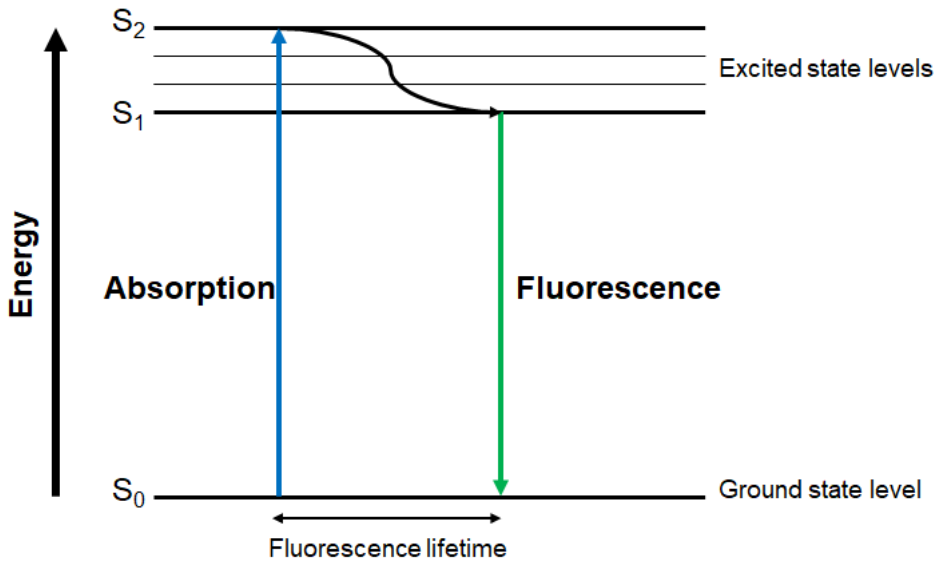

Figure 3.5: Simplified Jablonski energy diagram for fluorescence fundamentals. A molecule not absorbing energy is confined to a ground state level S_0; when a photon excites the molecule, the molecule absorbs energy and goes from S_0 to S_2 excited state level. Finally, the excited molecule relaxes to S_1 and returns to the S_0 ground state level, re-emitting a photon with fluorescence light.

The emission energy is generally less than the one of absorption; in fact, fluorescence takes place at longer wavelengths or lower energies. This shift, known as Stokes shift from Sir G. G. Stokes, who first observed the phenomenon, is caused by the rapid decay to the lowest S_1 vibrational level [*121*].

According to Kasha's rule and the Valivov rule, a general fluorescence property is that the same fluorescence emission spectrum is usually observed independent of the excitation wavelength. The photon emission is expected in significant yield only from the lowest excited state S_1.

The relaxation to the lowest vibrational level occurs in about 10^{-12} s; because of this fast relaxation, the emission spectra are typically independent of the excitation wavelength.

Exceptions are molecules, which exhibit two ionization states, each presenting distinct absorption and emission spectra. Moreover, some fluorophores emit from the S_2 level, but this emission is uncommon and mostly not observed in biology [*121*].

Fluorescence is applied to study various scientific issues; it can supply information on a wide range of molecular processes, conformational variations, and binding interactions, especially thanks to fluorescence microscopy, which is widespread as a useful tool in various scientific and technological fields.

3.2.2 Confocal Microscopy

The principle of confocal microscopy was studied by Marvin Minsky and aimed to overcome some limitations of fluorescence (widefield) microscopes.

In a traditional fluorescence microscope, a beam of light, provided by a xenon or mercury bulb, is filtered by an excitation filter; a dichroic mirror directs the light to the whole specimen, which is illuminated (widefield). The emitted fluorescence light from the sample crosses an emission filter, and a camera detects it.

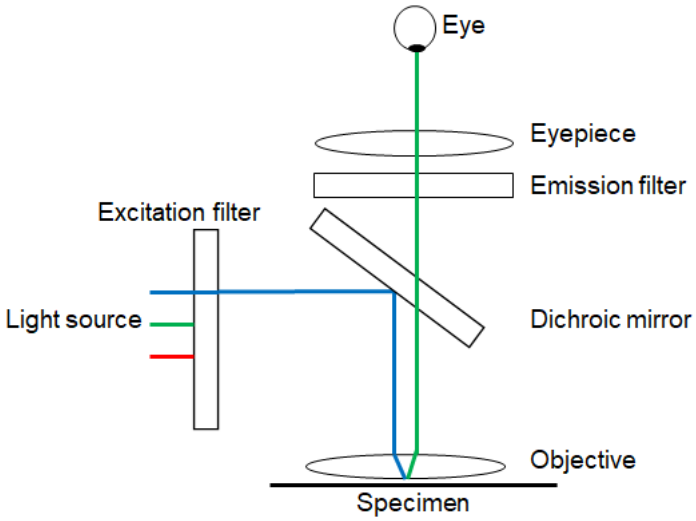

Figure 3.6 Scheme of a fluorescence microscope.

The fluorescence concepts also apply to confocal microscopy; the significant differences are the excitation source (a bright point source such as a laser), a sequential scanning method of the illumination point source, and the detector of the emitted light is a photomultiplier tube (PMT).

The light out of focus is rejected thanks to a pinhole aperture: the light that reaches the detector comes only from the "confocal point" in the specimen where the excitation light is focused.

The image is created pixel by pixel by scanning the confocal excitation and detection point across the specimen and recording the fluorescence at each point. The laser and pinhole remain stationary; a pair of oscillating orthogonal mirrors optically direct the laser light across the sample [*122*].

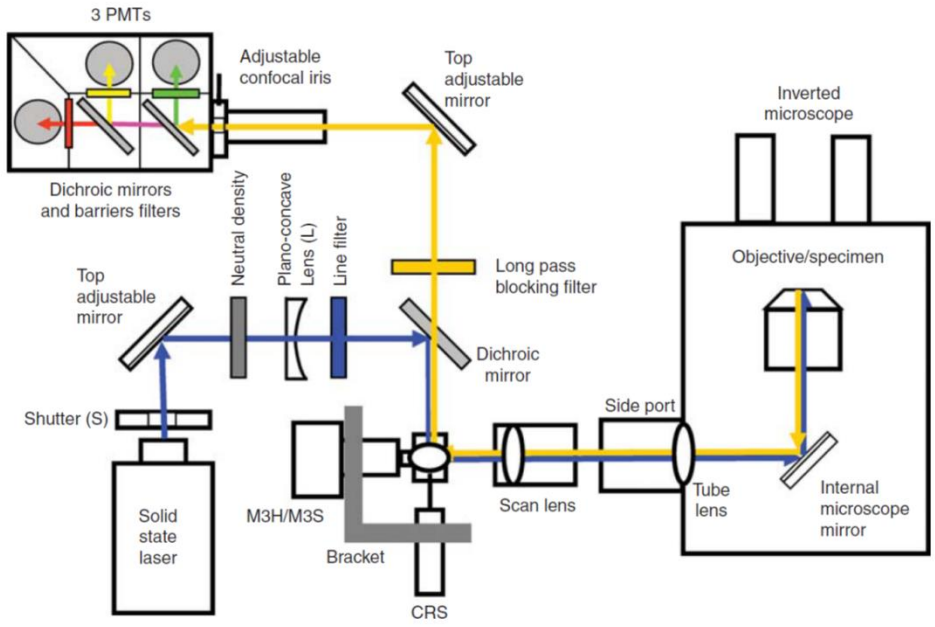

Figure 3.7: Laser scanning confocal microscope (LSCM) fundamental elements. The laser light reaches the specimen by a dichroic mirror and scan mirrors; the laser is scanned across the sample, the emitted fluorescence light is descanned by the scan mirrors, and transmitted by the dichroic mirror. It passes across an emission filter; it is focused onto the pinhole (adjustable confocal iris) and arrives at the photomultipliers. Extra dichroic mirrors are added to separate fluorescence wavelengths. Copyright © 2014 Cold Spring Harbor Laboratory Press. Used with permission from Sanderson M. J., Smith I., Parker I., Bootman M. D. (2014). Fluorescence microscopy. Cold Spring Harb Protoc, 2014 (10): pdb.top071795. doi: 10.1101/pdb.top071795 [*122*].

The image formation is produced using the image of a point, the point spread function (PSF), and determined the level of detail observed [*123*]. The PSF depends on the wavelength and the numerical aperture of an objective; it is a measure of the resolving power: narrow PSF, better in the resolution, even if aberrations of the optical setup may distort the PSF.

Ideally, the PSF is the 3D diffraction pattern of light emitted from an infinitely point source object and transmitted to the image plane through a high NA. The emitted light is collected by the objective and focused on a corresponding point image plane. At the focal point, the light waves converge and interfere and produce a diffraction pattern of concentric rings of light surrounding a central bright disk; the NA determines the radius of this disk (Airy disk), and the resolution power depends on its measure size.

$$r_{Airy} = 0.61 \frac{\lambda_0}{NA} \tag{3.3}$$

The Rayleigh criterion declares that it is only possible to resolve a pair of sources if the two diffraction patterns' central peaks are no closer than the radius of the Airy disk.

3.2.3 Two-Photon Microscopy

The confocal microscope improves spatial resolution by forming the image through a pinhole in front of the detector, which allows avoiding the emission light out of focus [*86*]. However, LSCM has a limitation in-depth penetration into tissues due to the use of short wavelength light produced by scattering and absorption [*122*]. Two-photon microscopy overcomes this limitation by employing longer wavelengths, which are not only less scattered by the specimen but may also not excite background autofluorescence [*124*].

Two-photon excitation (2PE) is a non-linear process made possible by the simultaneous absorption of two photons; the total energy must be sufficient to reach a transition to an excited electronic state [*124*].

This phenomenon occurs with very high photon density and is achieved when the laser, with a pulse duration (τ_p) of about 100 fs at a repetition rate (f_p) of about 80 MHz [*86*], is focused on a diffraction-limited spot centered on the focal plane of the objective [*122*].

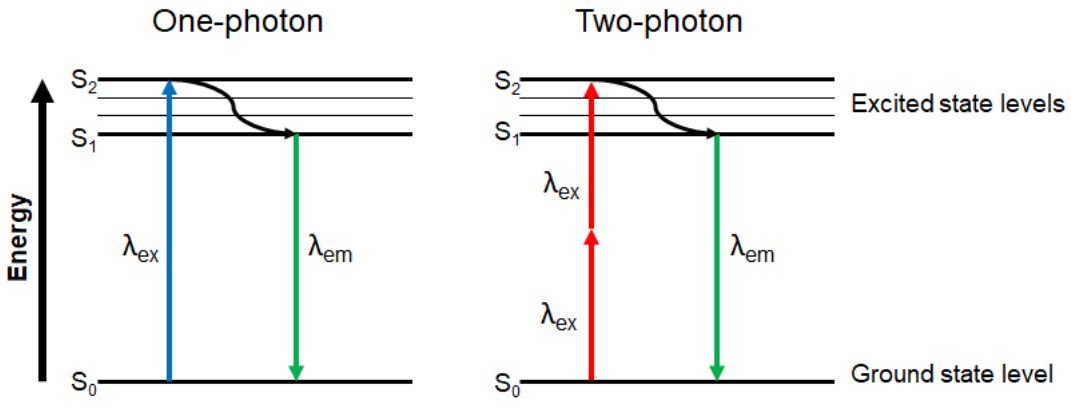

Figure 3.8: Simplified Jablonski diagrams for one- (left) and two-photon (right) fluorescence.

The number of photons (n_a) absorbed per fluorophore pulse is:

$$n_a \approx \frac{p_0^2 \delta}{\tau_p f_p^2} \left(\frac{NA^2}{2\hbar c \lambda} \right)^2 \tag{3.4}$$

Where p_0 is the laser power, δ the two-photon cross-section, τ_p the pulse duration, f_p the pulse repetition rate, NA the numerical aperture, $\hbar$ the Planck quantum of action, c the speed of light and λ the wavelength [*86*]. Hence, the photon density increases as a quadratic function approaching the focal point, the fluorescence is strictly stimulated in this zone, and, for this reason, a pinhole is not necessary as in LSCM [*122*].

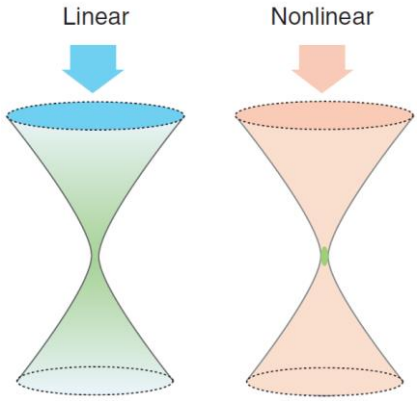

Figure 3.9: Excitation volume of one- (left) and two-photon (right) process. When the blue light is used for exciting a sample during the one-photon regime, a double cone of green fluorescence is produced. In comparison, near-infrared light is used during 2PE, and non-linear signal production is localized to the proximity of the focal spot. Copyright (2005) Wiley. Used with permission from Helmchen F., Denk W. Deep tissue two-photon microscopy. Nat Methods, Springer Nature [*123*].

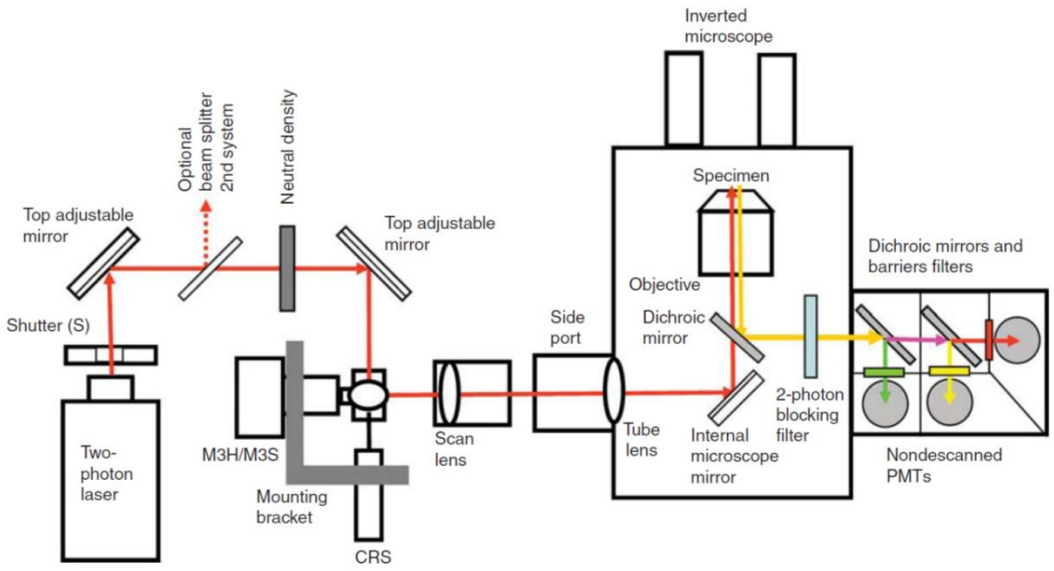

Figure 3.10: Two-Photon microscope fundamental elements. The detectors do not require pinholes or focused images and are located immediately below the objective. Copyright © 2014 Cold Spring Harbor Laboratory Press. Used with permission from Sanderson M. J., Smith I., Parker I., Bootman M. D. (2014). Fluorescence microscopy. Cold Spring Harb Protoc, 2014 (10): pdb.top071795. doi: 10.1101/pdb.top071795 [*122*].

Multiphoton absorption, compared to LSCM, offers some advantages for commonly fluorescent probes, the main of which are more penetration into thick tissues and generally less phototoxicity due to the use of near-infrared wavelength range (700-1000 nm) with visible spectral range emission. Also, it allows highly localized photo-manipulations, i.e., photobleaching and photolytic release of caged compounds, within femtoliter volumes [*123*].

Moreover, the capability to reject out of focus signal gives a resolution increase of about $\sqrt{2}$ compared to the diffraction-limited spot of excitation light. It is not a real genuine superresolution; in fact, the double wavelength causes an increase of diffraction spot size of a factor of 2 compared to the single-photon process [*125*].

Chapter 4: Materials and methods

4.1 Cell cultures

The cell cultures allow the growth of cells *in vitro* from tissues and biological fluids. In suitable supports such as plates, flasks, and bottles, the cells are kept alive thanks to *medium*, serums, and metabolites necessary for their growth.

They have different advantages: they are simplified and reproducible systems that enable several studies in different fields (i.e., cellular, molecular biology, pharmacology and toxicology, genetics, oncology) with lower costs than animal experimentation and controlled chemical, physical, and physiological conditions. On the other hand, they do not allow reproducing the complexity of the organism *in toto*. It is difficult to correlate the concentrations *in vitro* with those *in vivo*, the substances used can interact with the culture *medium*, and the exposure conditions to the various metabolites differ from the *in vivo* system [*126*].

Cell cultures involve the use of a series of actions aimed to maintain sterility, avoiding contamination with microorganisms (more typically bacteria, viruses, fungi, and mycoplasmas): stoves, UV rays, and autoclaves are used for sterilizing the laboratory material, and laminar biological safety cabinet for avoiding contamination during the cell manipulations.

Cell cultures can be adherent, as monolayer cells, or in suspension. They may have a finite life (limited expansion over time), continuous (indefinite replication), clonal (derived by mitosis from a single cell). The growing trend of a cell culture follows three phases characterized by the adaptation of the cell culture (primary culture), cell growth (expansions that allow originating subcultures), and senescence (decay), or development of a new cell line.

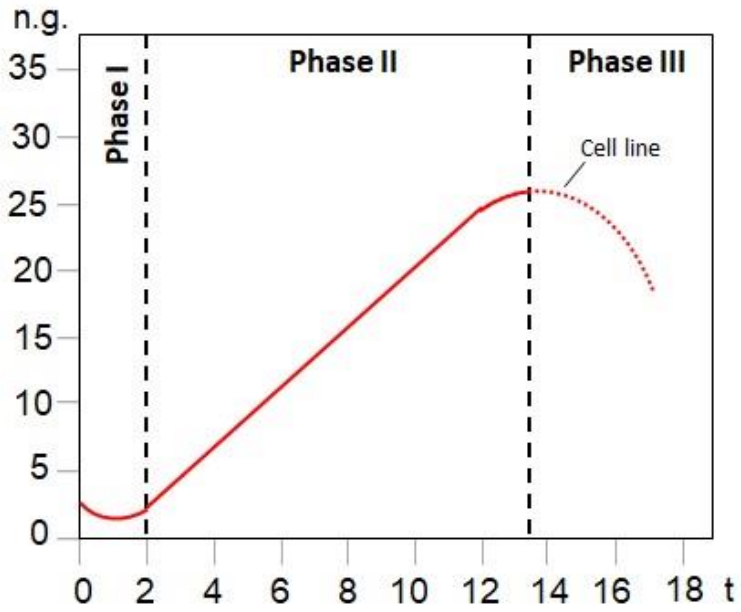

Figure 4.1: Trend of a cell culture *vs.* time; phase I represents a primary culture; phase II, in which it is possible to obtain subcultures, indicates the cell growth, phase III is the decay or development of a cell line.
On Y-axis, n.g. is the number of generations (n.g.), and on X-axis, the time is expressed in weeks (t).

The cell culture growth *medium* must ensure the supply of all the necessary substances and survival stability through the control of temperature, pH, and osmolarity. For this reason, it is crucial to choose a suitable culture *medium*, possibly enriched with serum, glutamine, and antibiotics. CO_2 incubators maintain the correct temperature and CO_2 concentration for guaranteeing the cell pH control.

The *medium* is necessary to reproduce an environment as similar as possible to that *in vivo*: they contain inorganic salts, energy molecules such as glucose, essential and non-essential amino acids for protein synthesis, vitamins, water, and trace elements.

Some *medium* compounds maintain an optimum of pH: sodium bicarbonate ($NaHCO_3$) is very used for its economical and not very toxic behavior, or HEPES (4-(2-Hydroxyethyl)piperazine-1-ethanesulfonic acid), a non-toxic synthetic molecule. Also, a compound, phenol red, is added, which allows a visual pH control. Depending on the pH value, phenol red changes color: at physiological pH, the *medium* appears red-orange; it turns yellow at low pH and red-violet for high pH.

It is usually added 5-20% of serum (bovine, equine, human) to the culture *medium* that contains growth (EGF, FGF, PDGF) and adhesion factors, hormones, and lipids [*127*]. Fetal bovine serum (FBS) and newborn bovine serum (NCS) are the most used. However, they can be a source of contamination, so they are tested to check for the absence of mycoplasmas and common bovine viruses.

The addition of antibiotics (i.e., penicillin-streptomycin and gentamicin) is common to avoid bacterial contamination, but they led to an increase in the selection of antibiotic-resistant bacterial strains; it becomes a good practice to use antibiotics for primary cell cultures or for "precious", rare cell cultures.

4.1.1 Cerebellar granule cell primary cultures

In the initial phase, it is necessary to sterilize the laboratory material, prepare the culture *medium*, and the solutions for the cerebellar granule cell isolation. After that, it is possible to remove the cerebella.

Sterilize in an oven for 30-60 minutes at 180 °C 1-2 trypsinization flasks, cylinders, beakers, tweezers, scissors, and in an autoclave at about 2 atm for 30 minutes Milli-Q water, tips for P1000 and P200, Pasteur pipettes with and without filter, 1.5 ml Eppendorf.

Prepare the culture *medium*: 90% BME (Basal Medium of Eagle) culture *medium*, 10% FCS, 100 μg/ml of glutamine, 100 μg/ml of antibiotics (gentamicin), and 25 mM KCl. The KCl must be filtered with a 0.2 μm Millipore filter after dissolving it with a small part of the *medium*.

The table below shows an example of the compounds' composition and quantity used to prepare the cerebellar granule cell *medium*.

Compounds	100 ml
BME	90 ml
FCS	10 ml
Glutamine	1 ml
Gentamicin	1 ml
KCl 25 mM	0.13 g

Table 4.1: *Medium* components for cerebellar granules and relative quantities on 100 ml.

During the cell preparation, it is necessary to use five solutions derived from 10x Krebs salts solution (basic solution). The composition is illustrated below.

Krebs Salt Solution 10x	500 ml	100 ml
NaCl	53.3 g	7.07 g
KCl	1.8 g	0.36 g
KH_2PO_4	0.83 g	0.166 g
Glucose	12.85 g	2.57 g
$NaHCO_3$	10.7 g	0.214 g
Phenol Red	0.072 g	0.015 g

Table 4.2: Krebs salts solution elements and relative quantities on 500 and 100 ml.

Sodium bicarbonate ($NaHCO_3$) is added on the day of cell preparation to prevent pH alterations, and the solution is brought to a volume of 100 ml with sterile Milli-Q water.

The 5 solutions used during cell preparation are listed below:

- Solution 1: 100 ml Krebs salt solution + 300 mg BSA (bovine serum albumine) + 800 µl di $MgSO_4$ (3.82% in Milli-Q water)
- Solution 2: 24 ml solution 1 + 1 ml trypsin (6.25 mg/ml)
- Solution 3: 13 ml solution 1 + 1 ml DNAse (1.2 mg/ml) + 1 ml trypsin inhibitor (7.8 mg/ml) + 150 µl $MgSO_4$ (3.82% in Milli-Q water).
- Solution 4: 21 ml solution 1 + 4 ml solution 3
- Solution 5: 12.5 ml soluzione 1 + 100 µl $MgSO_4$ (3.82% in Milli-Q water) + 15 µl $CaCl_2$ (1.2% in in Milli-Q water)

All solutions are filtered with a sterile 0.2 µm Millipore filter: 10 ml of solution 1 in a 50 ml Falcon, 10 ml of solution 2 in a 15 ml Falcon, 5.5 ml of solution 3 in a 50 ml Falcon, 10 ml of solution 4 in a 50 ml Falcon and 3 ml of solution 5 in a 15 ml Falcon.

The cerebella are obtained from 6-8 day Sprague-Dawley rats; the cerebella are removed, deposited in a Petri dish containing DPBS filtered with a 0.2 µm Millipore filter, and the meninges are eliminated with the fine tweezers (n.5 sa, DMR).

The cerebella are placed side by side on a plastic disc and cut with the Tissue Chopper (*The Mickle laboratory engineering CO.LTD*): a cut is made along the longitudinal axis, the disc is rotated 90° to allow its transversal cutting.

They are then transferred to the Falcon containing 10 ml of solution 1 with a Pasteur pipette with filter and centrifuged at 1000 rpm for 10-15 seconds.

The supernatant must be aspirated, and 10 ml of solution 2 containing trypsin, an enzyme that promotes tissue dissociation, is added to the sediment; the Falcon must be stirred with a rotating movement to resuspend all the cells, the contents are poured into a trypsinization flask which is incubated in a thermostated bath at 37 °C for 15 minutes with a stirring of 120-150 movements per minute.

10 ml of solution 4 are added to block the trypsin's action and, after stirring with rotary movements, centrifuge at 1000 rpm for 10-15 seconds.

The supernatant is aspirated, and a Pasteur of solution 3 is added. The pellet is resuspended at least 25 times with a pipette or in any case until the solution becomes homogeneous.

The solution is transferred to a 15 ml Falcon and left to settle for 10-15 minutes; the supernatant is mixed in solution 5, the sediment is again resuspended with a Pasteur of solution 3 and then transferred to solution 5.

It is left to settle for 10 minutes, with a Pasteur the supernatant containing the granules is brought into a 15 ml Falcon, it is decanted for 5 minutes, and if the solution is clear, the supernatant is centrifuged at 1500 rpm for 5 minutes.

The supernatant is aspirated, and 5-6 ml of the culture *medium* is added to the sediment to resuspend the cells.

In a 1.5 ml Eppendorf, 900 µl of culture *medium* and 100 µl of the cell suspension are combined to proceed with cell counting and then plating; 20 µl are taken from the Eppendorf and transferred to the Thoma chamber: the cells in the upper and lower chambers are counted under the microscope and, after averaging the two counts, 5 zeros are added to the final value to obtain the number of cells/ml.

1.5-2.5 · 10^6 cells/well are plated; to calculate the amount of cell suspension to add in each well, set the proportion based on the count.

Each Petri dish has previously been treated with 10 µg/ml poly-L-lysine: the polylysine is prepared in a concentrated solution (10x) containing 1 mg/10 ml Milli-Q water; the sterilized solution is kept at –20 °C.

Petri dishes must be left for 15-20 minutes under UV rays, then the polylysine is aspirated, and the plates are left to dry for 30 minutes, partially covering with the lids; for plating the cells on slides, the coverslips are first soaked in a solution with detergent, sonicated, dried and left in absolute alcohol for a few hours.

The slides are sterilized by passing them over a flame and putting in the Petri Dish before treating them with polylysine.

18 hours after plating, within 24 hours, 10 µM AraC (Cytosine Arabinoside) is added; it is an antimitotic prepared on the day of use. In essence, 1-2 mg AraC is weighed and diluted according to the proportion of 1.1 mg/1 ml to obtain a concentration of 4 mM. The solution is sterilized with a 0.2 µm Millipore filter, diluted with 1/10 medium to obtain a concentration of 400 µM, and added to the culture according to the proportion 50 µl/ 2 ml.

48 hours after plating, the culture *medium* is refreshed: the old culture *medium* is aspirated and replaced with a new one prepared on the day of collection.

AraC was added again in the way described above.

4.2 Solutions

4.2.1 External and internal solutions

The cells are kept in an external solution; the microelectrode is filled with an internal solution that mimics the intracellular liquid composition.

The composition of the solutions is shown in the following tables:

Standard External Solution	Molecular Weight	mM	g/l
NaCl	58.44	135	7.8894
KCl	74.55	5.4	0.4026
$CaCl_2$	147	1.8	0.2646
$MgCl_2$	203.3	1	0.2033
Hepes	238.3	5	1.1915
Glucose	180.2	10	1.802

Table 4.3: Standard external solution composition

The external solution is brought to pH 7.4 with 2 M NaOH.

Internal Solution	Molecular Weight	mM	g/100 ml
KCl	74.55	142	1.0586
$MgCl_2$	203.3	2	0.0406
Hepes	238.35	10	0.2383
EGTA	380.35	2	0.0760
ATP	551.1	3	0.1653

Table 4.4: Internal solution composition

The internal solution is brought to pH 7.3 with 1 M and 0.1 M Tris base. It is kept at -20 °C in aliquots of 5-6 ml; on the day of use, it is thawed and kept in ice to avoid hydrolysis of the ATP, which could compromise the success of the experiments.

4.2.2 Solutions employed during the experiments

The solutions used during the measurements are: 10 μM RuBi-GABA, 1 μM Antisecretory Factor, 10 μM RuBi-GABA + 1 μM Antisecretory Factor, 10 μM RuBi-GABA + 1 mM Furosemide, and 10 μM RuBi-GABA + 1 mM Furosemide + 1 μM Antisecretory Factor.

- *10 μM RuBi-GABA*
  A 10 mM RuBi-GABA solution (stock solution) is prepared by dissolving 0.01 g RuBi-GABA in 1.08 ml of sterile Milli-Q water. 50 μl are taken from this stock solution and brought to a volume of 50 ml with the external solution to reach the concentration of 10 μM RuBi-GABA.

- *1 μM Antisecretory Factor (AF-16)*
  A 100 μM AF-16 stock solution is prepared by dissolving 0.003 g Antisecretory Factor in 17 ml of the external solution; 500 μl are taken from this stock solution and brought to a volume of 50 ml with the external solution to reach the concentration of 1 μM.

- *Solution with 10 μM RuBi-GABA and 1 μM Antisecretory Factor (AF-16)*
  50 μl of 10 mM RuBi-GABA stock solution and 500 μl of 100 μM AF-16 were diluted in 50 ml of the external solution to obtain the concentration of 10 μM RuBi-GABA and 1 μM AF-16.

- *Solution with 10 μM RuBi-GABA and 1 mM Furosemide*
  A 10 mM Furosemide stock solution is prepared by dissolving 0.1654 g Furosemide in 50 ml of the external solution; 5 ml are taken from this stock solution and added with 50 μl of 10 mM RuBi-GABA stock solution. The solution was brought to a

volume of 50 ml with the external solution to obtain 1 mM Furosemide and 10 μM RuBi-GABA concentrations.

- *Solution with 10 μM RuBi-GABA, 1 mM Furosemide and 1 μM Antisecretory Factor (AF-16)*

  5 ml are taken from the 10 mM Furosemide stock solution and added with 50 μl of 10 mM RuBi-GABA stock solution and 500 μl of 100 μM AF-16. The solution was brought to a volume of 50 ml with the external solution to obtain 1 mM Furosemide, 10 μM RuBi-GABA, and 1 μM AF-16 concentrations.

4.3 Preparation of the micropipettes

Essential for the success of the experiments is the possibility of using micropipettes capable of originating a Gigaohm seal; borosilicate glass capillaries are used for this purpose, which not only allow the achievement of a high-strength seal with the cell membrane but also cause little background noise during recording.

The capillaries are washed in acetone, rinsed with deionized or milli-Q water, dried in an oven at 80 °C on aluminum foil to eliminate any impurities that can interfere with the formation of the seal; subsequently, they are subjected to a series of phases which foresee the heating and the draft by a vertical puller (*P-30 model, Sutter Instruments Co*) for the realization of micropipettes.

The capillary is heated and pulled to reach a diameter of 200 μm; after being repositioned, it is heated again, withdrawn, and separated in the two microelectrodes. The parameters that define the draft and the two heating phases are fixed to obtain many similar microelectrodes; small variations can give rise to peaks that differ by a few μm [*114*].

4.4 Experimental apparatus

The patch-clamp instrumentation is placed on an anti-vibration table, with compressed air shock absorbers, to prevent any mechanical vibrations that could avoid the seal formation.

The setup used for the experiments consists of an inverted three-channel laser scanning confocal microscope (*Leica TCS SP5, Leica Microsystems, Germany*) equipped with 458-, 476-, 488-, 514-, 543-, and 633-nm excitation lasers and a plan-apochromatic oil immersion objective × 63/1.4.

LAS AF (*Leica Microsystems, Germany*) was the software used for acquiring the images before and after the uncaging confirming the absence of relevant cell displacements, using a 633 nm laser source coupled to a photomultiplier tube.

The two-photon excitation and uncaging were performed with a Ti: Sapphire laser (*Chameleon II, Coherent Inc., Santa Clara, CA, USA*). This laser operates with pulses of 100 fs at the repetition frequency of 80 MHz.

The laser power was measured at the objective focal point by a PM100A power meter (*Thorlabs Inc., Newton, NJ, USA*), and the laser stability was checked after considering a balance between pulse width and power performances, suggesting the utilization of 750 nm.

FRAP Wizard Leica was used to set up the bleach point in terms of coordinates, laser power, and exposure time during the uncaging experiments.

On the microscope stage is placed a chamber for the samples connected to a system of free fall perfusions by a manipulator (*MP-225, Sutter Instrument, Novato, CA, USA*) used for approaching the tip of the micropipette to the cell, and an electrode holder formed by a Teflon body and an opening for positioning the chlorinated silver electrode; on it, thanks to a screwed plastic cap, the glass microelectrode, containing the internal solution, is inserted, and a silicone tube is connected for applying negative pressure during the seal formation.

An amplifier (*Axopatch 200B, Axon Instruments, USA*) allows the reading of the current values, the filtering of the background noise, and other operations such as the compensation of the electrode resistance, the cell capacity, and the series resistance; this amplifier consists of two units, a pre-amplifier, and a controller.

An analog-to-digital converter enables the amplifier signal to be recorded on the computer.

The computer and software are used to monitor the experiment, store the data, and analyze them.

The software considers the conversions applied and displays an appropriate scale for the recorded current represented by a trace on the monitor.

The acquisition and analysis of the currents were carried out using the pClamp software (*Axon Instruments, USA*), particularly version 10 of Clampex and Clampfit.

4.5 Electrophysiological measurements

The electrophysiological measurements were performed on rat cerebellar granule cells in culture to verify the modulation of the currents activated by the uncaging of RuBi-GABA using the patch-clamp technique in whole-cell configuration. A protocol was followed that took into account the currents activated by the passage of chloride ions through the $GABA_A$ channel receptor.

The slide with the samples was placed in the bath chamber with an external solution; the glass microelectrode was brought closer to the neuron's cell membrane for the recording using macro and micromanipulators and, creating negative pressure, a seal was formed to achieve the cell-attached configuration.

The amplifier was set to the voltage-clamp configuration; a suitable potential was fit for the current measurements activated by the GABA (typically -80 mV), and the plasma membrane was then broken with a slight suction to reach the whole-cell configuration.

The washing solution (external solution), the caged compound solutions, and the pharmacological molecules flow thanks to the perfusion system.

Before carrying out the measurements, it was checked that the compound did not determine a $GABA_A$ receptor response before the uncaging.

The typical experiment consists of measuring the 10 μM uncaged RuBi-GABA activated current on the same cell in different experimental conditions. The current activated by uncaged RuBi-GABA alone is compared with that activated by uncaged RuBi-GABA with the pharmacological compounds.

The various measurements are interspersed by washing the cell with the external standard solution to eliminate any compound in the bath and avoid the receptor desensitization phenomenon.

Chapter 5: Results

Initially, it was checked that photolyzed RuBi-GABA determined the activation of $GABA_A$ receptors. When 10 μM RuBi-GABA is uncaged, a maximum current value (peak) is recorded, reflecting a population of $GABA_A$ ionotropic receptors associated with Cl^- channels. After the photoexcitation, the measured current returns to the original value (Figure 5.1).

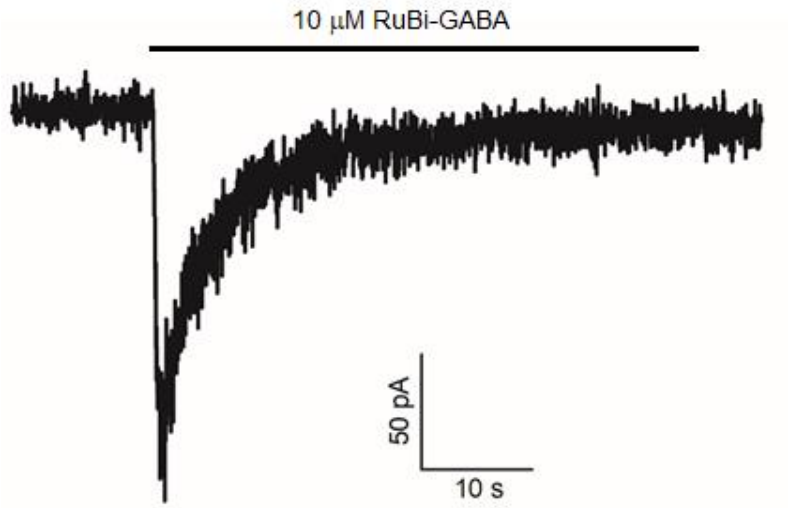

Figure 5.1: Current (pA) *versus* time (s). Current trace recorded at a holding potential V = -80 mV during the photoactivation of 10 μM RuBi-GABA with 1PE (458 nm, 100 ms, 6.7 μW).

Moreover, experiments were performed to verify that uncaged RuBi-GABA directly acted on $GABA_A$ receptors using the competitive antagonist bicuculline.
1 μM RuBi-GABA was photolyzed to activate $GABA_A$ receptors (Figure 5.2 left trace); after the administration of 20 μM bicuculline, which competes for the GABA site, no relevant current alterations were recorded even if 1 μM RuBi-GABA was uncaged (Figure 5.2 right trace).
These measurements confirm that $GABA_A$ receptors are the target of photoactivated RuBi-GABA.

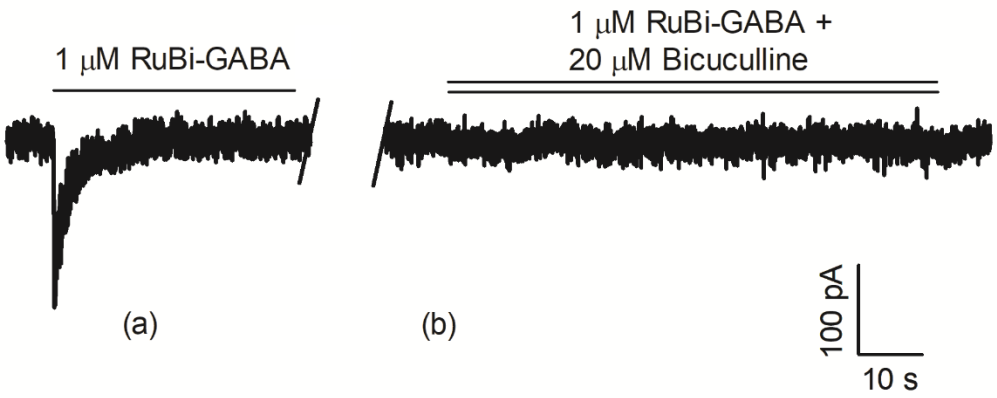

Figure 5.2: Current (pA) *versus* time (s). Current traces recorded on the same cell during the uncaging of 1 μM RuBi-GABA by 1PE (458 nm, 100 ms, 6.7 μW) at a holding potential V = -80 mV before (a) and after the administration of 20 μM bicuculline (b).

For characterizing the uncaging technique, critical parameters that could influence the electrophysiological measurements have been extensively explored and correlated in a temporally and spatially confined way: one and two-photon excitation (1PE and 2PE), laser power, exposure time, X-, Y-, Z- distance uncaging point from the target cell, different holding potentials.

For each parameter variation, it was decided to perform experiments on the same cell for avoiding alterations due to cell-to-cell differences [*11*].

5.1 1PE, 2PE, Laser Power

The excitation volumes of one and two-photon regimes are considerably different. During the one-photon process, the caged molecules are photolyzed along the entire laser optical path, and the amount of photo-released compound, conserved plane by plane following the distribution of the photon density, is proportional to the light absorbed in each plane.

The uncaging with 2PE is a process spatially localized due to the simultaneous absorption of two photons that results in a volumetrically confined event.

Therefore, experiments were performed to evaluate the effects of these distinct processes, changing the laser power for both 1PE and 2PE.

The current peaks, measured during both 1P and 2P uncaging after $GABA_A$ receptor activation, increase, spanning from low to high laser power, though the localized volume of 2P uncaging determines lower current peaks than the ones due to 1PE (Figure 5.3 A, B).

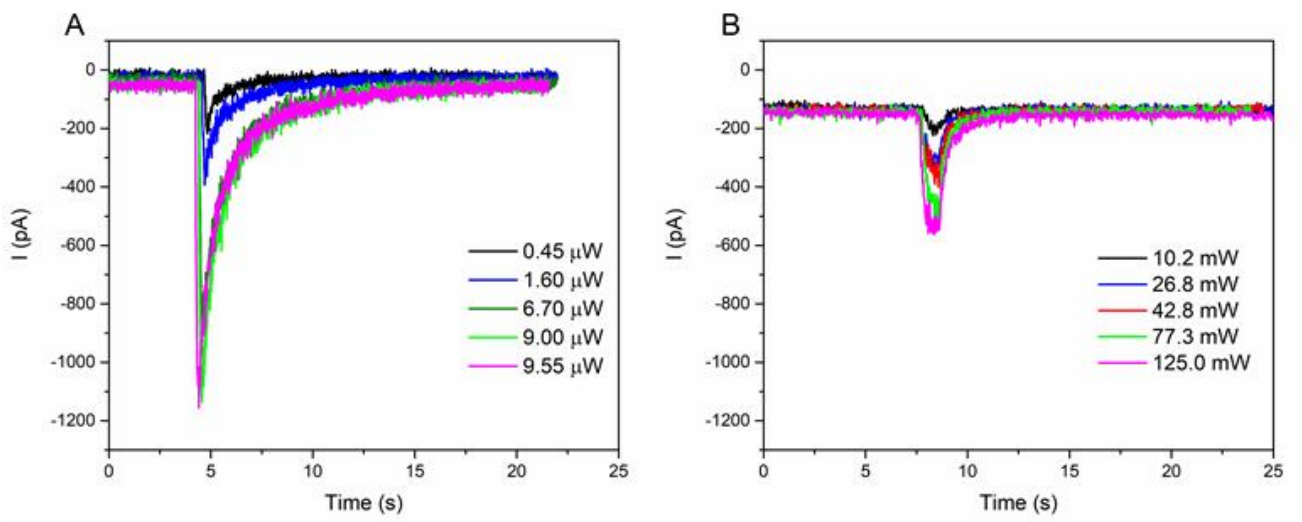

Figure 5.3: Current (pA) *versus* time (s). Typical traces of chloride current peaks evoked by 10 µM RuBi-GABA uncaged at V = -80 mV by using different laser power for 1PE (458 nm, 100 ms) (A) and 2PE (750 nm, 100 ms) (B) on the same cell.

When the laser power rises, the amount of uncaged GABA increases, resulting in an increase of the activated $GABA_A$ receptors until reaching a saturation because of the photoactivation of all molecules in the excitation volume.

The experiments were repeated by doubling the RuBi-GABA concentration to ensure it was not due to a receptor saturation effect.

Figure 5.4 A and B report the curves for 1PE and 2PE, respectively, of the normalized current peak values as a function of the laser power for 10 µM and 20 µM RuBi-GABA. The plateau is reached for the same relative laser power, and the curves show the same trend. Consequently, the peak current saturation is due to a limited number of uncaged molecules, not to the receptor saturation; otherwise, saturation should occur at a lower laser power [*11*].

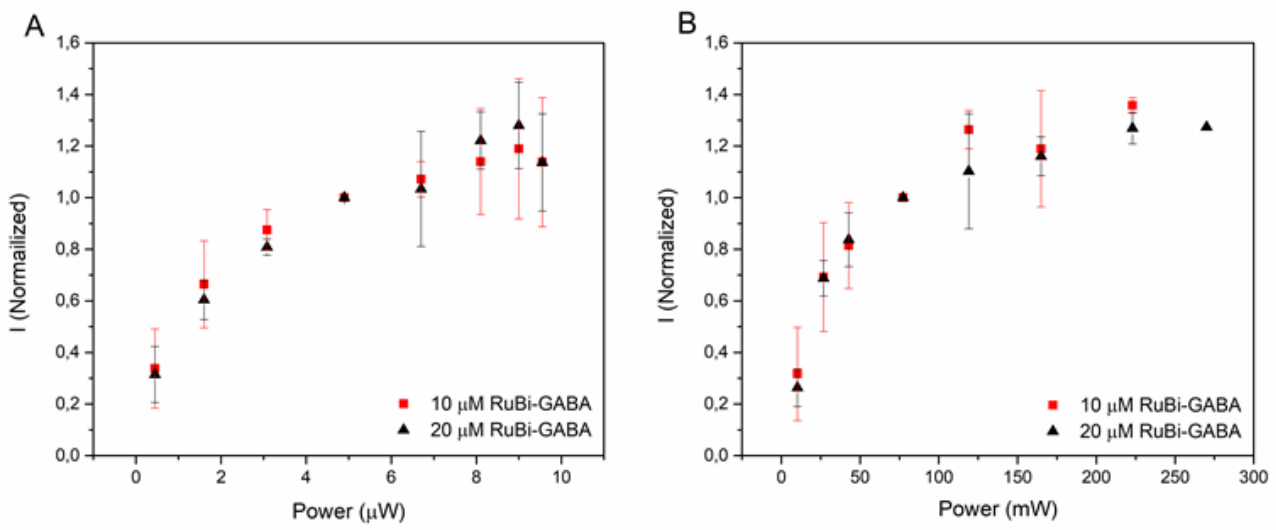

Figure 5.4: Current *versus* laser power. Current peaks (normalized values to the peak current value evoked using 4.9 µW for 1PE and 77.3 mW for 2PE) evoked by the uncaging of 10 µM (red squares) and 20 µM (black triangles) RuBi-GABA using different laser power for 1PE (458 nm, 100 ms) (A) and 2PE (750 nm, 100 ms) (B).

5.2 Exposure Time

During 1P or 2P processes, the photolyzed molecules spread out of the excitation volume and diffuse in the solution. An exposure time longer than this diffusion time involves a replacement by new caged molecules that come into the excitation volume, becoming photoactivated.

Therefore, a "cloud" of uncaged molecules shapes around the uncaging volume for long exposure time.

Figure 5.5 A and B show the experiments performed, at least on 4 cells per session, changing the exposure time.

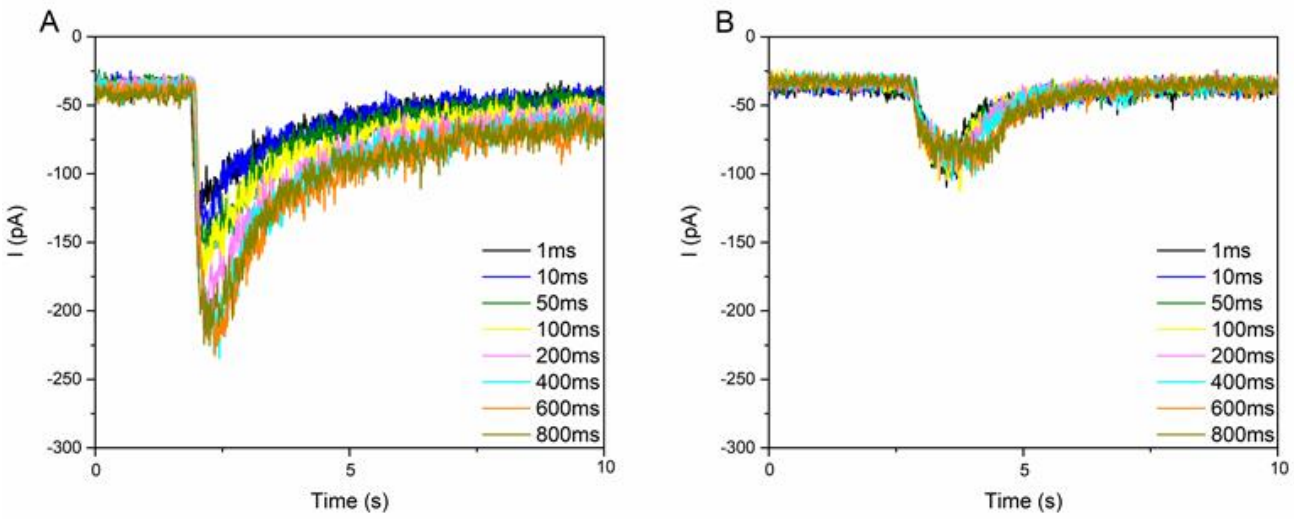

Figure 5.5: Current (pA) *versus* time (s). Typical traces of chloride current peaks evoked by 10 µM RuBi-GABA uncaged at V = -80 mV using different exposure time for 1PE (458 nm, 9.36 µW) (A) and 2PE (750 nm, 125 mW) (B) on the same cell.

The current peak intensity (Figure 5.5 A, Figure 5.6 A) and the time of decay (Figure 5.6 C) rise to a plateau value, raising the exposure time during 1PE. The full width at half maximum (FWHM) shows a linear trend (Figure 5.6 E).

On the other hand, the current peak intensity and the time of decay do not change during 2P uncaging (Figure 5.5 B, Figure 5.6 B, D), but the FWHM linearly increases while raising the exposure time (Figure 5.6 F) [*11*].

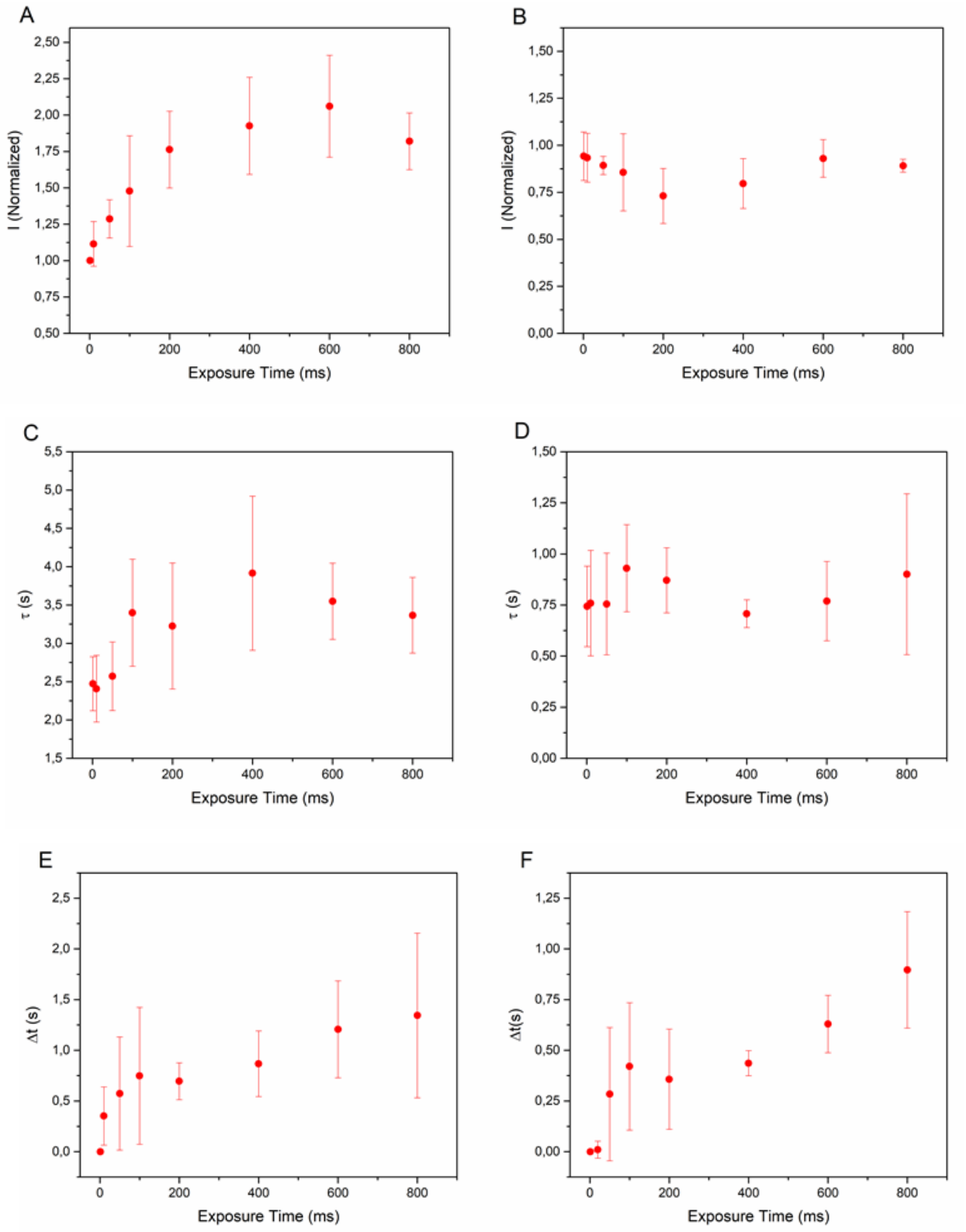

Figure 5.6: Chloride current peaks, normalized to the current measured for the lowest exposure time (1 ms), evoked by 10 µM RuBi-GABA uncaged at V = -80 mV using different exposure time during 1P uncaging (458 nm, 9.36 µW) (A) and 2PE (750 nm, 125 mW) (B) on the same cell. Time of decay (τ) *versus* the exposure time for 1PE (458 nm, 9.36 µW) (C) and 2PE (750

nm, 125 mW) (D). Full width at half maximum (FWHM) as a function of exposure time for 1PE (458 nm, 9.36 µW) (E) and 2PE (750 nm, 125 mW) (F). The data are collected on at least 4 cells, and each value is estimated by calculating the mean ± SEM.

5.3 X, Y, Z Distance from the target cell

Changing the distance of the uncaging point along the X-Y plane (Figure 5.7 A), the peak current intensities decrease both for 1PE and 2PE (Figure 5.7 B, C, D); in particular, when the uncaging occurs in the confined volume of 2PE (Figure 5.7 B, black circles), the current peaks exhibit a faster decrease compared to 1PE (Figure 5.7 B, red squares) as the distance in X-Y increases.

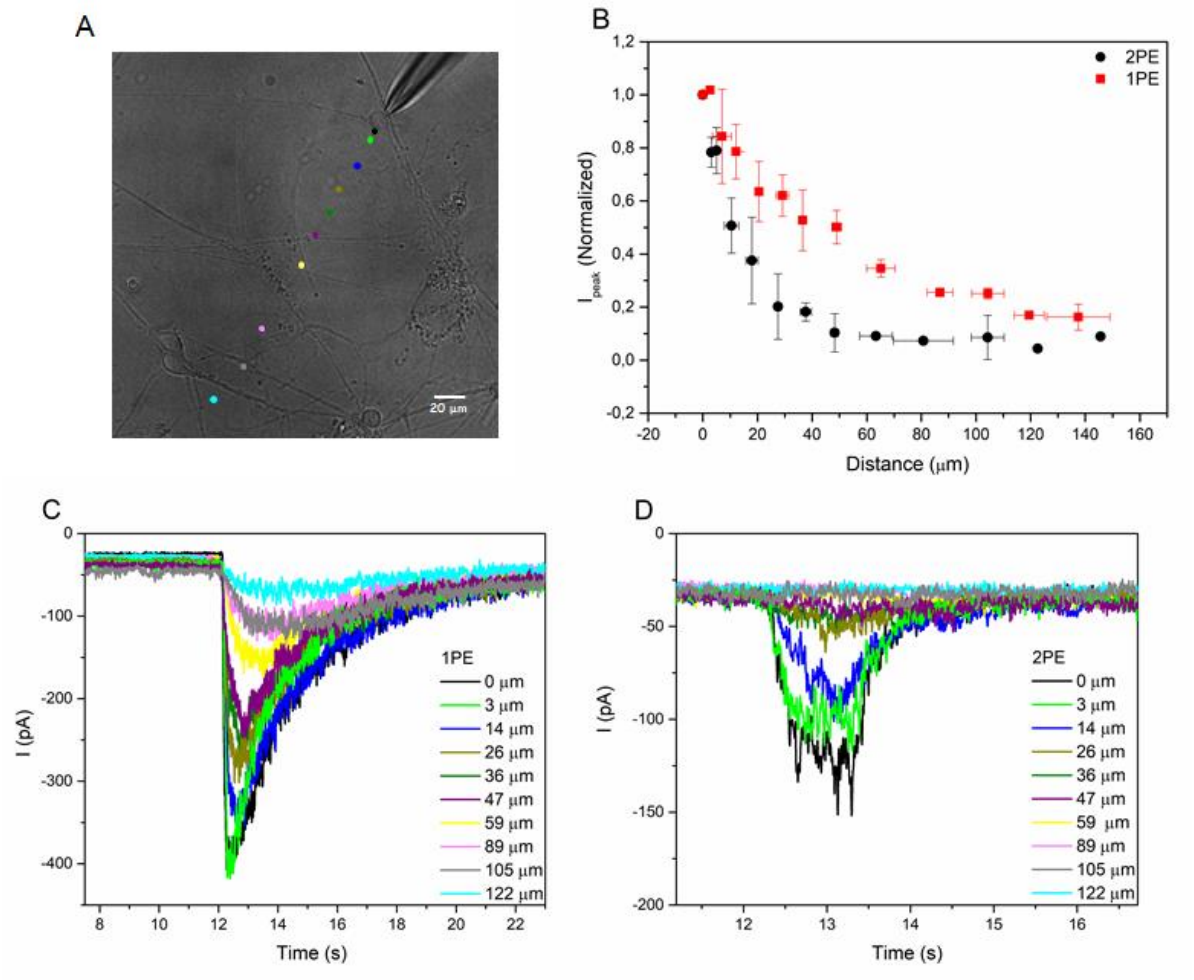

Figure 5.7: Uncaging points at different distances from the target along the X-Y plane (A). Current peak values, normalized to the distance 0 µm far from the cell, *versus* the distance after the uncaging of 10 µM RuBi–GABA at V = -80 mV with 1PE (458 nm, 100 ms, 9.36 µW-red squares) and 2PE (750 nm, 100 ms, 77.3 mW-black circles) (B). Current peaks recorded for the

uncaging points reported in (A) for 1PE (458 nm, 100 ms, 9.36 µW) (C) and 2PE (750 nm, 100 ms, 77.3 mW) (D).

The amount of photolyzed RuBi-GABA that binds the receptors may diverge because of the isotropic diffusion of uncaged molecules, and when the distance increases, the rise time grows (Figure 5.8).

If the diffusion dynamics of the uncaged molecules is approximated as the diffusion of an instantaneous point source, it is possible using the equation:

$$C(x,t) = \frac{A}{\sqrt{4\pi D \cdot t}} e^{\left(-\frac{x^2}{4Dt}\right)} \quad (5.1)$$

C is the concentration of the molecules, D the diffusion coefficient, x the distance from the point source, t the time, and A an arbitrary constant.

Therefore, the current rise time was fitted with equation 1 (Figure 5.8). At a temperature of 25 °C and viscosity of 1 mPa s, the diffusion coefficient analyzed for four distance values of four different cells, $(6 \pm 3)\ 10^{-10}\ m^2\ s^{-1}$, agrees with the theoretical one estimated for GABA [*11*].

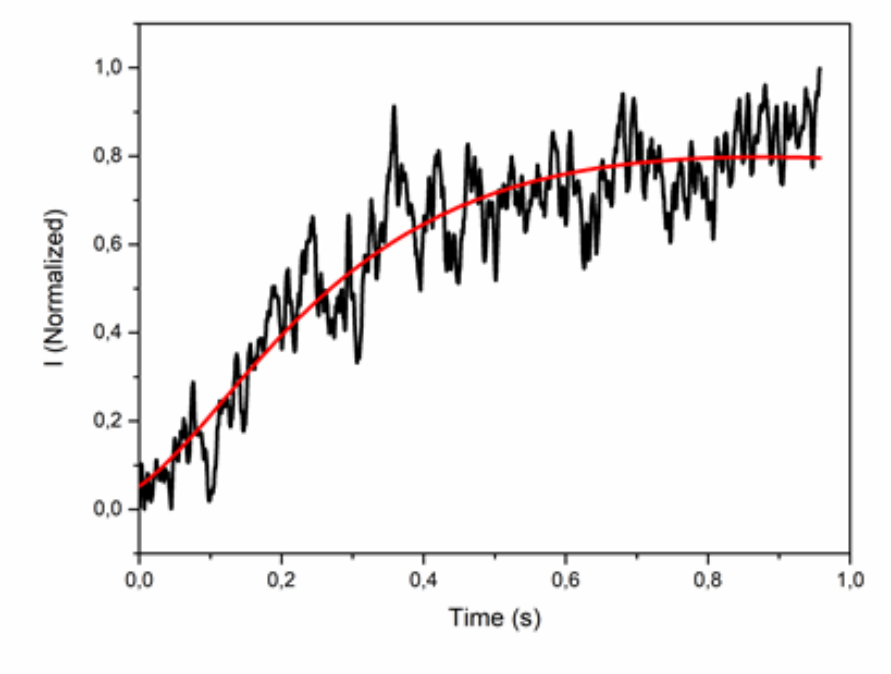

Figure 5.8: Rising current peak (black line) fitted (red line) with equation 1 *versus* the time (uncaging distance point of 50 µm with 1PE at 458 nm, 9.36 µW).

The current peaks recorded during 1PE (458 nm, 100 ms, 9.36 µW) and 2PE (750 nm, 100 ms, 77.3 mW) at different uncaging Z-distances (Figure 5.9) show a distinct behavior.

The measured current peak remains constant within a distance of about 10 µm, a distance comparable to a granule cell size, from the coverslip surface, then it linearly decreases during 2PE (Figure 5.9 black circles).

On the other hand, during 1PE, the current peak increases, and, after that, it remains constant (Figure 5.9 red squares) [*11*].

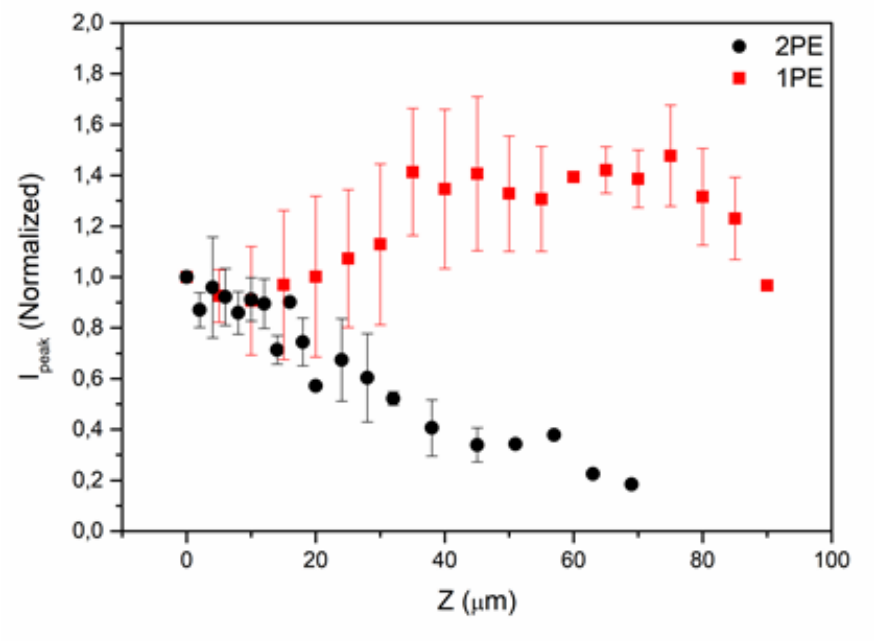

Figure 5.9: Current peak values, normalized to the distance Z=0 µm far from the coverslip surface, *versus* the Z-distance during the uncaging of 10 µM RuBi–GABA at V = -80 mV with 1PE (458 nm, 100 ms, 9.36 µW-red squares) and 2PE (750 nm, 100 ms, 77.3 mW-black circles).

5.4 Current-Voltage Curves

Experiments were performed at different holding potentials for evaluating possible different effects on current peak values using the neurotransmitter GABA and caged compound RuBi-GABA.

Figure 5.10 reports the current-voltage (I-V) curve recorded with 10 µM GABA and 10 µM RuBi-GABA, applying a voltage bias from -60 mV to +60 mV with steps of 20 mV.

10 µM GABA curve shows an ohmic trend, as previously described by *Robello et al. 1994* [*128*]; the I-V curve recorded after the uncaging of 10 µM RuBi-GABA (1PE, 458 nm, 9 µW, 100 ms) has an ohmic trend comparably to that of GABA [*11*].

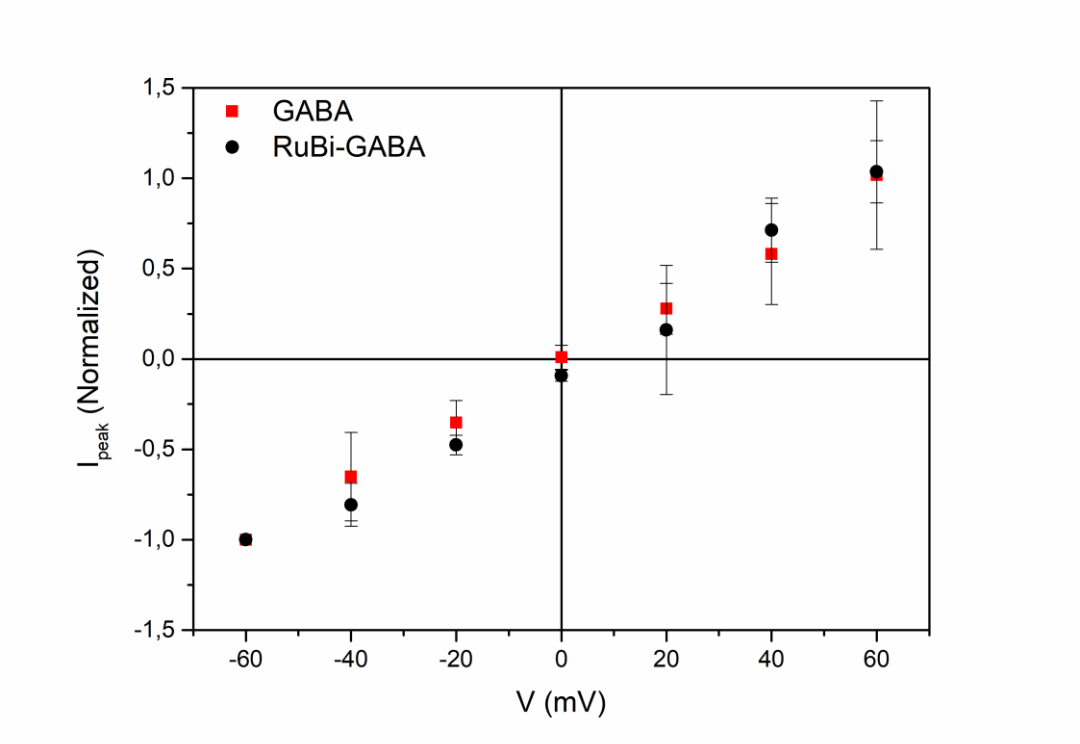

Figure 5.10: Current-voltage curves. The current peak values, normalized to the current peak recorded for -60 mV, are measured using 10 µM GABA (red squares) and after uncaging 10 µM RuBi-GABA with 1PE (458 nm, 100 ms, 9 µW-black circles).

5.5 RuBi-GABA dose-response

Different RuBi-GABA concentrations were tested: 1, 10, 20, 50, 100 µM. Hence, a dose-response graph was constructed, reporting the RuBi-GABA concentrations on the X-axis and the peak current on the Y-axis (Figure 5.11) [*11*].

The data were fitted in according to the Hill equation [*129*]:

$$I_p = I_{max} \frac{C^n}{C^n + K_a^n} \tag{5.2}$$

Where I_p is the dependent variable corresponding to the current peak values, I_{max} is the maximum current peak value, C is the concentration (independent variable), n the Hill coefficient, K_a a constant. The results were: K_a = 1.98 µM , I_{max} = 247 pA, and a Hill coefficient of 1.1.

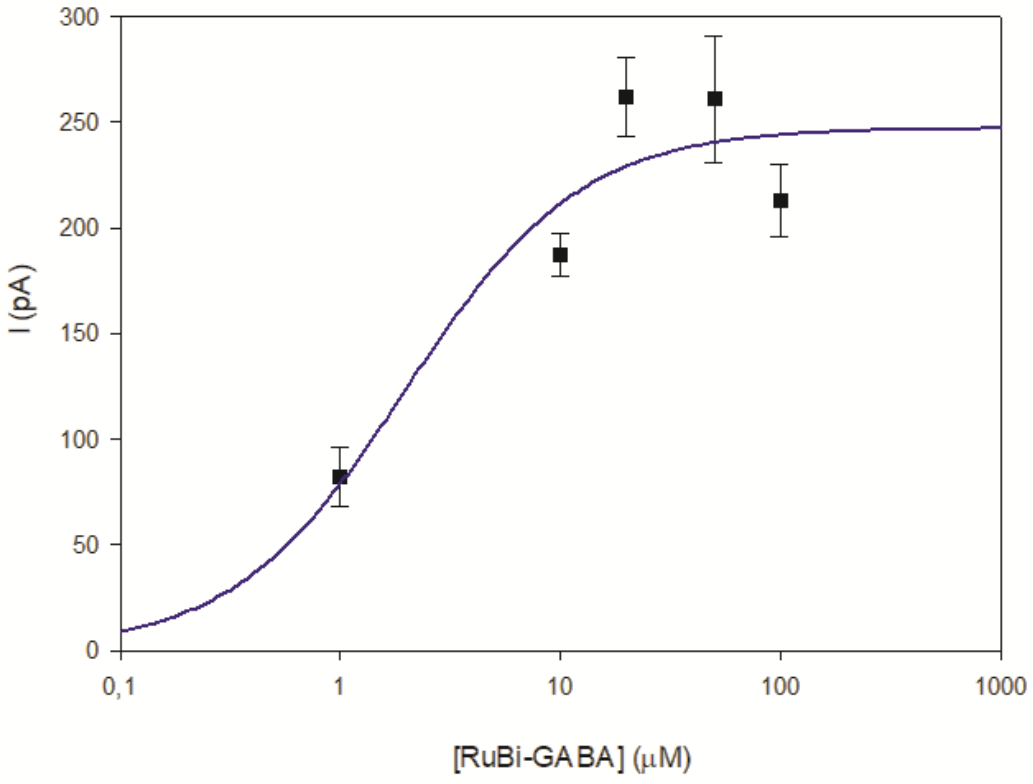

Figure 5.11: RuBi-GABA dose-response curve measured using 2PE (750 nm, 100 ms, 45 mW, -80 mV). Peak current (pA) *versus* RuBi-GABA concentrations (µM). The vertical bars represent the SEMs. The curve fit is calculated according to the Hill equation $I_p = I_{max} \cdot (C^n)/(C^n + K_a^n)$.

5.6 RuBi-GABA and pharmacological molecules

After the characterization of the main physical parameters that occur during the uncaging of the caged compound RuBi-GABA, it was decided to evaluate the effects of the pharmacological molecule Antisecretory Factor (AF-16) in well-defined areas of the neuron: soma, the growth cone, and neurites.

The results of the Antisecretory Factor effect on the modulation of the current activated by GABA on rat cerebellum granule cells were previously tested and reported in the paper *Bazzurro et al. 2018*: measurements of currents activated by 10 μM GABA after the pretreatment with Antisecretory Factor showed an increase in the current induced by GABA [*12*].

For these new sets of experiments with RuBi-GABA and Antisecretory Factor, 2PE was considered the most suitable uncaging parameter, precisely due to its characteristic that endures the photo-release of molecules in a confined volume. Hence, it allows the study of the Antisecretory Factor response on a limited number of $GABA_A$ receptors in a defined region and, consequently, how its action changes in a precise, specific, and limited neuron area.

Firstly, the current induced by the uncaging of 10 μM RuBi-GABA was checked. After the incubation for 3 minutes with Antisecretory Factor, RuBi-GABA was uncaged combined with AF-16 (Figure 5.12).

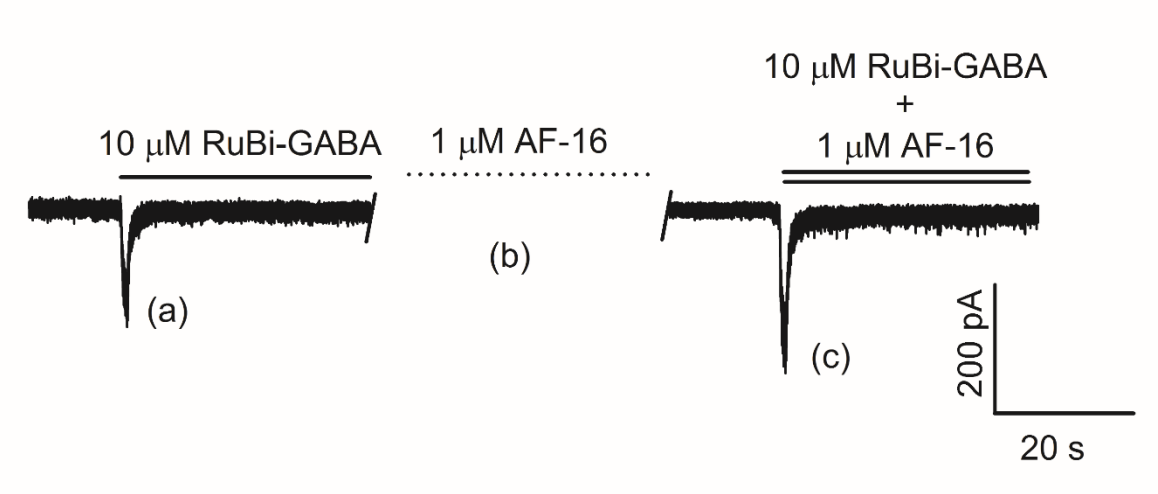

Figure 5.12: Current (pA) *versus* time (s). (a) Current trace after the uncaging of 10 μM RuBi-GABA (750 nm, 100 ms, 30 mW, -80 mV), (b) pretreatment for 3 minutes with 1 μM AF-16, (c) current measured after the photo-release of 10 μM RuBi-GABA in combination with 1 μM AF-16.

The response increases after the treatment with Antisecretory Factor, just like in the results obtained with GABA.

Since the preliminary results confirmed the past ones, experiments were performed in the three different areas of the neuron (Figure 5.13).

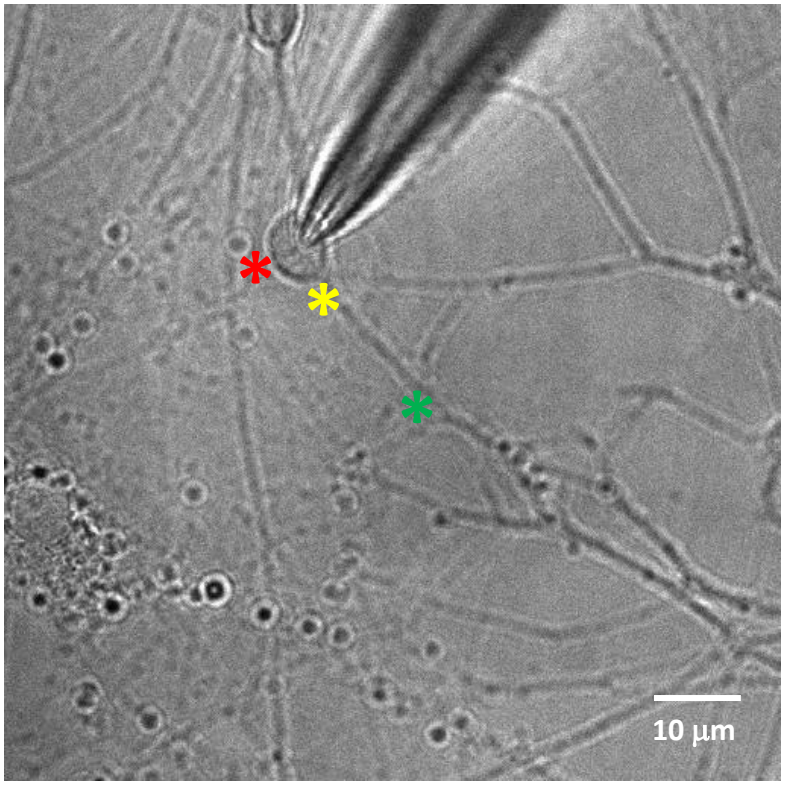

Figure 5.13: Uncaging points on soma (red asterisk), growth cone (yellow asterisk), and neurite (green asterisk) of a cerebellar granule cell.

The uncaging of RuBi-GABA combined with AF-16 after the treatment with Antisecretory Factor for 3 minutes increases the current (facilitating action) due to the activation of $GABA_A$ receptors on the soma, cone, and neurites (Figure 5.14 A, B, C respectively).

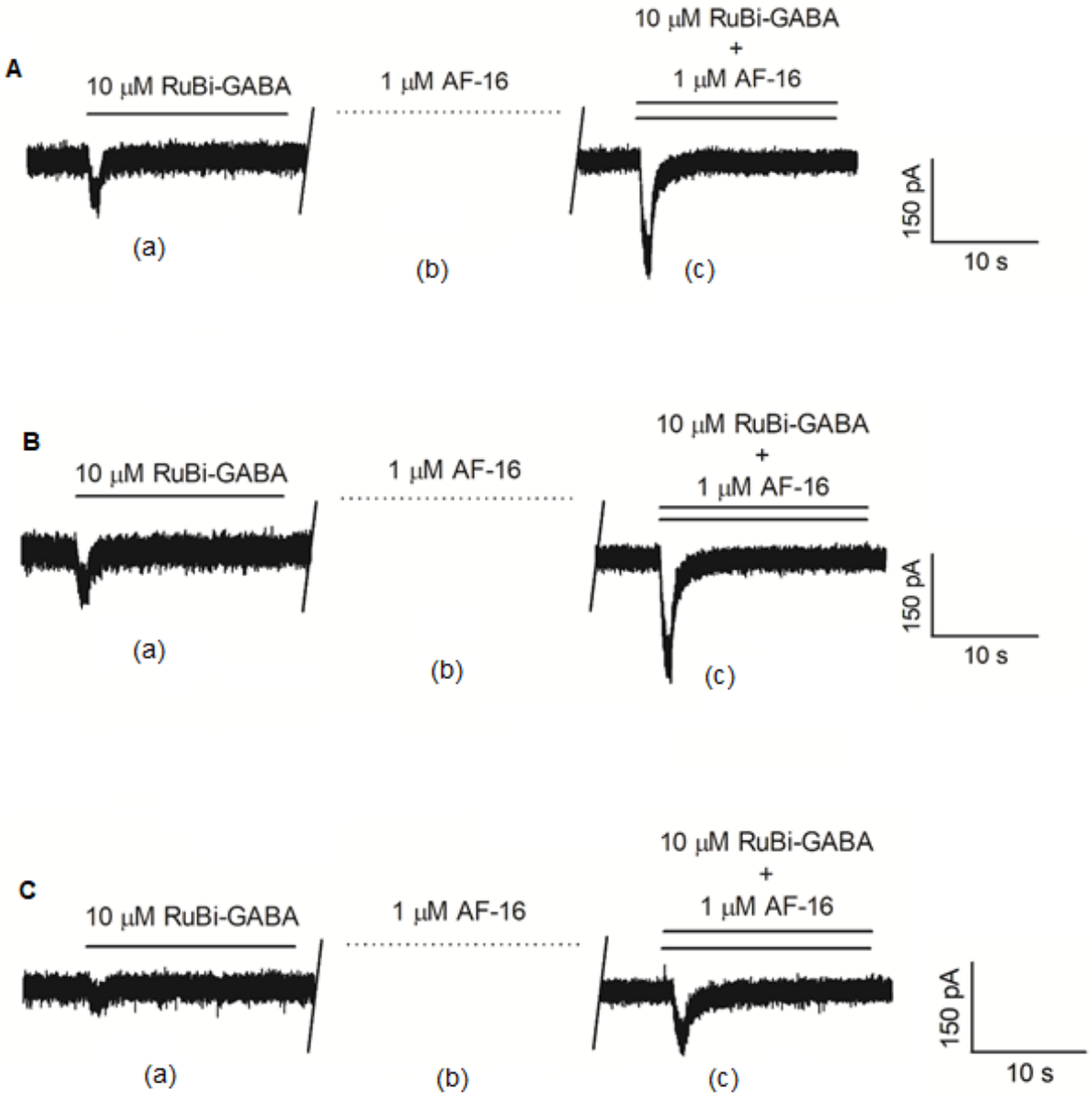

Figure 5.14: Example of chloride current traces evoked by 10 µM uncaged RuBi-GABA (750 nm, 100 ms, 30 mW, -80 mV) on soma (A), growth cone (B), and neurite (C) on the same cell: (a) Current trace after the uncaging of 10 µM RuBi-GABA, (b) pretreatment for 3 minutes with 1 µM AF-16, (c) current measured after the photo-release of 10 µM RuBi-GABA in combination with 1 µM AF-16.

The effect induced by the Antisecretory Factor was calculated by the percentage effect (E%) deducted from the current measurements:

$$E\% = \left(\frac{I_{RuBi-GABA+AF} - I_{RuBi-GABA}}{I_{RuBi-GABA}}\right) \cdot 100 \quad (5.3)$$

	E% ± SEM	**n**
Soma	(37 ± 3) %	25
Cone	(27 ± 4) %	13
Neurite	(40 ± 3) %	14

Table 5.1: Effect of AF-16 on uncaged RuBi-GABA induced current after the pretreatment for 3 minutes of the Antisecretory Factor on soma, growth cone, and neurite. The significance of the result is indicated for each data series.

	Statistical Significance
Soma-Cone	$p < 0.05$
Soma-Neurite	n.s.
Cone-Neurite	$p < 0.05$

Table 5.2: Statistical significance of the differences in the effect of 1 µM AF-16 on soma-cone, soma neurite, cone-neurite. Statistical comparisons were analyzed with Student's t-test.

A series of experiments were carried out on the soma, using the selective pharmacological molecule furosemide, for understanding which receptor subtypes may be involved in the Antisecretory Factor mechanism of action. Furosemide is a selective blocker for the α_6 subunit of $GABA_A$ receptors.

Figure 5.15 reports the traces of the current measurements.

Firstly, the current induced by the uncaging of 10 µM RuBi-GABA was verified (Figure 5.15 A (a)); after the incubation for 3 minutes with Antisecretory Factor (Figure 5.15 A (b)), RuBi-GABA was uncaged combined with AF-16 (Figure 5.15 A (c)).

As expected, the response increases after the treatment with Antisecretory Factor.

On the same cell, RuBi-GABA was uncaged in combination with 1 mM Furosemide (Figure 5.15 B (c)) after a wash-out for 1 minute with the external solution (Figure 5.15 B (b)).

In this case, the current peak decreases because of the blocking of α_6 receptor subtypes.

Finally, after a new treatment with antisecretory factor for 3 minutes (Figure 5.15 C(b)), RuBi-GABA was uncaged combined with 1 µM AF-16 and 1 mM Furosemide (Figure 5.15 C (c)). It can be observed that the current measurement is quite similar to that in the absence of Antisecretory Factor and the presence of the selective blocker.

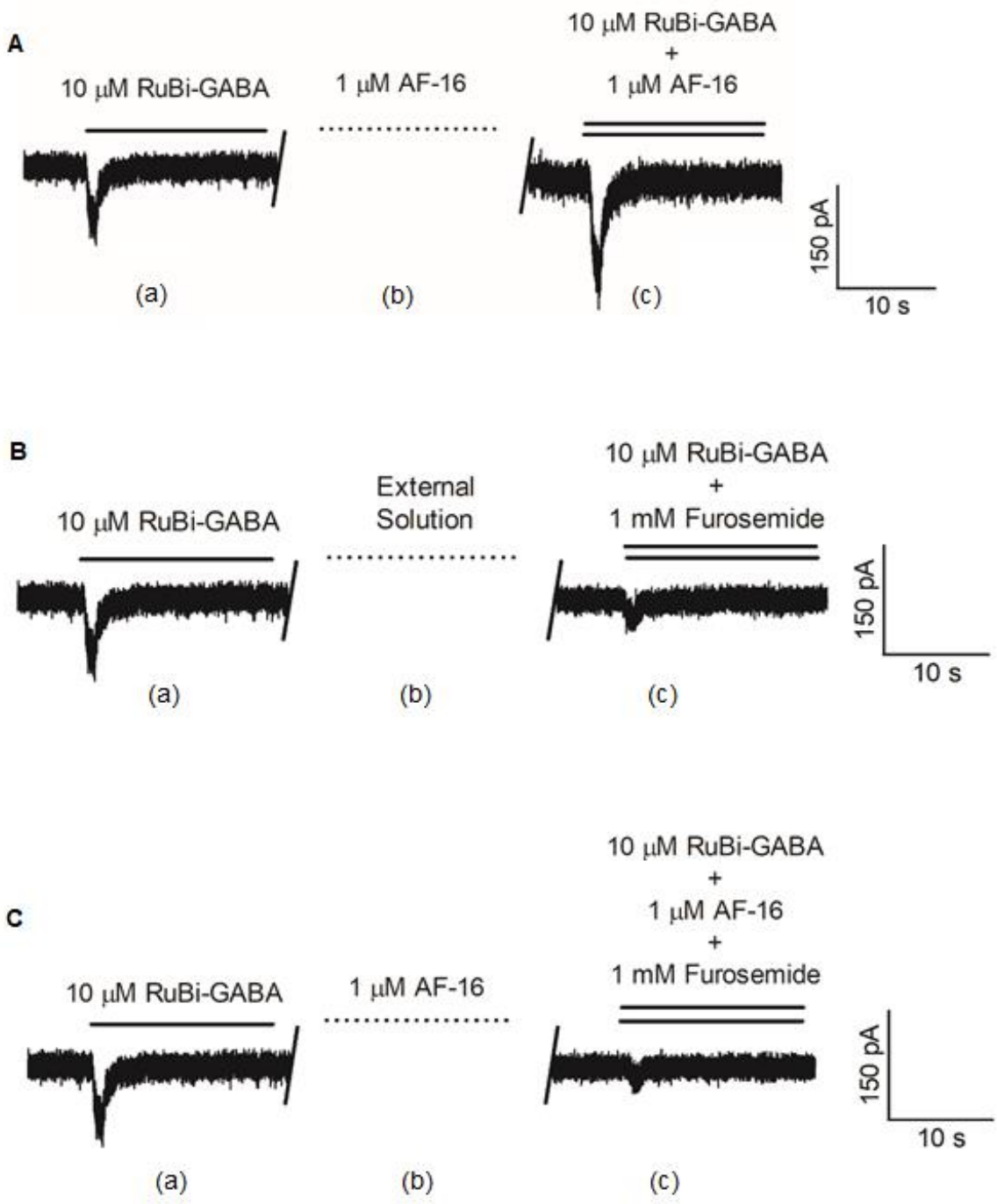

Figure 5.15: Example of chloride current traces evoked by 10 µM uncaged RuBi-GABA (750 nm, 100 ms, 30 mW, -80 mV) on the same cell. A: (a) Current trace measured after the uncaging of 10 µM RuBi-GABA, (b) pretreatment for 3 minutes with 1 µM AF-16, (c) current recorded after the photo-release of 10 µM RuBi-GABA in combination with 1 µM AF-16.

B: (a) Current trace measured after the uncaging of 10 µM RuBi-GABA, (b) wash-out for 1 minute with external solution, (c) current recorded after the photo-release of 10 µM RuBi-GABA in combination with 1 mM furosemide.
C: (a) Current trace measured after the uncaging of 10 µM RuBi-GABA, (b) pretreatment for 3 minutes with 1 µM AF-16, (c) current recorded after the photo-release of 10 µM RuBi-GABA in combination with 1 mM furosemide and 1 µM AF-16.

In Table 5.3 the results are reported in detail.

	E% ± SEM	**n**	**Significance**
10 µM RuBi-GABA + 1 µM AF-16	(45 ± 5)	8	$p < 0.05$
10 µM RuBi-GABA + 1 mM Furosemide	(65 ± 2)	9	$p < 0.001$
10 µM RuBi-GABA + 1 mM Furosemide + 1 µM AF-16	(64 ± 2)	9	$p < 0.001$

Table 5.3: Effect of 1 µM AF-16 (first raw), 1 mM Furosemide (second raw), and 1 mM Furosemide + 1 µM AF-16 (third raw) on 10 µM uncaged RuBi-GABA induced current after the pretreatment for 3 minutes with the Antisecretory Factor. The significance of the result is indicated for each data series.

Chapter 6: Discussion

In this thesis project, it has been explored how the uncaging method can be a useful technique to investigate the GABAergic transmission in cerebellar neurons by studying the variation of the current of the chloride channels associated with the activation of $GABA_A$ receptors in well-defined areas of the cell.

GABA is the principal inhibitory neurotransmitter of the mammalian Central Nervous System, and the photoactivation of the compound RuBi-GABA, a caged GABA, allows controlling the release of a defined neurotransmitter amount in a precise and specific location.

In the first part of the work, the uncaging method has been characterized by studying how physical parameters may affect $GABA_A$ receptor activation and response when the neurotransmitter is released, as reported in the paper Cozzolino et al. 2020 [*11*].

The photophysical condition variations are crucial tools for understanding and differentiating how biological issues and responses are affected during electrophysiological measurements.

The fundamental parameters identified and studied were:

- Excitation method (1PE and 2PE) and laser power
- Exposure time
- X, Y, Z distance from the target

In addition to these parameters, different holding potentials used during the electrophysiological recordings and the variation of RuBi-GABA concentrations were considered.

In the second part of the project, the uncaging method has been applied to the study of $GABA_A$ receptor modulation by pharmacological molecules, i.e., Antisecretory Factor and furosemide, in different neuronal regions during the 2PE photo-release of RuBi-GABA.

Initially, it has been verified that the measured current induced by RuBi-GABA uncaging (Figure 5.1) was due to $GABA_A$ receptor activation by using bicuculline (Figure 5.2); bicuculline occupies the GABA site in the channel preventing the link between the neurotransmitter and the receptor.

After making sure that RuBi-GABA acts as the neurotransmitter GABA, the current curves have been analyzed either as peak values and signal shape by changing the physical parameters for identifying the best experimental conditions to set.

1P excitation volume can be approximated to a double cone, while 2PE is confined to a localized ellipsoid [*130*].

The amount of photolyzed molecules under the 1P process is larger than during the 2P regime and results in differences in the recorded current peaks (Figure 5.3 A, B).

Laser intensity variations may change the number of uncaged molecules in both processes (Figure 5.4 A, B); the lower beam power, the fewer molecules are released.

The number of uncaged GABA gradually increases, raising the laser power until all the molecules in the excitation volume are photoactivated.

The modification of the laser exposure time allows changing the time of uncaged molecules photo-releasing. The effects in the recording currents are different for 1PE and 2PE (Figure 5.5, 5.6).

In the 1P regime, the increase of the exposure time produces a rise in the current intensity that reflects a larger uncaging volume (Figure 5.5 A). Far from the focal point, the photon density is small, and low is the probability of the interaction between uncaged molecules and receptors.

This probability grows for longer exposure time: in fact, the excitation volume increase and, consequently, also the number of uncaged molecules that bind the receptors (Figure 5.6 A).

The activation of more receptors raises the current signal and the decay time (Figure 5.6 C). The full width at half maximum (FWHM) increases because of the interaction of a longer decay time and longer extent of time in the administration of the neurotransmitter (Figure 5.6 E).

On the other hand, the 2PE excitation volume does not increase with the excitation time, and the number of activated receptors remains constant. Hence the peak current intensity and the decay time keep steady (Figure 5.6 B, D).

The FWHM linearly rises, increasing the exposure time because the neurotransmitter is photo-released for a longer time (Figure 5.6 F).

Considering the distance variations along X, Y, and Z-axes, 2PE is more localized than 1PE.

By setting the uncaging point at various X-Y distances and moving away from the target cell (Figure 5.7 A), the current peak measurements decrease both for 1PE and 2PE (Figure 5.7 B) because the number of activated receptors reduces due to the isotropic diffusion of the uncaged molecules.

The effect of the distance variations is more sensitive for 2P compared to the 1P process.

The molecules uncaged far from the cell need more time to reach the target; the increase of the uncaging point distance fits well with long signal rise time (Figure 5.7 C, D, Figure 5.8).

The analysis of the GABA diffusion coefficient experimental data (Figure 5.8) has the result of (6 ± 3) 10^{-10} m^2 s^{-1}; this is comparable to the theoretical one (7 10^{-10} m^2 s^{-1}), evaluated for GABA molecules with the Stokes-Einstein equation, considering water as a *medium* and 10 µM as a concentration.

The peak current variation is due to the diffusion phenomenon.

Regarding the Z-axis variations, the effects on the electrophysiological measurements are different for 1PE and 2PE (Figure 5.9).

During 1PE (Figure 5.9, red squares), the current peaks increase until Z=40 µm from the target, then remain steady between 40 µm < Z < 80 µm. Initially, at Z=0 µm, the low excitation cone is under the glass slice; from 0 to 40 µm, the increase is due to the displacement of this cone within the solution that uncaged more molecules. Finally, at Z > 40 µm, the uncaging of RuBi-GABA in the lower and upper cones is balanced, and the current peaks reach a plateau.

Instead, during 2PE (Figure 5.9, black circles), the current values remain constant within the first 10 µm and then decrease, increasing the distance. The cerebellar granule cells have a size of about 10 µm; for this reason, the current measurements keep steady. Moving the uncaging point from the target, the amount of photo-released molecules diminishes because of the diffusion, as occurs in the case of the variations along the X-Y plane.

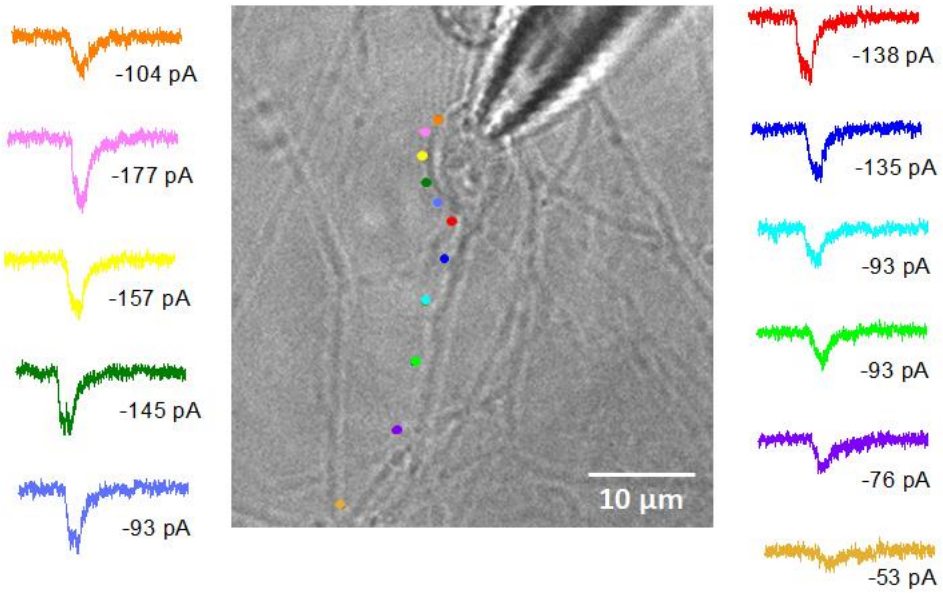

Figure 6.1: Current trace map recorded uncaging 10 µM RuBi–GABA at different points during 2PE (750 nm, 100 ms, 77.3 mW). The color of the current trace and the dot, indicating the uncaging point on the optical image, is the same.

The uncaging method is useful for investigating how the distribution of $GABA_A$ receptors is. The electrophysiological currents evoked by the photo-release of 10 µM RuBi-GABA while changing the uncaging point along the neuron (Figure 6.1) decrease moving away from the soma. These results suggest a different receptor density in the different neuronal areas, and in particular, the receptor density is lower in the neurites than in the cell body.

The technique can be used to study how the receptor density may vary in an area after pharmacological treatments.

It has been investigated how the AF-16 peptide acts on GABAergic transmission in cerebellar neurons by studying the variation of the current of the chloride channels associated with the activation of $GABA_A$ receptors in particular neuronal zones (Figure 5.14).

Although the mechanism of action of the antisecretory effect of AF-16 is unknown, the use of models such as the one presented here can improve the comprehension of how it works.

In particular, the results revealed significant differences in the effects of AF-16 in the cone compared to the cell body and neurites (Tables 5.1, 5.2). These results indicate that the Antisecretory Factor acts on a specific subtype of $GABA_A$ receptors.

Using the selective pharmacological molecule furosemide, a blocker of the receptors constituted by the α_6 subunit, it is possible to verify how effectively the action of the Antisecretory Factor is almost completely blocked (Figure 5.15). It can be hypothesized that its action is mainly carried out on the receptor subtypes formed by this subunit.

Chapter 7: Conclusions

With this research work, the uncaging method was studied, a technique developed in recent decades as a useful tool for observing cellular phenomena localized in specific regions of interest.

The use of caged compounds in electrophysiology and, in particular, the use of two-photon microscopy allows accurate analysis for locating precise and specific responses of a neuronal area and becomes a powerful approach in biophysical issues.

The coupling of electrophysiology and molecular uncaging facilitates defining a complete map of physiological receptor distribution, kinetics, and pharmacology.

In this case, the attention was focused on the pentameric $GABA_A$ receptor in different areas (cell body, growth cone, neurite) of the cerebellar granule cells; comparison between 1PE and 2PE were made for characterized the system and elaborating protocols for experiments related to understanding specific mechanisms that affect the neuronal communications by several pharmacological molecules, i.e., benzodiazepines, neurosteroids, barbiturates.

2P process imaging and uncaging provide 3D localization and define the threshold doses of pharmacological treatments; it is necessary to understand how the measurement conditions affect neuron physiological responses.

For this reason, the principal physical parameters intervening during the measurements (1P and 2P excitation, laser power, exposure time, uncaging point) were analyzed and studied to know better how they influence the signal recorded during the $GABA_A$ receptor activation.

After investigating all these parameters, the method was used to map the receptor electrophysiological distribution response in different regions; this allows deducing that the density of the receptor is higher in the soma than in neurites.

The technique, extensively explored in this project, was also applied to the study of the pharmacological treatment with the protein Antisecretory Factor; in fact, it can be utilized for studying how the receptor density changes in a region of interest after the use of drugs.

The Antisecretory Factor was previously tested in cerebellar granule cells, as reported by *Bazzurro et al. 2018* [*12*], and the results showed a facilitated action on $GABA_A$ receptors.

With the new approach of uncaging, it has been possible to confirm the previous data obtained with the classical electrophysiological technique and verify the importance and the role of this factor, whose mechanism of action is partly unknown. Moreover, uncaging reveals a different action on the different neuronal areas to indicate a different effect on the receptor subtypes of $GABA_A$. In particular, it seems to act on the receptor subtypes composed of the α_6 subunit.

Further experiments in this area would be useful to deepen the topic, for example, using other selective pharmacological molecules for the different receptor subtypes (i.e., flumazenil, a selective antagonist for the benzodiazepine site) and investigating the possible intracellular mechanisms activated by the Antisecretory Factor with selective fluorescent labels for ions as chloride and calcium. A fascinating perspective could be developing this research by coupling 2-photon excitation with an optical super-resolution technique, such as stimulated emission depletion (STED) microscopy.

STED allows resolving details bypassing the diffraction limit of light microscopy by depleting fluorescence in specific regions of the sample while leaving a center focal spot active to emit fluorescence [*131*].

The study with the super-resolution of the possible intracellular mechanisms activated by the Antisecretory Factor could lead to an understanding of how this factor can act *in vivo* and how it can be employed in other parts of the body and on other tissues and organs such as on the Enteric Nervous System where it would seem performing most of its action.

Another development of this work could concern the study of lifetimes (FLIM) by selectively labeling the subunits of $GABA_A$ receptors with specific fluorophores and verifying how the Antisecretory Factor's administration can modify environmental conditions and, consequently, cellular conditions over time.

The $GABA_A$ receptor activation analysis with this research may pave the way to translate similar studies in other models. E.g., it may apply it in the study of the action and effect of different drugs in three-dimensional organoid models or activate specific photoactivable pharmacological molecules in situ to improve the drugs' bioavailability would otherwise be metabolized during standard administration.

References

[1] **Adams S. R., Tsien R. Y. (1993).** Controlling cell chemistry with caged compounds. Annu Rev Physiol, 55: 755-784. DOI: https://doi.org/10.1146/annurev.ph.55.030193.003543

[2] **Rial Verde E. M., Zayat L., Etchenique R., Yuste R. (2008).** Photorelease of GABA with visible light using an inorganic caging group. Front Neural Circuits, 2: 2. DOI: https://doi.org/10.3389/neuro.04.002.2008

[3] **Warther D., Gug S., Specht A., Bolze F., Nicoud J. F., Mourot A., Goeldner M. (2010).** Two-photon uncaging: New prospects in neuroscience and cellular biology. Bioorg Med Chem, 18(22): 7753-7758. DOI: https://doi.org/10.1016/j.bmc.2010.04.084

[4] **Araya R., Andino-Pavlovsky V., Yuste R., Etchenique R. (2013).** Two-photon optical interrogation of individual dendritic spines with caged dopamine. ACS Chem Neurosci, 4(8): 1163-1167. DOI: https://doi.org/10.1021/cn4000692

[5] **Bort G., Gallavardin T., Ogden D., Dalko P. I. (2013).** From one-photon to two-photon probes: "caged" compounds, actuators, and photoswitches. Angew Chem Int Ed Engl, 52(17): 4526-4537. DOI: https://doi.org/10.1002/anie.201204203

[6] **Amatrudo J. M., Olson J. P., Lur G., Chiu C. Q., Higley M. J., Ellis-Davies G. C. R. (2014).** Wavelength-selective one- and two-photon uncaging of GABA. ACS Chem Neurosci, 5(1): 64-70. DOI: https://doi.org/10.1021/cn400185r

[7] **Hess G. P., Lewis R. W., Chen Y. (2014).** Caged neurotransmitters and other caged compounds: design and application. Cold Spring Harb Protoc, 2014(10): pdb.top084152. DOI: https://doi.org/10.1101/pdb.top084152

[8] **Amatrudo J. M., Olson J. P., Agarwal H. K., Ellis-Davies G. C. R. (2015).** Caged compounds for multichromic optical interrogation of neural systems. Eur J Neurosci, 41(1): 5-16. DOI: https://doi.org/10.1111/ejn.12785

[9] **Ellis-Davies G. C. R. (2019).** Two-Photon Uncaging of Glutamate. Front Synaptic Neurosci,10: 48. DOI: https://doi.org/10.3389/fnsyn.2018.00048

[10] **Ellis-Davies G. C. R. (2020).** Useful Caged Compounds for Cell Physiology. Acc Chem Res, 53(8): 1593-1604. DOI: https://doi.org/10.1021/acs.accounts.0c00292

[11] **Cozzolino M., Bazzurro V., Gatta E., Bianchini P., Angeli E., Robello M., Diaspro A. (2020).** Precise 3D modulation of electro-optical parameters during neurotransmitter uncaging experiments with neurons in vitro. Sci Rep, 10(1): 13380. DOI: https://doi.org/10.1038/s41598-020-70217-5

[12] **Bazzurro V., Gatta E., Cupello A., Lange S., Robello M. (2018).** Antisecretory factor modulates $GABA_A$ receptor activity in neurons. J Mol Neurosci, 64(2): 312-320. DOI: https://doi.org/10.1007/s12031-017-1024-8

[13] **Lönnroth I., Lange S. (1984).** Purification and characterization of a hormone-like factor which inhibits cholera secretion. FEBS Lett, 177(1): 104-108. DOI: https://doi.org/10.1016/0014-5793(84)80990-4

[14] **Lange S., Martinsson K., Lönnroth I., Göransson L. (1993).** Plasma level of antisecretory factor (ASF) and its relation to post-weaning diarrhoea in piglets. Zentralbl Veterinarmed B, 40(2): 113-118. DOI: https://doi.org/10.1111/j.1439-0450.1993.tb00117.x

[15] **Lange S., Jennische E., Johansson E., Lönnroth I. (1999).** The antisecretory factor: synthesis and intracellular localisation in porcine tissues. Cell Tissue Res, 296(3): 607-617. DOI: https://doi.org/10.1007/s004410051322

[16] **Lange S., Lönnroth I. (2001).** The antisecretory factor: synthesis, anatomical and cellular distribution, and biological action in experimental and clinical studies. Int Rev Cytol, 210: 39-75. DOI: https://doi.org/10.1016/s0074-7696(01)10003-3

[17] Gravielle M. C. (2016). Activation-induced regulation of $GABA_A$ receptors: Is there a link with the molecular basis of benzodiazepine tolerance? Pharmacol Res 109: 92-100. DOI: https://doi.org/10.1016/j.phrs.2015.12.030

[18] Awapara J., Landua A.J., Fuerst R., Seale B. (1950). Free γ – aminobutyric acid in brain. J Biol Chem, 187(1): 35-39.

[19] Roberts E., Frankel S. (1950). γ-Aminobutyric acid in brain: its formation from glutamic acid. J Biol Chem, 187(1): 55-63.

[20] Roberts E., Frankel S. (1951). Glutamic acid decarboxylase in brain. J Biol Chem, 188(2): 789-795.

[21] Roberts E., Frankel, S. (1951). Further studies of glutamic acid decarboxylase in brain. J Biol Chem, 190(2): 505-512.

[22] Roberts E., Younger F., Frankel S. (1951). Influence of dietary pyridoxine on glutamic decarboxylase activity of brain. J Biol Chem, 191(1): 277-285.

[23] Bessman S. P., Rossen J., Layne E. C. (1953). γ-Aminobutyric acid-glutamic acid transamination in brain. J Biol Chem, 201(1): 385-391.

[24] Clementi F., Fumagalli G. (2012). Farmacologia generale e molecolare, IV edizione. UTET.

[25] Yoon B. E., Woo J., Chun Y. E., Chun H., Jo S., Bae J. Y., An H., Min J. O., Oh S. J., Han K. S., Kim H. Y., Kim T., Kim Y. S., Bae Y. C., Lee C. J. (2014). Glial GABA, synthesized by monoamine oxidase B, mediates tonic inhibition. J Physiol, 592(22): 4951-4968. DOI: https://doi.org/10.1113/jphysiol.2014.278754

[26] Ben-Ari Y., Tseeb V., Raggozzino D., Khazipov R., Gaiarsa J. L. (1994). γ-Aminobutyric acid (GABA): a fast excitatory transmitter which may regulate the development of hippocampal neurones in early postnatal life. Prog Brain Res, 102: 261-273. DOI: https://doi.org/10.1016/S0079-6123(08)60545-2

[27] **Cupello A. (2003).** Neuronal transmembrane chloride electrochemical gradient: A key player in $GABA_A$ receptor activation physiological effect. Amino Acids, 24: 335-346. DOI: https://doi.org/10.1007/s00726-002-0350-4

[28] **Silverthorn D. U. (2007).** Fisiologia, terza edizione. Casa editrice Ambrosiana.

[29] **Sieghart W. (2015).** Allosteric modulation of $GABA_A$ receptors via multiple drug-binding sites. Adv Pharmacol, 72: 53-96. DOI: https://doi.org/10.1016/bs.apha.2014.10.002

[30] **Olsen R. W., Li G. D., Wallner M., Trudell J. R., Bertaccini E. J., Lindahl E., Miller K. W., Alkana R. L., Davies D. L. (2013).** Structural models of ligand-gated ion channels: sites of action for anesthetics and ethanol. Alcohol Clin Exp Res, 38(3): 595-603. DOI: https://doi.org/10.1111/acer.12283

[31] **Antkowiak B. (2015).** Closing the gap between the molecular and systemic actions of anesthetic agents. Adv Pharmacol, 72: 229-262. DOI: https://doi.org/10.1016/bs.apha.2014.10.009

[32] **Bowery N. G., Hill D. R., Hudson A. L. (1983).** Characteristics of $GABA_B$ receptor binding sites on rat whole brain synaptic membranes. Br J Pharmac, 78: 191-206. DOI: https://doi.org/10.1111/j.1476-5381.1997.tb06835.x

[33] **Kerr D. I. B., Ong J. (1995).** $GABA_B$ receptors. Pharmacol Ther, 67(2): 187-246. DOI: https://doi.org/10.1016/0163-7258(95)00016-a

[34] **Jones K. A., Borowsky B., Tamm J. A., Craig D. A., Durkin M. M., Dai M., Yao W. J., Johnson M., Gunwaldsen C., Huang L. Y., Tang C., Shen Q., Salon J. A., Morse K., Laz T., Smith K. E., Nagarathnam D., Noble S. A., Branchek T. A., Gerald C. (1998).** $GABA_B$ receptors function as a heteromeric assembly of the subunits $GABA_BR1$ and $GABA_BR2$. Nature, 396(6712): 674-679. DOI: https://doi.org/10.1038/25348

[35] Takahashi T., Kajikawa Y., Tsujimoto T. (1998). G-protein-coupled modulation of presynaptic calcium currents and transmitter release by a $GABA_B$ receptor. J Neurosci, 18(9): 3138-3146. DOI: https://doi.org/10.1523/JNEUROSCI.18-09-03138.1998

[36] Bowery N. G., Enna S. J. (2000). γ-Aminobutyric $acid_B$ receptors: first of the functional metabotropic heterodimers. J Pharmacol Exp Ther, 292(1): 2-7

[37] Watanabe M., Maemura K., Kanbara K., Tamayama T., Hayasaki H. (2002). GABA and GABA receptors in the central nervous system and other organs. Int Rev Cytol, 213: 1-47. DOI: https://doi.org/10.1016/s0074-7696(02)13011-7

[38] Feigenspan A., Bormann J. (1998). GABA-gated Cl^- channels in the rat retina. Prog Retin Eye Res, 17(1): 99-126. DOI: https://doi.org/10.1016/s1350-9462(97)00008-6

[39] Olsen R. W., Sieghart W. (2008). International Union of Pharmacology. LXX. Subtypes of γ-aminobutyric $acid_A$ receptors: classification on the basis of subunit composition, pharmacology, and function. Update. Pharmacol Rev, 60(3): 243-260. DOI: https://doi.org/10.1124/pr.108.00505

[40] Olsen R. W., Tobin A. J. (1990). Molecular biology of $GABA_A$ receptors. Faseb J, 4(5): 1469-1480. DOI: https://doi.org/10.1096/fasebj.4.5.2155149

[41] Puthenkalam R., Hieckel M., Simeone X., Suwattanasophon C., Feldbauer R. V., Ecker G. F., Ernst M. (2016). Structural studies of $GABA_A$ receptor binding sites: which experimental structure tells us what? Front Mol Neurosci, 9: 44. DOI: https://doi.org/10.3389/fnmol.2016.00044

[42] Fritschy J.M., Mohler H. (1995). $GABA_A$-receptor heterogeneity in the adult rat brain: differential regional and cellular distribution of seven major subunits. J Comp Neurol, 359(1): 154-194. DOI: https://doi.org/10.1002/cne.903590111

[43] Benke D., Fritschy J. M., Trzeciak A., Bannwarth W., Mohler H. (1994). Distribution, prevalence, and drug binding profile of gamma-aminobutyric acid type A receptor subtypes differing in the beta-subunit variant. J Biol Chem, 269(43): 27100-27107.

[44] MacLennan A. J., Brecha N., Khrestchatisky M., Sternini C., Tillakaratne N. J., Chiang M. Y., Anderson K., Lai M., Tobin A. J. (1991). Independent cellular and ontogenetic expression of mRNAs encoding three α polypeptides of the rat $GABA_A$ receptor. Neuroscience, 43(2-3): 369-380. DOI: https://doi.org/10.1016/0306-4522(91)90301-4

[45] Chandra D., Jia F., Liang J., Peng Z., Suryanarayanan A., Werner D. F., Spigelman I., Houser C. R., Olsen R. W., Harrison N. L., Homanics G. E. (2006). $GABA_A$ receptor α4 subunits mediate extrasynaptic inhibition in thalamus and dentate gyrus and the action of gaboxadol. Proc Natl Acad Sci USA, 103(41): 15230-15235. DOI: https://doi.org/10.1073/pnas.0604304103

[46] Varecka L., Wu C. H., Rotter A., Frostholm A. (1994). GABAA/benzodiazepine receptor alpha 6 subunit mRNA in granule cells of the cerebellar cortex and cochlear nuclei: expression in developing and mutant mice. J Comp Neurol, 339(3): 341-352. DOI: https://doi.org/10.1002/cne.903390304

[47] Whiting P. J., McAllister G., Bonnert T., Heavens R. P., Rigby M. R., Sirinathsinghji D. J., Marshall G., Thompson S. A., Wafford K. A. (1997). The use of expressed sequence tag databases to identify novel human γ-aminobutyric acid type receptor genes. Biochem Soc Trans, 25(3): 817-819. DOI: https://doi.org/10.1042/bst0250817

[48] Hedblom E., Kirkness E. F. (1997). A novel class of $GABA_A$ receptor subunit in tissues of the reproductive system. J Biol Chem, 272(24): 15346-1550. DOI: https://doi.org/10.1074/jbc.272.24.15346

[49] Khom S., Baburin I., Timin E. N., Hohaus A., Sieghart W., Hering S. (2006). Pharmacological properties of $GABA_A$ receptors containing γ1 subunits. Mol Pharmacol, 69(2): 640-649. DOI: https://doi.org/10.1124/mol.105.017236

[50] Korpi E. R., Gründer G., Lüddens H. (2002). Drug interactions at $GABA_A$ receptors. Prog Neurobiol, 67(2): 113-159. DOI: https://doi.org/10.1016/s0301-0082(02)00013-8

[51] Nolan S. J., Marson A. G., Weston J., Tudur Smith C. (2016). Carbamazepine versus phenobarbitone monotherapy for epilepsy: an individual participant data review. Cochrane Database Syst Rev, 12: CD001904. DOI: https://doi.org/10.1002/14651858.CD001904.pub3

[52] Mihic S. J., Ye Q., Wick M. J., Koltchine V. V., Krasowski M. D., Finn S. E., Mascia M. P., Valenzuela C. F., Hanson K. K., Greenblatt E. P., Harris R. A., Harrison N. L. (1997). Sites of alcohol and volatile anaesthetic action on $GABA_A$ and glycine receptors. Nature, 389(6649): 385-389. DOI: https://doi.org/10.1038/38738

[53] Ambrosi G., Cantino D., Castano P., Correr S., D'Este L., Donato R. F., Familiari G., Fornai F., Gulisano M., Iannello A., Magaudda L., Marcello M. F., Martelli A. M., Pacini P., Rende M., Rossi P., Sforza C., Tacchetti C., Toni R., Zummo G. (2008). Anatomia dell'uomo, II edizione. Edi – ermes.

[54] Gilbert S. F. (2005). Biologia dello sviluppo, III edizione. Zanichelli.

[55] Mosconi M. W., Wang Z., Schmitt L. M., Tsai P., Sweeney J. A. (2015). The role of cerebellar circuitry alterations in the pathophysiology of autism spectrum disorders. Front Neurosci, 9: 296. DOI: https://doi.org/10.3389/fnins.2015.00296

[56] Ghez C. (1994). "Il cervelletto", in Kandel E.R., Schwartz J.H., Jessel T.M. "Principi di Neuroscienze". Casa Editrice Ambrosiana, Milano, pp 642-662.

[57] Johansson E., Lönnroth I., Lange S., Jonson I., Jennische E., Lönnroth C. (1995). Molecular cloning and expression of a pituitary gland protein modulating intestinal fluid secretion. J Biol Chem, 270(35): 20615-20620. DOI: https://doi.org/10.1074/jbc.270.35.20615

[58] Johansson E., Lange S., Lönnroth I. (1997). Identification of an active site in the antisecretory factor protein. Biochim Biophys Acta, 1362(2-3): 177-182. DOI: https://doi.org/10.1016/s0925-4439(97)00066-5

[59] Rapallino M. V., Cupello A., Lange S., Lönnroth I. (2003). Antisecretory factor peptide derivatives specifically inhibit [^{3}H]-γ-amino-butyric acid/$^{36}Cl^{-}$ out→in permeation across the isolated rabbit Deiters' neuronal membrane. Acta Physiol Scand, 179(4): 367-371. DOI: https://doi.org/10.1111/j.1365-201X.2003.01173.x

[60] Björck S., Bosaeus I., Ek E., Jennische E., Lönnroth I., Johansson E., Lange S. (2000). Food induced stimulation of the antisecretory factor can improve symptoms in human inflammatory bowel disease: a study of a concept. Gut, 46(6): 824-829. DOI: https://doi.org/10.1136/gut.46.6.824

[61] Jennische E., Bergström T., Johansson M., Nyström K., Tarkowski A., Hansson H. A., Lange S. (2008). The peptide AF-16 abolishes sickness and death at experimental encephalitis by reducing increase of intracranial pressure. Brain Res., 1227: 189-197. DOI: https://doi.org/10.1016/j.brainres.2008.05.083

[62] Matson Dzebo M., Reymer A., Fant K., Lincoln P., Nordén B., Rocha S. (2014). Enhanced cellular uptake of antisecretory peptide AF-16 through proteoglycan binding. Biochemistry, 53(41): 6566-6573. DOI: https://doi.org/10.1021/bi5010377

[63] Davidson T. S., Hickey W. F. (2004). Distribution and immunoregulatory properties of antisecretory factor. Lab Invest, 84(3): 307-319. DOI: https://doi.org/10.1038/labinvest.3700036

[64] Edwards Y. J., Perkins S. J. (1996). Assessment of protein fold predictions from sequence information: the predicted α/β doubly wound fold of the von Willebrand factor type A domain is similar to its crystal structure. J Mol Biol, 260(2): 277-285. DOI: https://doi.org/10.1006/jmbi.1996.0398

[65] Kim M., Wasling P., Xiao M. Y., Jennische E., Lange S., Hanse E. (2005). Antisecretory factor modulates GABAergic transmission in the rat hippocampus. Regul Pept, 129(1-3): 109-118. DOI: https://doi.org/10.1016/j.regpep.2005.01.018

[66] Johansson E., Lönnroth I., Jonson I., Lange S., Jennische E. (2009). Development of monoclonal antibodies for detection of Antisecretory Factor activity in human plasma. J Immunol Methods, 342(1-2): 64-70. DOI: https://doi.org/10.1016/j.jim.2008.11.018

[67] Bodrikov V., Pauschert A., Kochlamazashvili G., Stuermer C. A. (2017). Reggie-1 and Reggie-2 (flotillins) participate in Rab11a-dependent cargo trafficking, spine synapse formation and LTP-related AMPA receptor (GluA1) surface exposure in mouse hippocampal neurons. Exp Neurol, 289: 31-45. DOI: https://doi.org/10.1016/j.expneurol.2016.12.007

[68] Torres J., Jennische E., Lange S., Lönnroth I. (1991). Clostridium difficile toxin A induces a specific antisecretory factor which protects against intestinal mucosal damage. Gut, 32(7): 791-795. DOI: https://doi.org/10.1136/gut.32.7.791

[69] Galligan J. J. (2002). Ligand-gated ion channels in the enteric nervous system. Neurogastroenterol Motil, 14(6): 611-623. DOI: https://doi.org/10.1046/j.1365-2982.2002.00363.x

[70] Galligan J. J. (2002). Pharmacology of synaptic transmission in the enteric nervous system. Curr Opin Pharmacol, 2(6): 623-629. DOI: https://doi.org/10.1016/s1471-4892(02)00212-6

[71] Krantis A., Shabnavard L., Nichols K., de Blas A. L., Staines W. (1995). Localization of $GABA_A$ receptor immunoreactivity in NO synthase positive myenteric neurones. J Auton Nerv Syst, 53(2-3): 157-165. DOI: https://doi.org/10.1016/0165-1838(94)00180-r

[72] Strandberg J., Lindquist C., Lange S., Asztely F., Hanse E. (2014). The endogenous peptide antisecretory factor promotes tonic GABAergic signaling in CA1 stratum radiatum interneurons. Front Cell Neurosci, 8: 13. DOI: https://doi.org/10.3389/fncel.2014.00013

[73] Ulgheri C., Paganini B., Rossi F. (2010). Antisecretory factor as a potential health-promoting molecule in man and animals. Nutr Res Rev, 23(2): 300-313. DOI: https://doi.org/10.1017/S0954422410000193

[74] Zaman S., Aamir K., Lange S., Jennische E., Silfverdal S. A., Hanson L. Å. (2014). Antisecretory factor effectively and safely stops childhood diarrhoea: a placebo-controlled, randomised study. Acta Paediatr, 103(6): 659-664. DOI: https://doi.org/10.1111/apa.12581

[75] Hanner P., Jennische E., Lange S., Lönnroth I., Wahlström B. (2004). Increased antisecretory factor reduces vertigo in patients with Ménière's disease: a pilot study. Hear Res, 190(1-2): 31-36. DOI: https://doi.org/10.1016/S0378-5955(03)00368-X

[76] Hanner P., Rask-Andersen H., Lange S., Jennische E. (2010). Antisecretory factor-inducing therapy improves the clinical outcome in patients with Ménière's disease. Acta Otolaryngol, 130(2): 223-227. DOI: https://doi.org/10.3109/00016480903022842

[77] Leong S. C., Narayan S., Lesser T. H. (2013). Antisecretory factor-inducing therapy improves patient-reported functional levels in Ménière's disease. Ann Otol Rhinol Laryngol, 122(10): 619-624.

[78] Ingvardsen C. J., Klokker M. (2016). Antisecretory therapy with no improvement in functional level in Ménière's disease. Acta Otolaryngol, 136(3): 232-235. DOI: https://doi.org/10.3109/00016489.2015.1115551

[79] Ishihara A., Gee K., Schwartz S., Jacobson K., Lee J. (1997). Photoactivation of caged compounds in single living cells: an application to the study of cell locomotion. Biotechniques, 23(2): 268-274. DOI: https://doi.org/10.2144/97232st01

[80] Passlick S., Ellis-Davies G. C. R. (2019). Chromatically independent, two-color uncaging of glutamate and GABA with one- or two-photon excitation. Methods Enzymol, 624: 167-196. DOI: https://doi.org/10.1016/bs.mie.2019.05.003

[81] Papageorgiou G., Corrie J. E. T. (2000). Effects of aromatic substituents on the photocleavage of 1-acyl-7-nitroindolines. Tetrahedron, 56: 8197-8205. DOI: https://doi.org/10.1016/S0040-4020(00)00745-6

[82] Ellis-Davies G. C. R. (2007). Caged compounds: photorelease technology for control of cellular chemistry and physiology. Nat Methods, 4(8): 619-628. DOI: https://doi.org/10.1038/nmeth1072

[83] Ellis-Davies G. C. R. (2009). Basics of photoactivation. Cold Spring Harb Protoc, 2009(2): pdb.top55. DOI: https://doi.org/10.1101/pdb.top55

[84] Klán P., Šolomek T., Bochet C. G., Blanc A., Givens R., Rubina M., Popik V., Kostikov A., Wirz J. (2013). Photoremovable protecting groups in chemistry and biology: reaction mechanisms and efficacy. Chem Rev, 113(1): 119-191. DOI: https://doi.org/10.1021/cr300177k

[85] Zayat L., Salierno M., Etchenique R. (2006). Ruthenium (II) bipyridyl complexes as photolabile caging groups for amines. Inorg Chem, 45(4): 1728-1731. DOI: https://doi.org/10.1021/ic0512983.

[86] Denk W., Strickler J. H., Webb W. W. (1990). Two-photon laser scanning fluorescence microscopy. Science 248(4951): 73-76. DOI: https://doi.org/10.1126/science.2321027.

[87] Kantevari S., Matsuzaki M., Kanemoto Y., Kasai H., Ellis-Davies G. C. R. (2010). Two-color, two-photon uncaging of glutamate and GABA. Nat Methods, 7(2): 123-5. DOI: https://doi.org/10.1038/nmeth.1413

[88] Kanemoto Y., Matsuzaki M., Morita S., Hayama T., Noguchi J., Senda N., Momotake A., Arai T., Kasai H. (2011). Spatial distributions of GABA receptors and local inhibition of Ca^{2+} transients studied with GABA uncaging in the dendrites of CA1 pyramidal neurons. PLoS One, 6(7): e22652. DOI: https://doi.org/10.1371/journal.pone.0022652

[89] Marlin J. J., Carter A. G. (2014). GABA-A receptor inhibition of local calcium signaling in spines and dendrites. J Neurosci, 34(48): 15898-15911. DOI: https://doi.org/10.1523/JNEUROSCI.0869-13.2014

[90] Passlick S., Kramer P. F., Richers M. T., Williams J. T., Ellis-Davies G. C. R. (2017). Two-color, one-photon uncaging of glutamate and GABA. PLoS One, 12(11): e0187732. DOI: https://doi.org/10.1371/journal.pone.0187732

[91] Kwon T., Merchán-Pérez A., Rial Verde E. M., Rodríguez J. R., DeFelipe J., Yuste R. (2019). Ultrastructural, Molecular and Functional Mapping of GABAergic Synapses on Dendritic Spines and Shafts of Neocortical Pyramidal Neurons. Cereb Cortex, 29(7): 2771-2781. DOI: https://doi.org/10.1093/cercor/bhy143

[92] Gurney A. M., Lester H. A. (1987). Light-flash physiology with synthetic photosensitive compounds. Physiol Rev, 67(2): 583-617. DOI: https://doi.org/10.1152/physrev.1987.67.2.583

[93] Shi D. D., Trigo F. F., Semmelhack M. F., Wang S. S-H (2014). Synthesis and biological evaluation of bis-CNB-GABA, a photoactivatable neurotransmitter with low receptor interference and chemical two-photon uncaging properties. J Am Chem Soc, 136(5): 1976-181. DOI: https://doi.org/10.1021/ja411082f

[94] Ellis-Davies G. C. R. (2013). A chemist and biologist talk to each other about caged neurotransmitters. Beilstein J Org Chem, 9: 64-73. DOI: https://doi.org/10.3762/bjoc.9.8

[95] Delcour A. H., Hess G. P. (1986). Chemical kinetic measurements of the effect of trans- and cis-3,3'-Bis[(trimethylammonio)methyl]azobenzene bromide on acetylcholine receptor mediated ion translocation in Electrophorus electricus and Torpedo californica. Biochemistry, 25(7): 1793-1798. DOI: https://doi.org/10.1021/bi00355a051

[96] Milburn T., Matsubara N., Billington A. P., Udgaonkar J. B., Walker J. W., Carpenter B. K., Webb W. W., Marque J., Denk W., McCray J. A., Hess G. P. (1989). Synthesis, photochemistry, and biological activity of a caged photolabile acetylcholine receptor ligand. Biochemistry, 28(1): 49-55. DOI: https://doi.org/10.1021/bi00427a008

[97] Shembekar V. R., Chen Y., Carpenter B. K., Hess G. P. (2007). Coumarin-caged glycine that can be photolyzed within 3 microseconds by visible light. Biochemistry, 46(18): 5479-5484. DOI: https://doi.org/10.1021/bi700280e

[98] Matsuzaki M., Honkura N., Ellis-Davies G. C. R., Kasai H. (2004). Structural basis of long-term potentiation in single dendritic spines. Nature, 429(6993): 761-766. DOI: https://doi.org/10.1038/nature02617

[99] Breitinger H. G., Wieboldt R., Ramesh D., Carpenter B. K., Hess G. P. (2000). Synthesis and characterization of photolabile derivatives of serotonin for chemical kinetic investigations of the serotonin 5-HT_3 receptor. Biochemistry, 39(18): 5500-5508. DOI: https://doi.org/10.1021/bi992781q

[100] Matsuzaki M., Hayama T., Kasai H., Ellis-Davies G. C. R. (2010). Two-photon uncaging of γ-aminobutyric acid in intact brain tissue. Nat Chem Biol, 6(4): 255-257. DOI: https://doi.org/10.1038/nchembio.321

[101] Trigo F. F., Papageorgiou G., Corrie J. E. T., Ogden D. (2009). Laser photolysis of DPNI-GABA, a tool for investigating the properties and distribution of GABA receptors and for silencing neurons in situ. J Neurosci Methods, 181(2): 159-169. DOI: https://doi.org/10.1016/j.jneumeth.2009.04.022

[102] Salierno M., Marceca E., Peterka D. S., Yuste R., Etchenique R. (2010). A fast ruthenium polypyridine cage complex photoreleases glutamate with visible or IR light in one and two photon regimes. J Inorg Biochem, 104(4): 418-422. DOI: https://doi.org/10.1016/j.jinorgbio.2009.12.004

[103] Ellis-Davies G. C. R. (2014). Nitrophenyl-based caged neurotransmitters. Cold Spring Harb Protoc, 2014(6): 584-590. DOI: https://doi.org/10.1101/pdb.top081794

[104] Senda N., Momotake A., Arai T. (2007). Synthesis and Photocleavage of 7-[{Bis(carboxymethyl)amino}-coumarin-4-yl]methyl-Caged Neurotransmitters. Bull Chem Soc Jpn, 80(12): 2384-2388. DOI: https://doi.org/10.1246/bcsj.80.2384

[105] Molnár P., Nadler J. V. (2000). γ-Aminobutyrate, α-carboxy-2-nitrobenzyl ester selectively blocks inhibitory synaptic transmission in rat dentate gyrus. Eur J Pharmacol, 391(3): 255-262. DOI: https://doi.org/10.1016/s0014-2999(00)00106-0

[106] Gee K. R., Wieboldt R., Hess G. P. (1994). Synthesis and photochemistry of a new photolabile derivative of GABA. Neurotransmitter release and receptor activation in the microsecond time region. J Am Chem Soc, 116: 8366-8367.

[107] Gee K. R., Carpenter B. K., Hess G. P. (1998). [2] Synthesis, photochemistry, and biological characterization of photolabile protecting groups for carboxylic acids and neurotransmitters. Methods Enzymol, 291: 30-50. DOI: https://doi.org/10.1016/S0076-6879(98)91005-9

[108] Zayat L., Noval M. G., Campi J., Calero C. I., Calvo D. J., Etchenique R. (2007). A new inorganic photolabile protecting group for highly efficient visible light GABA uncaging. Chembiochem, 8(17): 2035-2038. DOI: https://doi.org/10.1002/cbic.200700354

[109] Svaasand L. O., Ellingsen R. (1983). Optical properties of human brain. Photochem Photobiol, 38(3): 293-299. DOI: https://doi.org/10.1111/j.1751-1097.1983.tb02674.x

[110] Nikolenko V., Yuste R., Zayat L., Baraldo L. M., Etchenique R. (2005). Two-photon uncaging of neurochemicals using inorganic metal complexes. Chem Commun (Camb), (13): 1752-1754. DOI: https://doi.org/10.1039/b418572b

[111] Kornreich B.G., (2007). The patch clamp technique: principles and technical considerations. J Vet Cardiol, 9:25-37. DOI: https://doi.org/10.1016/j.jvc.2007.02.001

[112] Ogden D., Stanfield P. (1994). Patch clamp techniques for single channel and whole-cell recording. Microelectrode Techniques (2nd edition). The Company of Biologists Ltd, Cambridge

[113] Karmažínová M., Lacinová L'. (2010). Measurement of cellular excitability by whole cell patch clamp technique. Physiol Res, 59(Suppl. 1): S1-S7.

[114] Hamill O. P., Marty A., Neher E., Sakmann B., Sigworth F. J. (1981). Improved patch-clamp techniques for high-resolution current recording from cells and cell-free membrane patches. Pflfigers Arch 391: 85-100. DOI: https://doi.org/10.1007/BF00656997

[115] Bébarová M. (2012). Advances in patch clamp technique: towards higher quality and quantity. Gen. Physiol. Biophys., 31: 131-140. DOI: https://doi.org/10.4149/gpb_2012_016

[116] Molleman A. (2003). Patch clamping: an introductory guide to patch clamp electrophysiology. John Wiley&Sons Ltd

[117] Evennett P. J., Hammond C. (2005). Microscopy/ Overview. Encyclopedia of Analytical Science (Second Edition): 32-41. DOI: https://doi.org/10.1016/B0-12-369397-7/00376-9

[118] Mondal P. P., Diaspro A. (2014). Fundamentals of Fluorescence Microscopy, Exploring Life with Light, Springer.

[119] Abbe E. (1873). Beiträge zur Theorie des Mikroskops und der mikroskopischen Wahrnehmung. Archiv für mikroskopische Anatomie, 9:413-418. DOI: https://doi.org/10.1007/BF02956173

[120] Mualla F., Aubreville M., Maier A. (2018). Microscopy. In: Maier A., Steidl S., Christlein V., Hornegger J. (eds) Medical Imaging Systems. Lecture Notes in Computer Science, vol 11111. Springer, Cham. DOI: https://doi.org/10.1007/978-3-319-96520-8_5

[121] Lakowicz J. R. (2006). Introduction to Fluorescence. In: Principles of Fluorescence Spectroscopy. Springer, Boston, MA. DOI: https://doi.org/10.1007/978-0-387-46312-4_1

[122] Sanderson M. J., Smith I., Parker I., Bootman M. D. (2014). Fluorescence microscopy. Cold Spring Harb Protoc, 2014(10): pdb.top071795. DOI: https://doi.org/10.1101/pdb.top071795

[123] Helmchen F., Denk W. (2005). Deep tissue two-photon microscopy. Nat Methods, 2(12): 932-940. DOI: https://doi.org/10.1038/nmeth818

[124] Diaspro A, Chirico G, Collini M. (2005). Two-photon fluorescence excitation and related techniques in biological microscopy. Q Rev Biophys, 38(2): 97-166. DOI: https://doi.org/10.1017/S0033583505004129

[125] Bianchini P., Harke B., Galiani S., Vicidomini G., Diaspro A. (2012). Single-wavelength two-photon excitation-stimulated emission depletion (SW2PE-STED) superresolution imaging. Proc Natl Acad Sci U S A, 109(17): 6390-6393. DOI: https://doi.org/10.1073/pnas.1119129109

[126] Mariottini G. L., Capicchioni V., Guida L., Mattioli F., Penco S., Romano P., Scarabelli L. (2010). Introduzione alle colture cellulari, II edizione. Tecniche Nuove.

[127] De Angelis I. (1994). Tecniche per la coltivazione delle cellule in vitro. In: Colture cellulari in tossicologia. F. Zucco, V. Bianchi (Eds.), Lombardo Editore, Roma, 31-54.

[128] Robello M., Baldelli P., Cupello A. (1994). Modulation by extracellular pH of the activity of $GABA_A$ receptors on rat cerebellum granule cells. Neuroscience, 61(4): 833-837. DOI: https://doi.org/10.1016/0306-4522(94)90406-5

[129] Goutelle S., Maurin M., Rougier F., Barbaut X., Bourguignon L., Ducher M., Maire P. (2008). The Hill equation: a review of its capabilities in pharmacological modelling. Fundam Clin Pharmacol, 22(6): 633-648. DOI: https://doi.org/10.1111/j.1472-8206.2008.00633.x

[130] Mazza D., Cella F., Vicidomini G., Krol S., Diaspro A (2007). Role of three-dimensional bleach distribution in confocal and two-photon fluorescence recovery after photobleaching experiments. Appl Opt, 46: 7401-7411. DOI: https://doi.org/10.1364/AO.46.007401

[131] Schermelleh L., Heintzmann R., Leonhardt H. (2010). A guide to super-resolution fluorescence microscopy. J Cell Biol, 190(2): 165-175. DOI: https://doi.org/10.1083/jcb.201002018

Acknowledgments

Writing this Ph.D. thesis, I had the opportunity to reflect on the origins of my interest in scientific topics.

A phrase that, despite being a very shy child, I clearly expressed to the mayor of my city has remained famous in my family: it was 1997, I participated with my parents in the laying of the “first stone” of a theater in Genoa, and, introducing myself directly to the mayor, I asked him for an autograph in my diary.

He kindly suggested to write me a short dedication, as long as I told him what my career choice would be for the future, I replied, "the scientist".

This was the moment that marked my history.

During these three years of Ph.D., I have discovered the beauty and complexity of scientific research, characterized by enthusiasm and sometimes moments of discouragement, but above all, I discovered that the world of science is fascinating, mysterious, and projected towards new frontiers without forgetting origins.

About this, I would like to thank everyone who took part in this work and made it possible with their participation, empathic support, and valuable suggestions.

I thank my supervisors, Professor Alberto Diaspro and Professor Mauro Robello, who have supported and directed me on this path with patience and attention.

I thank Dr. Elena Gatta and Dr. Elena Angeli, with whom I collaborated and found precious tutors and advisers.

I thank Dr. Cupello for his kind suggestions and advice.

I thank Dr. Marco Cozzolino, colleague and friend, with whom I shared ups and downs during the first phase of the experiments.

I thank Dr. Paolo Bianchini, Michele Oneto, Marco Scotto, and Mattia Pesce (IIT) for their technical support.

I thank Dr. Stefan Lange of the University of Gothenburg (Sweden), who provided the Antisecretory Factor (AF-16) used during the laboratory experiments.

A great thanks to Davide, Ester, Giacomo, Giulia, Marzia, Michele, and Paolo, whom every day shared joys, sacrifices, and successes with me without ever turning their backs. The affection and support they have shown me make this achievement even more valuable.

A special thanks to my family and Emanuele, who were close to me, understood me, and comforted me when I thought I was far from the result. It is thanks to their support and encouragement that today I have reached this goal.

Entering this world was extremely formative; in fact, it allowed me to exercise, together with the knowledge I learned in the field, the patience, tenacity, and stubbornness that I believe belong to those who love this job and want to continue on this path.